Durham E-Theses

Very high energy gamma rays from isolated pulsars and non-pulsating objects

Rayner, Stephen Mark

How to cite:

Use policy

ABSTRACT

This thesis is concerned with the detection of very high energy γ-rays from isolated pulsars and objects that are not known to emit pulsed radiation, using the atmospheric Cerenkov technique.

The first chapter summarises the processes by which celestial γ-rays can be generated and absorbed. A discussion of the criteria for selecting objects for study is given. The second chapter describes the atmospheric Cerenkov technique and gives a brief outline of its historical development. Details of the design and operation of the current Durham university V.H.E. γ-ray telescopes are given. The third chapter describes the standard analysis techniques used to search for pulsed and unpulsed emission.

The fourth chapter presents results of new observations of four isolated pulsars. Upper limits to the V.H.E. γ-ray flux are derived for each pulsar. A summary of the results is given and conclusions drawn regarding the consequences of the observations for the most popular pulsar model.

The fifth chapter deals with new analysis techniques that have been developed to test data for the presence of a signal which is not necessarily periodic. A number of different approaches is described. The results of these techniques when applied to simulated data are presented and conclusions are drawn regarding the relative effectiveness of the tests. The sixth chapter applies the most successful test to data from three objects. Upper limits to the flux from Centaurus A and SN1987a

are derived from our observations. Evidence for V.H.E. γ-ray emission from Scorpius X-1 is presented, together with evidence that this emission is modulated with the period of the binary orbit of this system.

The final chapter summarises the preceding results and conclusions and indicates areas where current research may lead to substantial improvements in telescope design and analysis techniques.

VERY HIGH ENERGY GAMMA RAYS

FROM ISOLATED PULSARS AND

NON-PULSATING OBJECTS

BY

Stephen Mark Rayner, BA

A thesis submitted to the University of Durham in accordance with the regulations for admittance to the degree of Doctor of Philosophy.

For Martin

VERY HIGH ENERGY γ-RAYS FROM ISOLATED PULSARS AND NON-PULSATING OBJECTS

Contents

The Durham University Mark III Telescope began operation in Narrabri, New South Wales, in October 1986. The author was involved in development of the online performance monitor used in this experiment. He was also one half of the two-person observing team for a total of 8 dark Moon periods. The author has been involved in the observation of all the objects studied in this thesis except PSR 0531+21.

The Mark IV telescope operated in La Palma from June to October 1988 and has been operating since June 1989. It is planned that it should continue until October 1989. The author was involved in the construction of the Mark IV in Durham before it was shipped to La Palma. He was also involved in the development of the Mark IV loggong software.

The author has been part of the team responsible for the routine pre-processing of data from both telescopes. In addition, he has been involved in much of the analysis of data from both telescopes, being largely responsible for the analysis of PSR 0531+21, PSR 1055-52, PSR 1509-58, and Scorpius X-1 and heavily involved in the latter stages of analysis of SN1987a.

The author wrote a number of programs based on curve fitting methods to search for unpulsed γ-ray emission. He wrote a program to simulate telescope data, which he then used to test the effectiveness of various different methods of searching for unpulsed signals. He also wrote the programs used in chapter 7 to show the effect of varying zenith angle on the two most common

methods of signal enhancement used by this research group.

None of the material contained in this thesis has been submitted previously for admittance to a degree in this or any other university.

CHAPTER 1

CELESTIAL γ-RAYS

1.1. Introduction

The γ-ray region of the electromagnetic spectrum runs from energies of 1 MeV upwards. There are several different methods used for detecting celestial γ-rays of various energies. For energies around 1 MeV, solid state detectors or scintillation counters are used in rockets, balloons or satellites. For energies from about 30 MeV to about 10 GeV, the most successful instrument is the spark chamber, in which high energy electrons produced by pair creation from the γ-ray primary are detected. These are carried in satellites and have proved very effective in such experiments as COS-B (Scarsi et al., 1977) and SAS-2 (Derdeyn et al., 1972). From around 100 GeV to around 100 TeV, the Atmospheric Cerenkov Technique has been the most successful method of detection. This will be discussed in detail in chapter 2. Above 100 TeV, the particles produced by the interactions of the γ-ray primary in the upper atmosphere survive to ground level and can be detected directly. Interest in the Astronomy of these energy ranges arose relatively recently.

Measurements of the flux of cosmic γ-rays were made in the early 1950s using balloons and rockets (Bergstrahl and Schroeder, 1951; Reiffel and Burgwald, 1954; Johnson et al., 1954) and an attempt was made by Jelley and Gold to observe the Crab Nebula (Jelley, 1987). However, the the first attempts at systematic

studies are generally thought to have started with a paper by Morrison (1958). Much experimental work was inspired by this. The first definite detection of celestial γ-rays was made by OSO-3 in 1967-1968 (Clark et al., 1968; Kraushaar et al., 1972). SAS-2 and COS-B mapped the Galaxy at energies above 50 MeV and studied point sources like the Crab pulsar (see for example, Fichtel et al., 1975; Pollock et al., 1985). In the energy range with which the current work is concerned (10^{11} - 10^{14} eV), the incident flux on a satellite proportional counter of area 1 m^2 would be about 10^{-4} min^{-1}, which would be too low for practical observations. In this region, therefore, ground-based techniques have proved more successful (see chapter 2).

1.2. Production Processes

1.2.1. Nuclear Interactions

Low energy γ-rays can be produced by the decay of radioactive nuclei or by the decay of π or κ mesons produced by the collision of high energy protons with nuclei.

e.g. $^{56}Co + e^- \longrightarrow {}^{56}Fe^* + \gamma \longrightarrow {}^{56}Fe + \gamma$
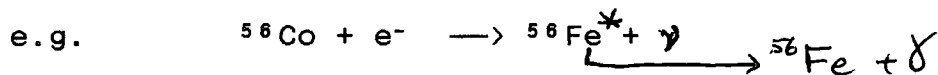
The Universe is old enough for effectively all primordial radioactive nuclei to have decayed. Most of the radioactive nuclei now present have their origin in supernova explosions. Thus, this kind of emission will be primarily associated with supernova remnants. Indeed, the γ-ray line from the above decay has been detected in SN1987a (see chapter 6). π and κ mesons are also produced by collisions between nucleons or nuclei at high energies

2

or by interactions of high energy nucleons with photons of the microwave background.

i.e.   p + p ——> π⁺ + n + p

or   p + γ(μ) ——> π⁺ + n
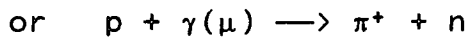
The former interaction will take place in regions containing high energy nucleons in the presence of large matter densities. This is typical of conditions in the immediate neighbourhood of a pulsar. The latter reaction will occur in interstellar space between cosmic ray protons and photons of the microwave background. The mesons produced in these reactions will decay with the production of γ-ray photons.

e.g.   π⁺ ——> e⁺ + ν + γ
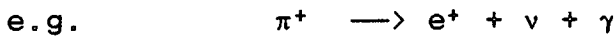
The typical energies of the γ-rays produced in these reactions range from ~1 MeV to ~100 MeV.

1.2.2. Particle Annihilation

An electron and a positron will annihilate on collision with production of ≥ 2 γ-ray photons.

e.g.   e⁺ + e⁻ ——> γ + γ
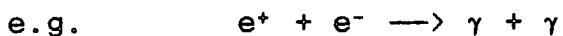
This interaction produces a characteristic sharp line at rest of 0.511 MeV. Positrons are produced in the decay of positively charged mesons. Thus, this interaction is found most commonly in sites of meson production, i.e. in the neighbourhood of pulsars producing beams of high energy electrons and protons. The galactic centre is also a source of this radiation (Barthelmy et al., 1989). Antinucleon production will occur under the same

3

conditions, but will be rarer due to the greater mass of the particle involved. Nucleons and antinucleons also annihilate with the production of mesons and γ-rays. The mesons then decay to produce more γ-rays as described above.

1.2.3. Charged Particle Acceleration in Electric or Magnetic Fields

Whenever a charged particle is accelerated, it will radiate electromagnetic waves at a rate given by

$$-\left[\frac{dE}{dt} \right] = \frac{e^2 |a|^2}{6\pi\varepsilon_o c^3} \qquad (1.1)$$

where E is the energy of the particle and a is the acceleration in the rest frame of the particle. This equation is subject only to the restriction that the particle does not lose a significant fraction of its total energy; a restriction that will generally be satisfied in the following discussion.

There are three main astrophysical processes in which this occurs: Bremsstrahlung, cyclotron and synchrotron radiation. Bremsstrahlung is produced when an electron is accelerated by the electric field of a nucleus or charged particle it passes close to (see fig. 1.1). The energy of the radiation depends on the amount by which the electron is deflected. As large deflections, implying very close approach to the nucleus in question, are much less common than smaller ones, most photons produced by this mechanism are in the lower region of the γ-ray spectrum. This process will

4
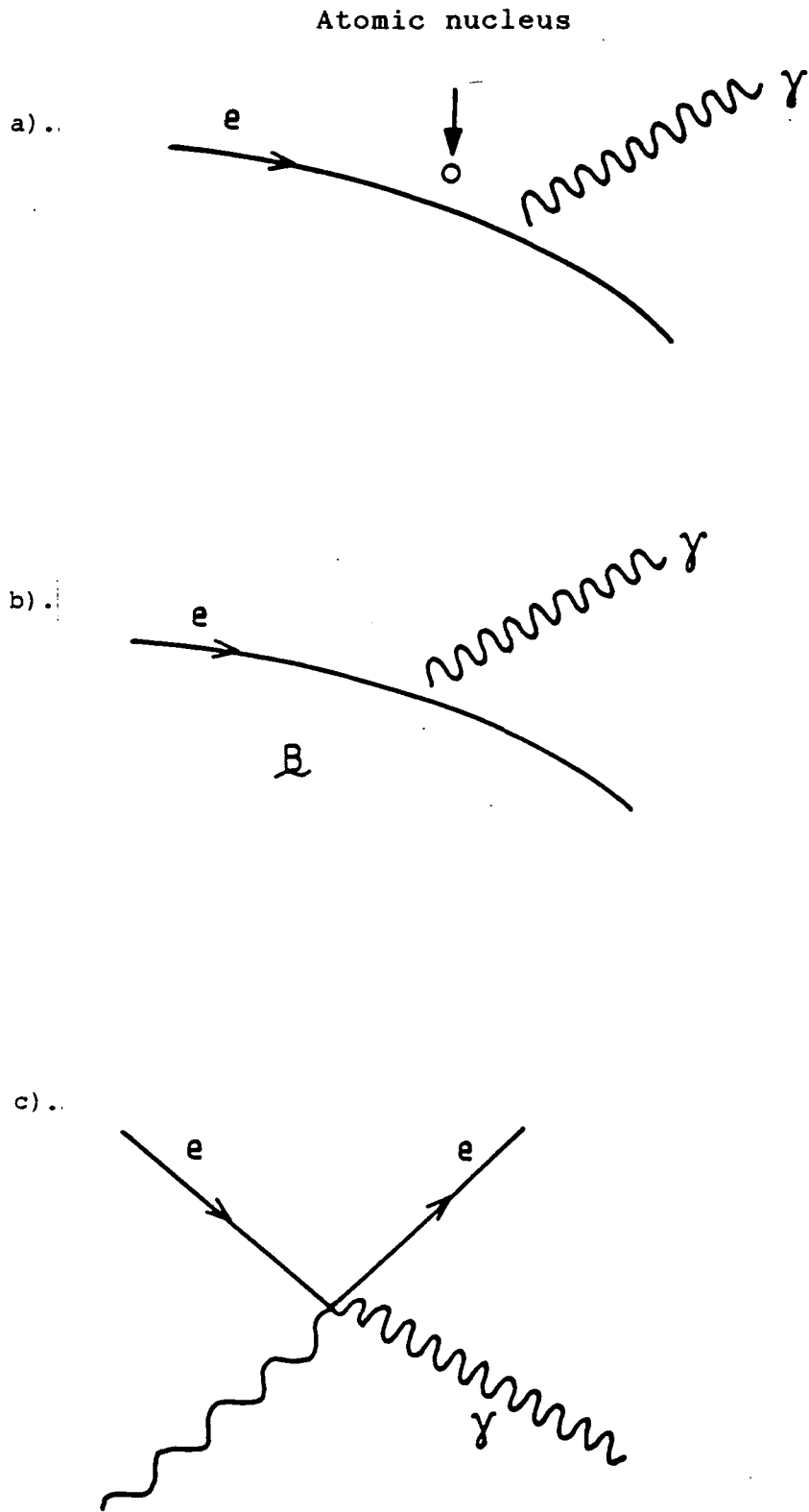
Figure 1.1 a)Bremsstrahlung emission, b)Synchrotron radiation and
c)The inverse Compton effect

produce high γ-ray fluxes only in areas of high matter density. When an electron travels through a magnetic field, B, at an angle θ to it, it undergoes an acceleration, a, given by

$$a = (e/m) \ v \cdot B / \gamma \qquad (1.2)$$

where γ is the usual relativistic factor, $(1-v^2/c^2)^{-1/2}$. Cyclotron radiation is produced when non-relativistic electrons are accelerated by magnetic fields (see fig. 1.1). The energy of the photons produced is many orders of magnitude below that of the original electron, so this will rarely produce γ-ray photons. Synchrotron radiation is produced by the same process occurring with relativistic electrons, i.e. when γ can not be approximated to 1. This can produce γ-rays, but will rarely produce V.H.E. γ-rays.

1.2.4. Inverse Compton Effect

When a low energy photon collides with a relativistic particle, energy is transferred from the particle to the photon (see fig. 1.1). The process is essentially the same as Compton scattering, where a photon is scattered off an electron, except for the direction of energy transfer. The phenomenon requires only the simultaneous presence of low energy photons and relativistic particles. This is a condition that is satisfied in the region of many pulsars, where large fluxes of relativistic particles are produced in the presence of a strong magnetic field. The synchrotron photons thus produced (see section 1.2.3) will then undergo inverse Compton scattering with the particles to produce

γ-rays. If the initial particle energy is sufficiently high, V.H.E. γ-ray photons can be produced. Hence, this may be an important method of production of cosmic V.H.E. γ-rays.

1.3. Absorption Processes

Interactions of V.H.E. γ-rays with the matter of the interstellar medium do not cause appreciable attenuation, due to the low interaction cross-section and low matter density involved. The radiation length for a typical photon is about 25 gcm^{-2}, whereas the column density for typical intragalactic distance of 10 kpc is about 0.05 gcm^{-2}. Much more important are photon-photon interactions. This is essentially the reverse of the electron-positron annihilation interaction. In this case, two photons interact to form an electron-positron pair.

i.e. $\gamma + \gamma \longrightarrow e^+ + e^-$

The reaction can only take place if the total energy of the photons in the zero momentum frame, E, is large enough to provide the mass of the particles produced.

i.e. $E \geq 2m_e c^2$ (1.3)

Interactions of this kind with the microwave background severely attenuate 10^{13} eV γ-rays over intergalactic distances. The other possible source of absorption is by magnetic fields. This is actually the same interaction as above, except that the γ-ray interacts with a virtual photon of the magnetic field. This is only important in regions of very intense ($\sim 10^8$ Gauss) field. Fields of this strength are only found near the surface of neutron

6

stars. This constrains the production region of a neutron star emitting V.H.E. γ-rays to be away from the star's surface.

1.4. Source Candidates

The above details must be borne in mind when deciding which objects to observe. Candidate sources must clearly be objects or regions where high energy processes are taking place. The most suitable objects under this criterion are quasars, active galaxies, pulsars and X-ray binaries. Quasars are unlikely to produce a detectable flux of V.H.E. γ-rays above 10^{14} eV, as attenuation by the microwave background over the very great distance to even the nearest quasar would be far too great. Similarly, most active galaxies would be too far away, the only likely exception being Centaurus-A, which is the closest at ~5 Mpc away. Galactic X-ray binaries are good candidates, since observation of synchrotron radiation from many of them indicates the production of high energy particles. They are also close enough that attenuation will not seriously affect the observed flux. Indeed, X-ray binaries are the most common source of V.H.E. γ-rays so far detected. Isolated pulsars are also promising candidates for V.H.E. γ-ray emission. They are to be found within the galaxy and therefore satisfy the distance criterion. Synchrotron radiation has also been observed from such candidates as the Crab (see section 4.2.1), indicating the presence of relativistic particles. These last two classes of object, then, are the principal targets of the V.H.E. γ-ray observer. Clearly,

7

any object detected in X-rays, Low Energy or Ultra High Energy γ-rays will be of considerable interest.

CHAPTER 2

THE ATMOSPHERIC CERENKOV TECHNIQUE

2.1. Introduction

The detection of V.H.E. γ-rays using the atmospheric Cerenkov technique relies on detecting Cerenkov light from cascades of high energy particles in the upper atmosphere produced by a cosmic V.H.E. photon. The technique has many advantages over alternatives like satellite detection. Being ground-based, it is much cheaper than a satellite. Also, typical fluxes of V.H.E. γ-rays are of the order of $10^{-10} cm^{-2} s^{-1}$, so a spark chamber capable of detecting them in a practical amount of time would be too large to be carried on a satellite. The effective collecting area of any Cerenkov detector, however, is the area of the pool of Cerenkov light on the ground, which is $\sim 10^4$ m^2 (Hillas and Patterson, 1987). Other ground-based detection techniques are not very effective up to 10^{13} eV, as the cascade particles do not reach the ground.

2.2 Cerenkov Radiation

2.2.1 Conditions for the Production of Cerenkov Radiation

When a charged particle moves through a medium, it induces charge polarisations on the atoms as it passes. Ordinarily, these

atoms return to the ground state randomly to give off radiation which interferes destructively and is therefore not seen. If, however, the particle is travelling faster than the phase velocity of light in that medium, there exists a direction in which this polarisation interferes constructively and is therefore observable. A Huygens construction illustrates this well (see fig 2.1). This radiation is known as Cerenkov radiation, after P. A. Cerenkov (1934, 1937), who did some of the first experimental work on the effect. It has recently come to light that the effect had been predicted in surprising detail 46 years earlier by Oliver Heaviside. In a fascinating paper, which first appeared in 'The Electrician' and was reprinted in a collection of his electrical papers (1892), he describes the effect and gives the correct relations for the 'Cerenkov' condition and 'Cerenkov' angle in terms of classical electrodynamics. Indeed, there could be a good case for referring to the effect as 'Heaviside-Cerenkov' radiation. The first modern theoretical treatment was given by Frank and Tamm (1937). The condition for the production of this radiation is

$$v > c/n \qquad\qquad (2.1)$$

where v is the speed of the particle; c is the speed of light in vacuum; and n is the refractive index of the medium. This is known as the Cerenkov condition. The Cerenkov angle θ between the radiation and the path of the particle is given by:

$$\cos\theta = \frac{c}{v * n} \qquad \text{(see fig 2.1)} \qquad (2.2)$$
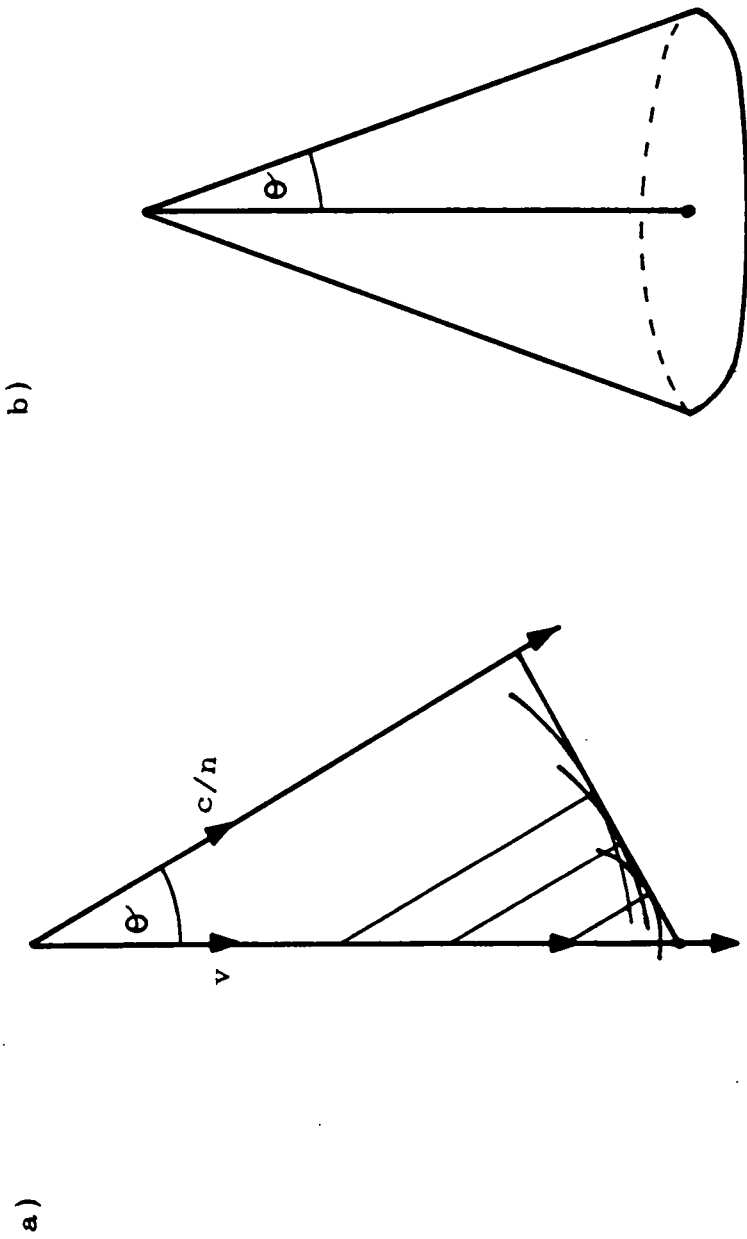
Figure.2.1 a)Huygens construction for Cerenkov radiation, showing
the Cerenkov angle and b)the formation of the Cerenkov light cone

Clearly, condition (2.1) cannot be satisfied if n < 1, so Cerenkov radiation can only be seen in the ultra-violet, visible, infra-red and microwave regions, since the refractive index is less than 1 outside this region of the spectrum.

2.2.2. Cerenkov Radiation from Air Showers

The first suggestion that Cerenkov light should be emitted in the atmosphere by cosmic ray particles was made by Blackett (1948). He calculated that Cerenkov radiation from cosmic ray primaries should account for 10^{-4} of the light from the night sky. Galbraith and Jelley (1953) later suggested that strong pulses of Cerenkov light should be observable from extensive air showers initiated by cosmic ray particles or photons, since these contain many particles satisfying the Cerenkov condition. The condition is most easily satisfied for particles of a given energy by those with the lowest mass. Hence it is the behaviour of the electrons and positrons in a shower that largely determine its Cerenkov emission. The Cerenkov condition implies an energy threshold for particles of a given mass:

i.e. $E = mc^2 / \sqrt{(1 - v^2/c^2)}$ (2.3)

$\Rightarrow E_{threshold} = mc^2 / \sqrt{(1 - 1/n^2)}$ (2.4)

This varies with n and therefore with altitude. For electrons at sea level, E = 21 MeV. Around 85 % of shower electrons at shower maximum have E > 21 MeV, whilst 36 % have E > 50 MeV (Richards and Nordheim, 1949). The angle of spread of the shower

11

particles is in general greater than the Cerenkov angle, so the Cerenkov light pool intensity profile at the ground is governed directly by the distribution of particles in the shower. Detailed computer simulations by Macrae (1985) suggest that the radius of a typical effective light pool is between 45 and 110 m, depending on the altitude of observation and the altitude at which the shower was initiated. Cerenkov pulses from these showers take less than 10 ns to pass an observer.

2.3. Outline of Experimental Techniques

The fundamental requirements for detection of Cerenkov light flashes are a photo-multiplier tube (PMT) at the focus of a flux collector (usually a mirror or array of mirrors with a common focus). Since typical Cerenkov pulses from air showers last <10 ns, fast response from the tube (~5 ns) is essential to prevent the pulse being 'smeared' in time and thus not firing the voltage discriminator. This will maintain good signal to noise ratios. Fast recording electronics are also important to reduce the system dead time and thus maximise the count rate. A single PMT would have to be run at very low gain to prevent any signal being swamped by electronic noise caused by general sky brightness. To increase the possible gain and thus sensitivity, it is necessary to operate 2 or more PMT/flux collector arrangements in fast coincidence, accepting only pulses triggering all tubes within a 10 ns gate. If this is done, most recorded events will be Cerenkov light flashes. The rate of 'accidental' coincidences can

be calculated quite easily (see section 2.4.1). The major problem is then to discriminate between photon-initiated and the much more common nucleon-initiated showers. Charged cosmic ray particles are deflected by interstellar electric and magnetic fields and carry no directional information when they arrive at Earth. Hence they form an isotropic background that is typically ~100 times that of the γ-ray signal. To maximise signal to noise ratio, therefore, it is necessary to reject events caused by these particles as efficiently as possible. Much effort has been made in the design of hardware and analysis techniques to combat this problem (see sections 2.4, 2.5 and chapters 3 and 5).

2.3.1. Historical note

The first use of the atmospheric Cerenkov technique for Astronomy was by Jelley and Gold in 1954 (Jelley, 1987). A mirror and phototube were mounted on a 6 inch refractor and used to observe the Crab with negative results. A detector was constructed in the Crimea in 1961 (Chudakov et al., 1962). This made scans across Cygnus A, Cassiopeia A, the Crab Nebula and Virgo A. Results were negative, but the feasibility of the method was demonstrated. In 1964, a group from University College Dublin started observations (Jelley and Porter, 1963). In 1970, the group moved to Malta. Also in 1972, Grindlay et al. (1975b) started observations at Narrabri, New South Wales and a V.H.E. γ-ray observatory was established at Mount Hopkins, Arizona, which was later named the Fred Whipple Observatory. In 1977 a Cerenkov

Location	Period of Observation	Energy Threshold (GeV)
Narrabri, NSW	1972-1974	200
Crimea	1960-64,1969-77, 1986-	5000,2000, 1000
Glencullen, Eire	1964-1970	2000
Malta	1970	2000
Mount Haleakala, Hawaii	1986-	500
Mount Hopkins, Arizona	1970-	300
Potchefstroom, RSA	1986-	1000
Ootacamund, India	1976	500
Gulmarg, India	1985-	1000
Pachmari, India	1987-	500
Dugway, Utah (Durham Mark I, II)	1981-1984	1000
Narrabri, NSW (Durham Mark III)	1986-	250
La Palma (Durham Mark IV)	June-October 1988, 1989	400

Table 2.1 V.H.E. γ-Ray Telescopes

detector was commissioned at Ootacamund, India. At the Dugway proving grounds in Utah, the Durham group operated an array of 4 spaced telescopes, referred to as the Mark I and Mark II, from 1981 until 1984. More recently, the Crimean group have been operating an array of 4 detectors at high altitude. A group from the University of Potchefstroom in the Republic of South Africa has operated a system of telescopes similar to the Mark II (Raubenheimer et al., 1986). Cerenkov detectors have also recently started operation at Mount Haleakala in Hawaii and in Gulmarg and Pachmari in India. A summary of the various V.H.E. γ-ray telescopes is given in table 2.1. In many cases, the telescopes were modified during their lifetimes. The energy threshold given, therefore, is the latest one and is not necessarily correct for the entire period of operation. The Durham group began observations in October 1986 with a new telescope, the Mark III, at Narrabri, New South Wales. The group has also deployed a Mark IV telescope on La Palma for the Summer of 1988 and, at time of writing, is reconstructing the instrument for the Summer 1989 observing season. For further details about the design and construction of these instruments, see sections 2.4 and 2.5.

2.4. The Mark III Telescope

In this section, the design and construction of the Mark III telescope will be described. Only those aspects which are necessary for the reader's understanding of the immediate work or

were the work of the author will be dealt with. For further details, see Chadwick (1987) or Brazier et al. (1989a)

2.4.1. Mechanics

The telescope is supported on an Alt-Azimuth mount constructed from a surplus gun mount. The weight of the telescope is taken by a single thrust bearing, allowing azimuth motion. Zenith motion is allowed by two smaller trunnion bearings. The steering is computer-controlled, making it relatively straightforward to drive the telescope separately in zenith and azimuth, as required by the Alt-Azimuth mount. The shaft encoders give the telescope position to 0.09°. The telescope consists of 3 large dishes. Each dish comprises 40 spherical mirrors with a common focus, having a reflective area of 11.4 m² per dish. Mirrors are arranged on each dish in 7 hexagons (see fig. 2.2). The framework holding them is made from Aluminium, which is light, strong and easily shaped. Each mirror is mounted on three adjustable studs for individual alignment. The mirrors are made with high reflectivity anodised aluminium sheet as the reflecting surface and 2 mm aluminium sheet as the backing plate. The space between reflective and backing surfaces is filled with crushed aluminium honeycomb. For details of mirror construction, see Chadwick (1987). The mirror surfaces are about 80% reflective (Weekes, private communication). There are two types; one with a focal length of 240 ± 8 cm; and one with a focal length of 260 ± 8 cm. The shorter focal length mirrors are mounted at the centre
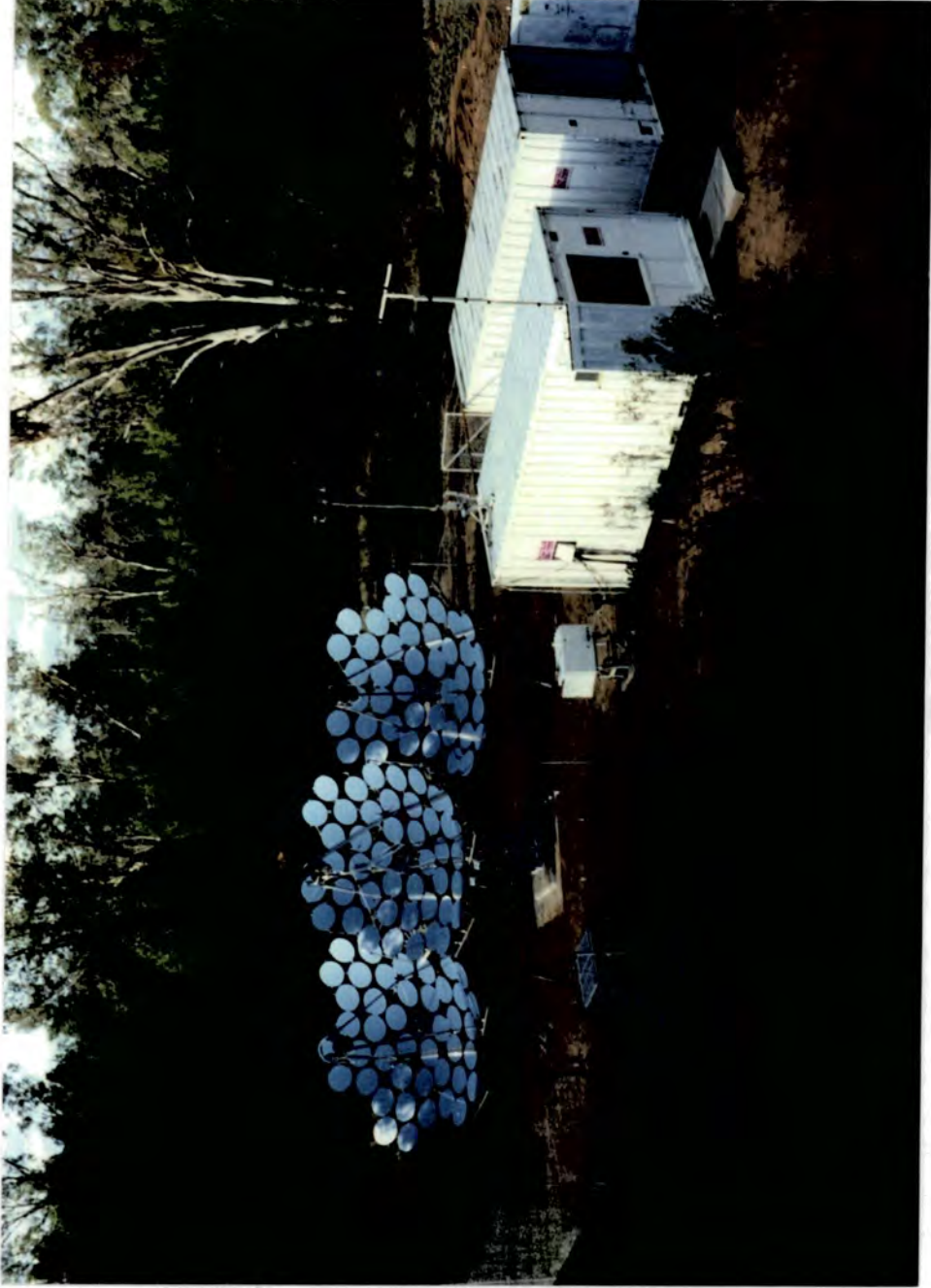
Figure 2.2 Photograph of the Mark III telescope in Narrabri, New South Wales

of the dish to improve image quality, although this is not of paramount importance in atmospheric Cerenkov work. Indeed, a very sharp image would cause problems since the variation in brightness at the photocathode between dark sky and a well-focussed bright star would be greater than could be compensated for by the AGC system (see section 2.4.2). Also, the intensity at the photocathode produced by a sharp image of a bright star might cause damage to the photocathode itself.

A matrix of seven tubes, consisting of a central tube surrounded by six outer ones (see fig. 2.3) is mounted at the focus of each dish. In the tracking mode of operation, the central tube tracks the source, while the others provide off-axis monitoring to allow rejection of nucleon-induced events. In the chopping mode, the telescope moves in azimuth every two minutes such that the central tube and the tube at the same zenith angle are pointing at the source alternately (see chapter 3).

2.4.2. Electronics

For a schematic diagram of the Mark III electronics, see figure 2.4. The phototubes used with the Mark III are RCA 8575's. They were chosen for stability of gain and low noise characteristic. The tubes are operated in 3-fold coincidence, i.e. to record an event, 3 paraxial tubes from the three matrices must trigger within 10 ns of each other. For example, if an on-axis event is to be recorded, the central tube on each dish must record a flash within a 10 ns period. The reason for this is to

DETECTOR
PACKAGE

SINGLE
PMT

BLACKENED
PERSPEX
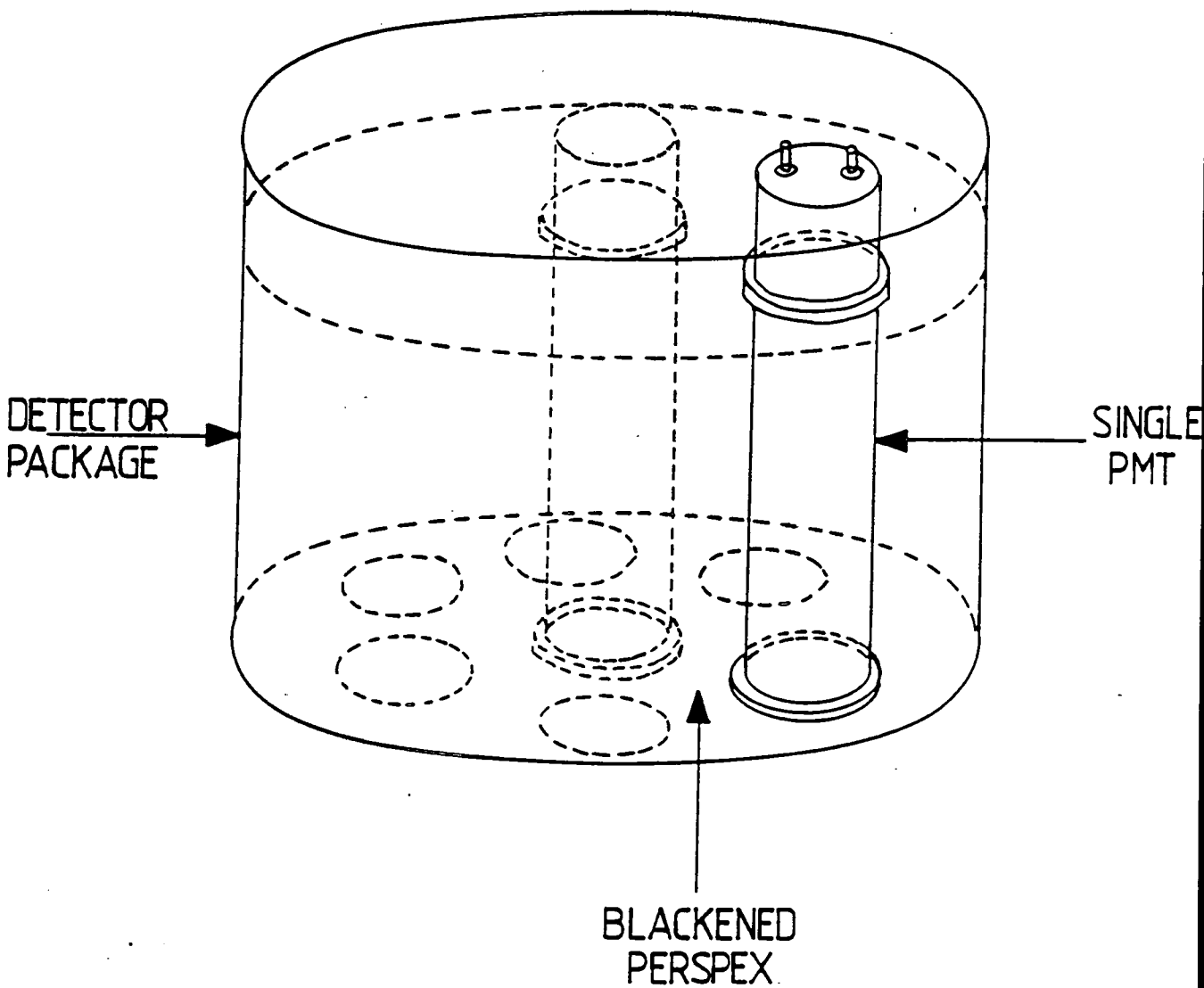
Figure 2.3 Diagram of the detector package used with both the
Mark III and Mark IV telescopes
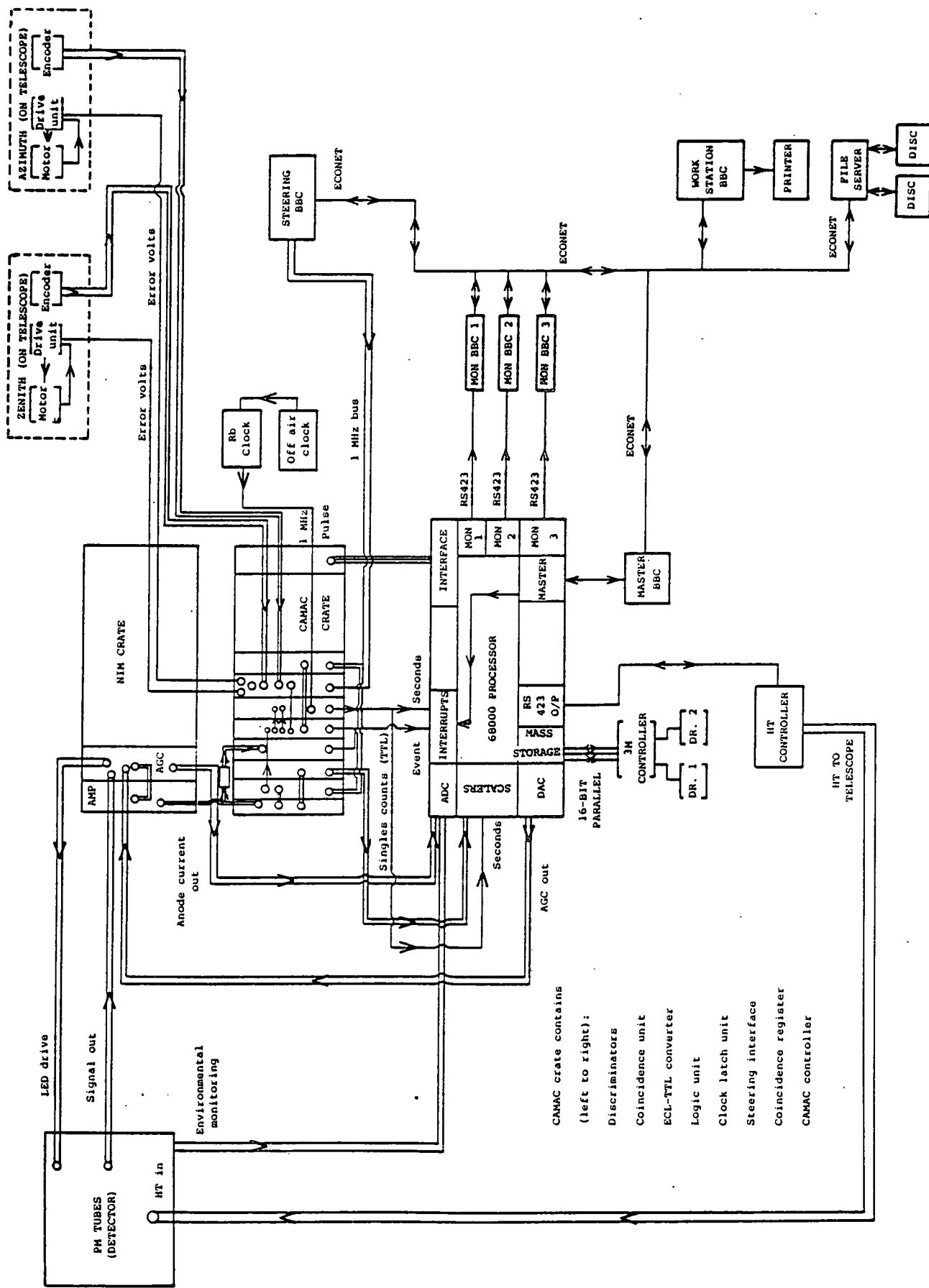
Figure 2.4 Schematic diagram of the Mark III control/logging system

ensure that only broad pulses of light cause events, rather than stray individual photons from such objects as stars. If each tube is individually registering n counts s⁻¹ (known as the 'singlefold' rate), then the rate at which coincidences will occur by chance is given by

$$R = C! * n^C * T^{(C-1)}$$

where C is the number of tubes from which coincidence is required and T is the coincidence resolution of the system, about 3.5 ns. Under typical operating conditions, each tube counts at a rate of ≤ 30 kHz, giving an 'accidental' rate of ≤ 6 per hour. A set of 3 corresponding PMTs constitutes a 'channel'. Each channel covers ~1.5° (Full Width Half Max.) of the sky, with channels 2-7 arranged symmetrically around channel 1, the centre channel. The PMTs are supplied with high voltage by a LeCroy HT unit, which communicates with the 'console' BBC (see fig. 2.4). Keeping PMT gain constant is vital, especially when using the telescope in chopping mode. The system used to achieve this is known as the Automatic Gain Control, or AGC. Each PMT contains a light emitting diode driven by a negative feedback circuit coupled to the PMT's anode current. This maintains constant anode current and thus PMT gain, despite varying sky brightness.

The PMTs produce 21 analogue signals, which are DC-coupled to the AGC unit before being passed to an amplifier (see fig. 2.4). The amplifier produces two outputs. One is sent to a charge to time converter (QT unit) which digitises the charge from the preceding 30 ns on the PMT's. The output from this unit is stored in scalers until needed by the 68000 (see section 2.4.3). The

18

other output from the amplifier is sent to the discriminator. The discriminator level is variable and is set by the 68000 at the beginning of an observation. The threshold used in all Mark III observations to date is 50 mV. Pulses greater than 50 mV cause output to be passed to the ECL to TTL converter. It then goes to the coincidence unit and scalers. There are 7 coincidence units; one for each channel. Pulses from all three PMTs in a channel are tested for overlap with a gate width of ~10 ns. If sufficient overlap occurs, an event is registered and the logic unit accessed. In fact, events can only be initiated in channels 1 to 4, since channels 5 to 7 were added some time after construction. Events not including channel 1 or channel 3 (for chopping mode) are useful only for performance monitoring and channels 2, 3 and 4 are sufficient for this purpose. More than 1 channel can fire from a single Cerenkov flash, so events from each unit are passed to the coincidence register which records which channels fired for a given event. This information is known as the "fire pattern" of the event.

The logic unit determines whether an event has occurred during the system dead time, i.e. when the system was busy handling a previous event. This interval has been measured to be ~350 μs (Brazier et al.,1989a). If an event has occurred, then the time is recorded, but no other information, and stored in a CAMAC 'first in first out' buffer with a capacity for 16 dead time events. When a normal event occurs, the logic unit latches the steering and CAMAC clock and accesses the coincidence register. It also interrupts the 68000 computer. When the 68000 has

finished handling the event (see section 2.4.3), it resets the logic unit, which then begins its cycle again.

2.4.3. The 68000

The core of the data logging system of the Mark III is a Motorola 68000 based micro-computer running a program written by the Durham University microprocessor centre. When the logic unit interrupts the 68000, previous operations are latched until the data logging routine has been completed. Information is read in the following order: all 21 QT's; the anode currents of all on-axis PMT's; the latched event time; the position and drive status of the telescope; and the fire pattern of the event. The information is formatted and stored in RAM until the tape drive is 'available' as defined by the tape drive controller. All events are recorded on tape via a 16-bit parallel interface. Every minute, the 68000 interrogates various devices for information on steering, PMT voltages, singlefold PMT rates and anode currents and stores the information in RAM for writing to tape, tagged as a 'housekeeping' block.

2.4.4. Timekeeping

For timing millisecond pulsars and pulsars with very accurate ephemerides, it is necessary to have a very accurate timing standard. The Mark III and Mark IV telescopes use a highly accurate Rubidium oscillator for this purpose. The oscillator is

checked regularly against an off-air signal, from VNG Lyndhurst, RAN Jervis Bay, or VNG Epping at various stages in the life of the experiment. During the period of operation of the telescope, VNG transmissions were discontinued for some months and later resumed, transmitting from a different place with different equipment. The RAN signal which had been broadcast in between the two periods of VNG emission was then discontinued. Hence the variety of signals used for checking the clock. Figures 2.5, 2.6 and 2.7 show the results of these checks. It can be seen that the clock drifted by about 1 ms month^{-1} from its initial synchronisation in October 1986 with respect to the various radio signals used. The radio signal is received after reflection off the ionosphere, so the measured delay is subject to diurnal and seasonal fluctuations in atmospheric conditions. The height of the ionosphere and its radio reflectivity vary over the course of a day due to the passage of the Sun and over the course of several days due to variations in weather conditions (see fig. 2.8). During the period when the off-air signal came from VNG Lyndhurst, it was possible to receive the signal on 4.5 or 7.5 MHz. The higher frequency was easier to receive during the day, whilst the lower was easier to receive at night. Hence, only 3 nearly simultaneous measurements were made. These are given in table 2.2. The 7.5 MHz delays are all higher than the corresponding 4.5 ones, though the long-term difference is impossible to quantify due to the uncertainties introduced by the systematic time-dependent variations mentioned above. The result of this is that for clock calibration purposes, one frequency
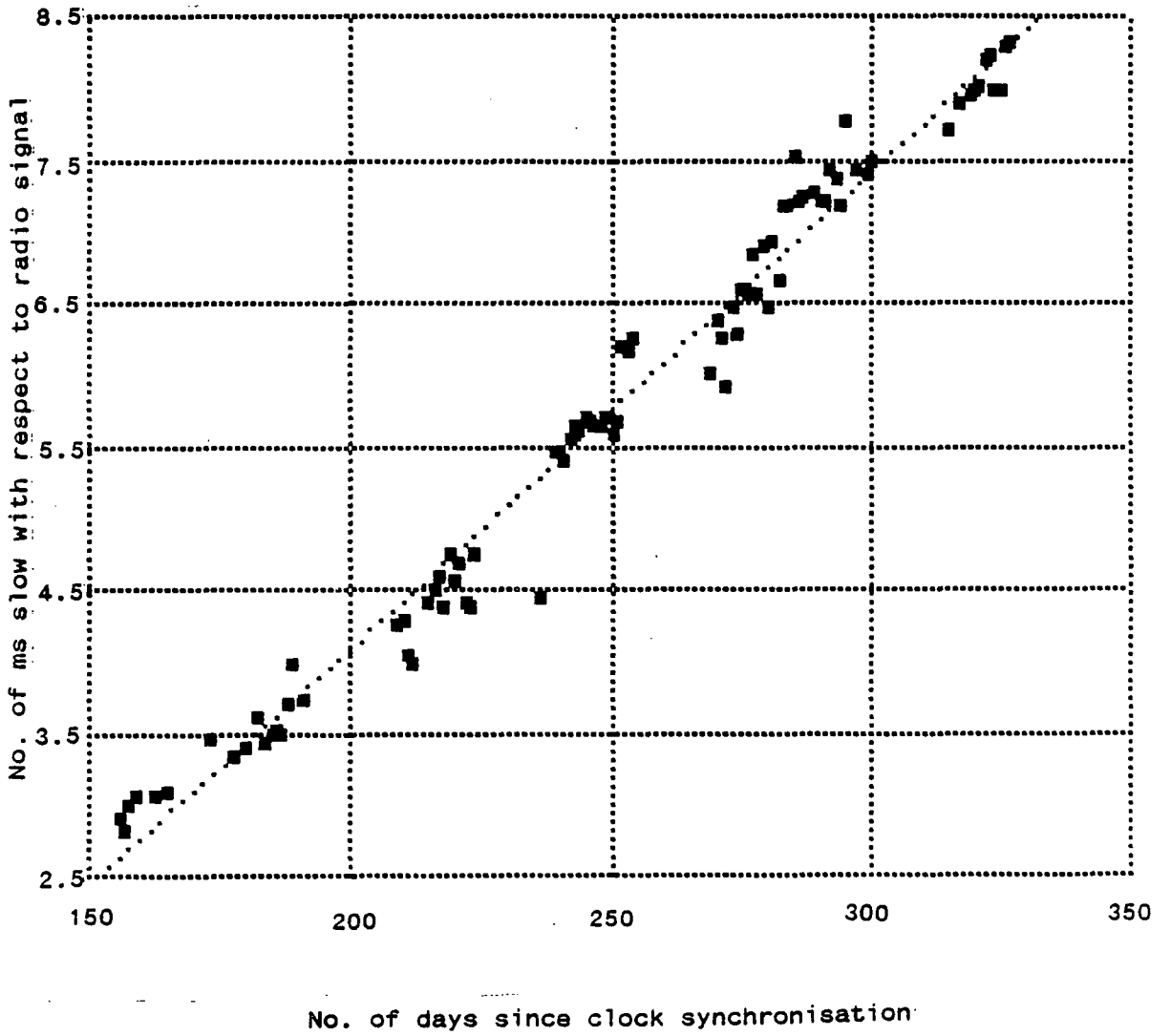
Figure 2.5 Graph of clock delay against time for VNG Lyndhurst
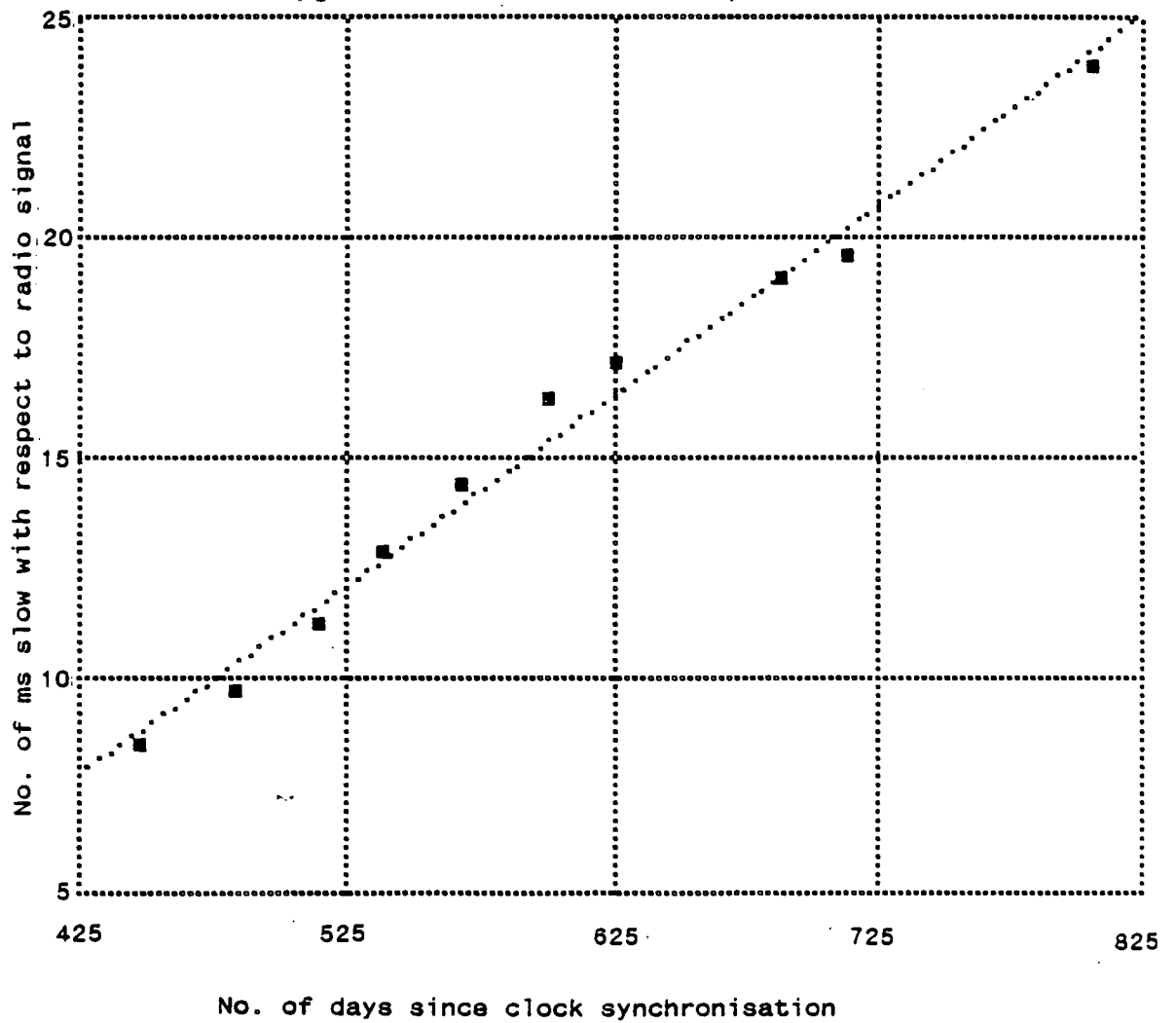
Figure 2.6 Graph of clock delay against time for RAN
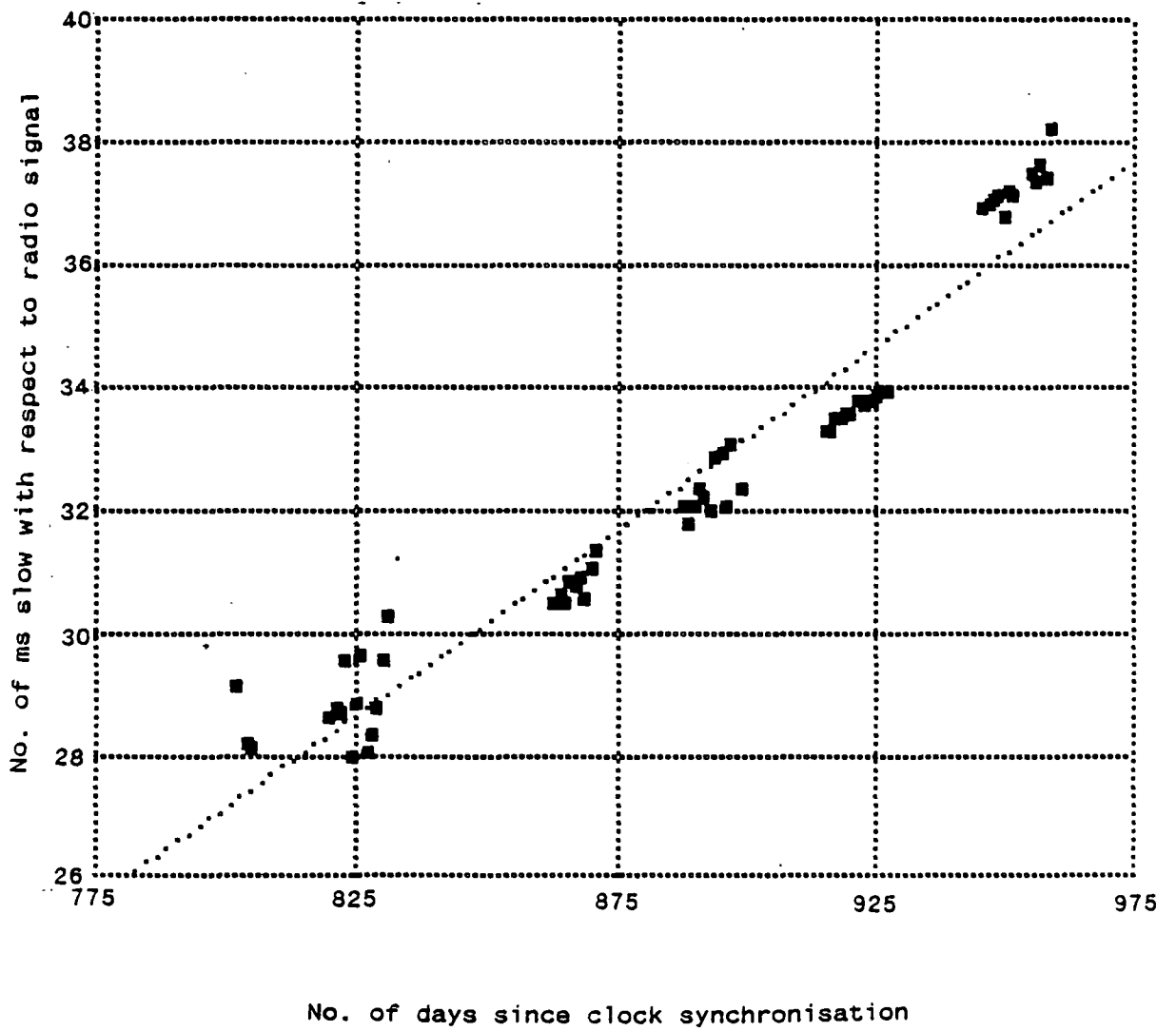
Figure 2.7 Graph of clock delay against time for VNG Epping
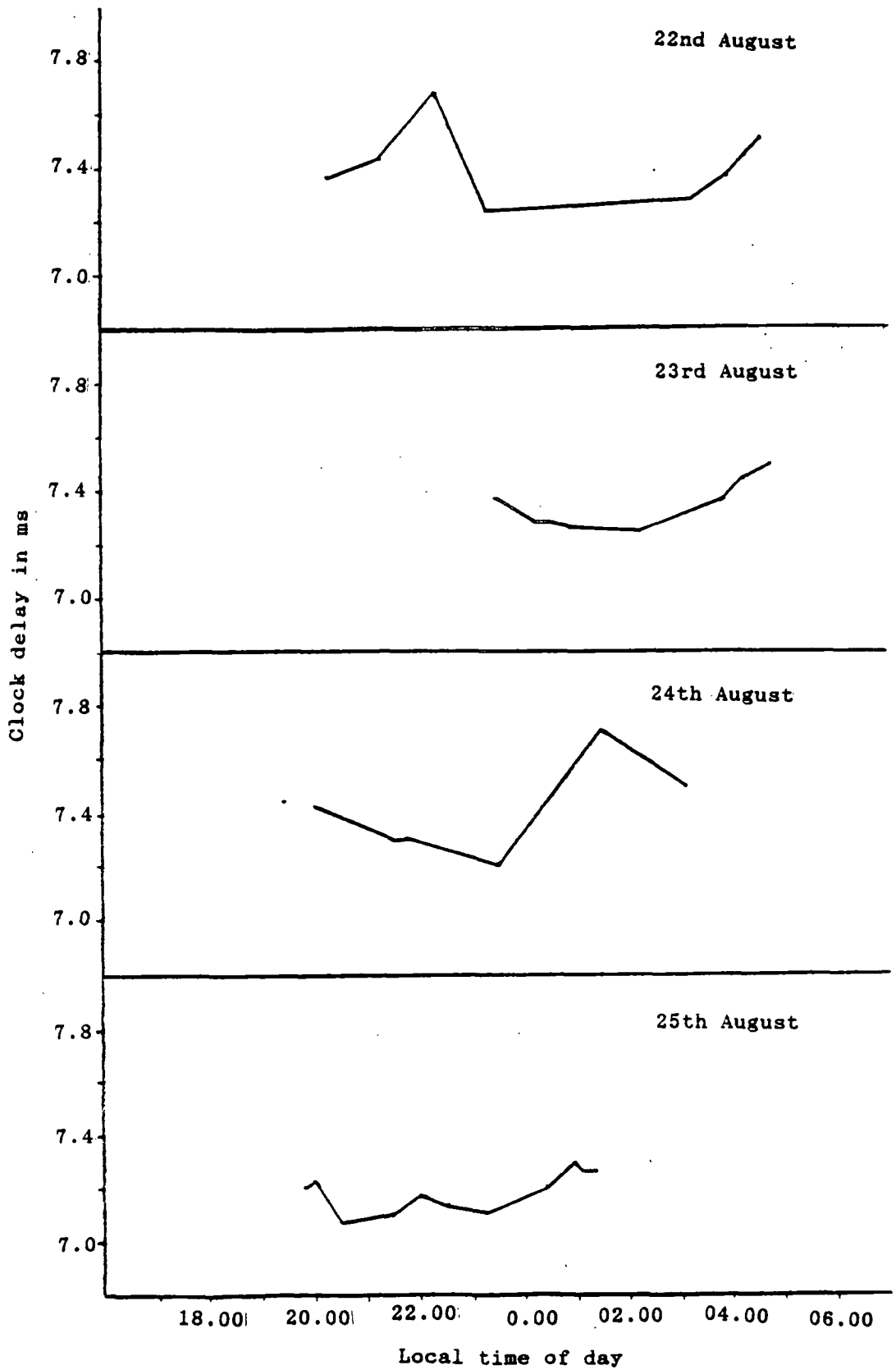
Figure 2.8 Graph of clock delay readings against time of day. All
clock delays are measured relative to 4.5 MHz VNG Epping accurate
to 0.01 ms

Date	Time (UT)	Clock Delay/ms	
		4.5MHz	7.5MHz
24-07-87	10.35	6.42 ± 0.01	6.74 ± 0.01
26-07-87	10.35	6.74 ± 0.01	6.94 ± 0.01
29-07-87	11.30	6.56 ± 0.01	6.96 ± 0.01

Table 2.2 Near-Simultaneous Clock Delay Measurements

should be used consistently. The data points used in fig. 2.5 therefore use only 4.5 MHz and are taken from the period 5 pm to 7 pm local time to reduce the effects of diurnal variation. From figs. 2.5 to 2.7 the clock slip rate is measured to be 1.166 ± 0.014 ms month^{-1}. This is due to errors in the initial frequency setting. There is probably a small quadratic term in the slip rate due to the drift in oscillator frequency, but consistent measurements have not been taken over a long enough timescale to show this yet.

2.4.5. Performance and Environment Monitoring

Control and monitoring of the telescope is achieved using a local area network, or 'Econet' of BBC micro-computers (see fig. 2.4). Information about telescope performance is displayed on various monitor BBC's. Monitor 1 shows the PMT singlefold rates. Monitor 2 displays the PMT anode currents. Both monitors have visual alarms if the readings get too high. Monitor 3 shows the wind speed and direction, the event rate for each channel, the external ambient temperature and humidity and the temperature of the centre dish bullet. An audible alarm sounds if the telescope has not steered in the last two minutes. A message is displayed if the mirror temperature falls below the dew point calculated from the ambient temperature and humidity. This warns the observers that the mirrors may be about to mist over. Misting has a deleterious effect on the count rate. However the problem can be solved or prevented by spraying the mirrors with a surfactant

liquid. This can be done in about 10 minutes in the middle of a run and restores count rates to near normal. Each treatment is effective for about 6 hours, so if misting is anticipated, the mirrors can be sprayed before the start of an observation to prevent any loss of counts. Monitors 1 and 2 are updated every second. Monitor 3 is updated only every 3 seconds, due to the extra complexity of its display. The weather information from monitor 3 is written to a file via the local area network every minute. This data from this file can then be displayed graphically after the observation and the graph printed for inclusion in the observers log (see fig. 2.9).

During an observation the values of all the anode currents, singlefold rates and 3-fold events displayed by monitors 1, 2 and 3 are written down about every half an hour. This record, along with a half-hourly report on the weather and any observations or actions from the observers are inserted in a file called the observers' log. The file is vital in assessing the quality of any given observation.

In addition to the monitors mentioned above, an online telescope performance monitoring program runs on another BBC micro. Each event causes an interrupt at its userport. The program reads the fire pattern and increments registers corresponding to channels 1 to 4. At the end of each minute, the graphical display is updated to show the event rate for each of these channels averaged over the preceding 3 minutes. This display allows the observers to spot long-term trends, such as icing or misting and take appropriate action. An alarm sounds if
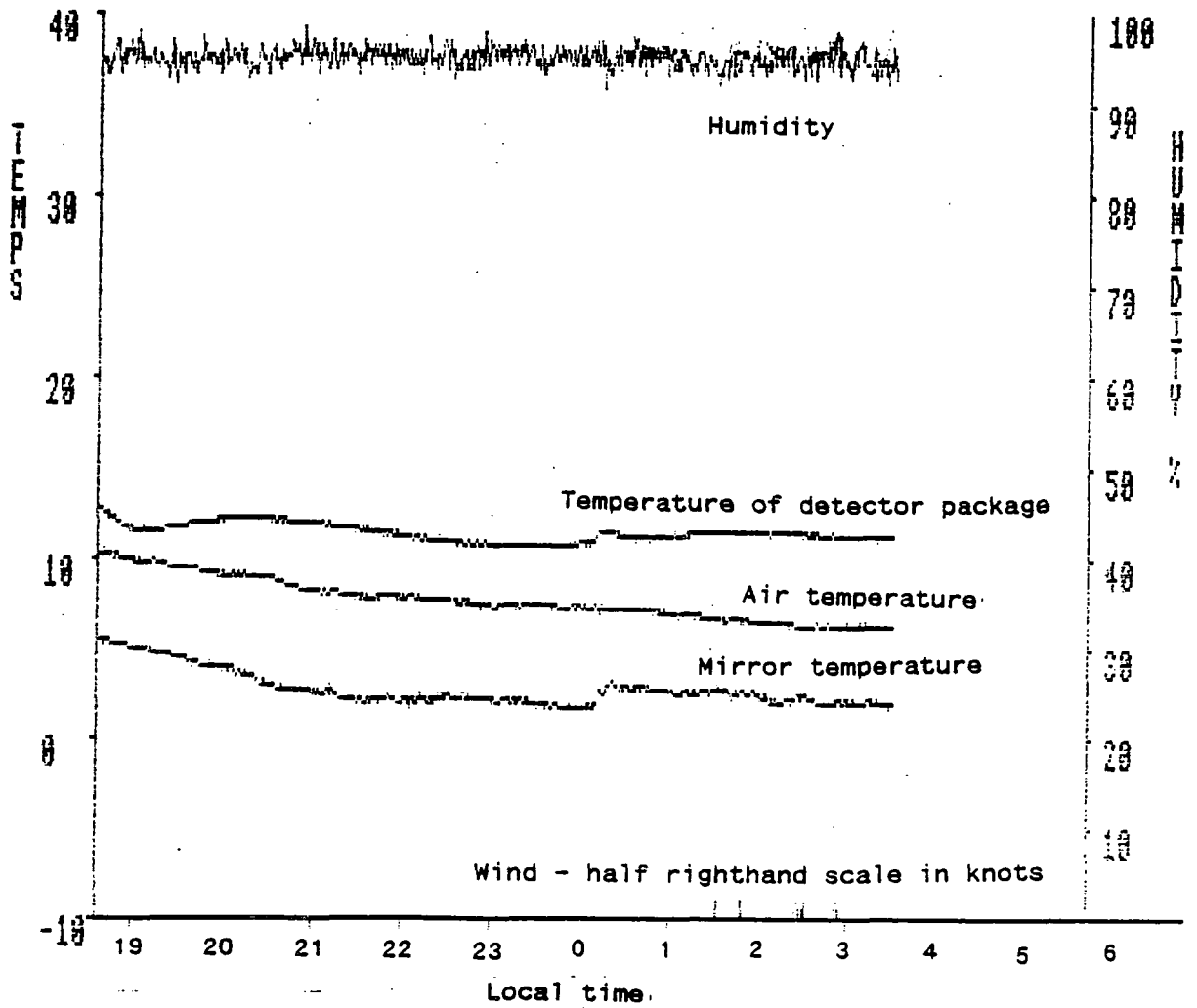
Figure 2.9   The weather file output for the 9th of July 1988

no event has been received for a period preset by the observer at the beginning of the observation. At the end of the night, the display is saved and printed out later for inclusion in the observers' log. This display, along with the information from the monitor 3 file give a clear impression of how good the observing conditions were for the observation in question. This is illustrated in figs 2.10 and 2.11. It is clear that the night of 09/07/88 was good and the data are suitable for analysis, assuming the log does not reveal any problems with the equipment, whereas the night of 28/06/87 was poor and the data should not be analysed.

2.5. The Mark IV Telescope

The Mark IV design is very similar to that of the Mark III. The mount is similar and the steering is identical. The dishes are smaller with an area of 5.1 m^2 each. The framework can thus be lighter with fewer mirrors to support. The QT unit has lower resolution than that of the Mark III (3 bits as opposed to 8). The high voltage for the PMTs is supplied by NIM units which are adjusted manually. The logging operation is overseen by a BBC micro, which writes data to a hard disc storage unit. The dead time of this system is ~1 ms (Dipper, private communication).
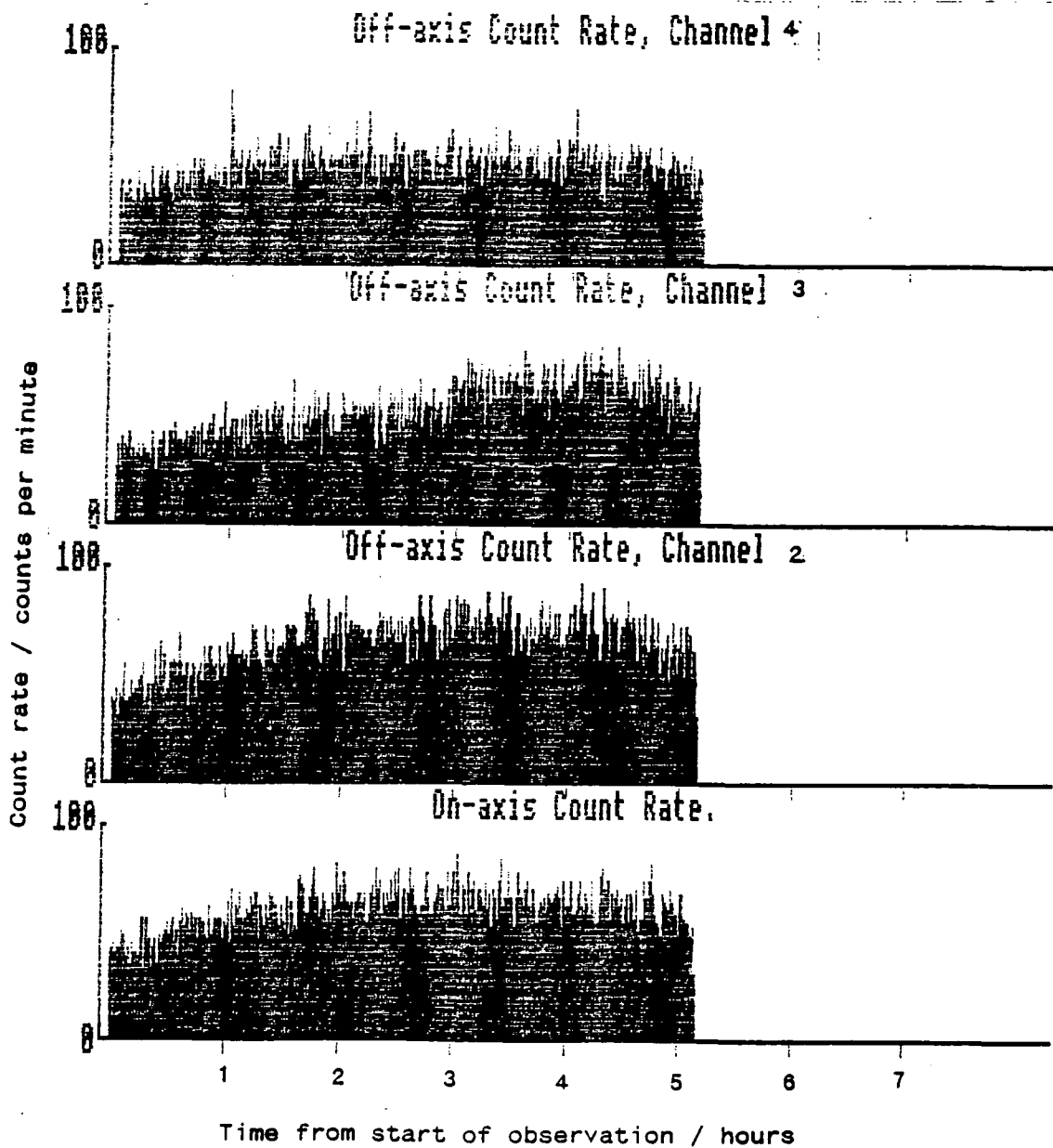
Figure 2.10 Online printout for the 9th July 1988
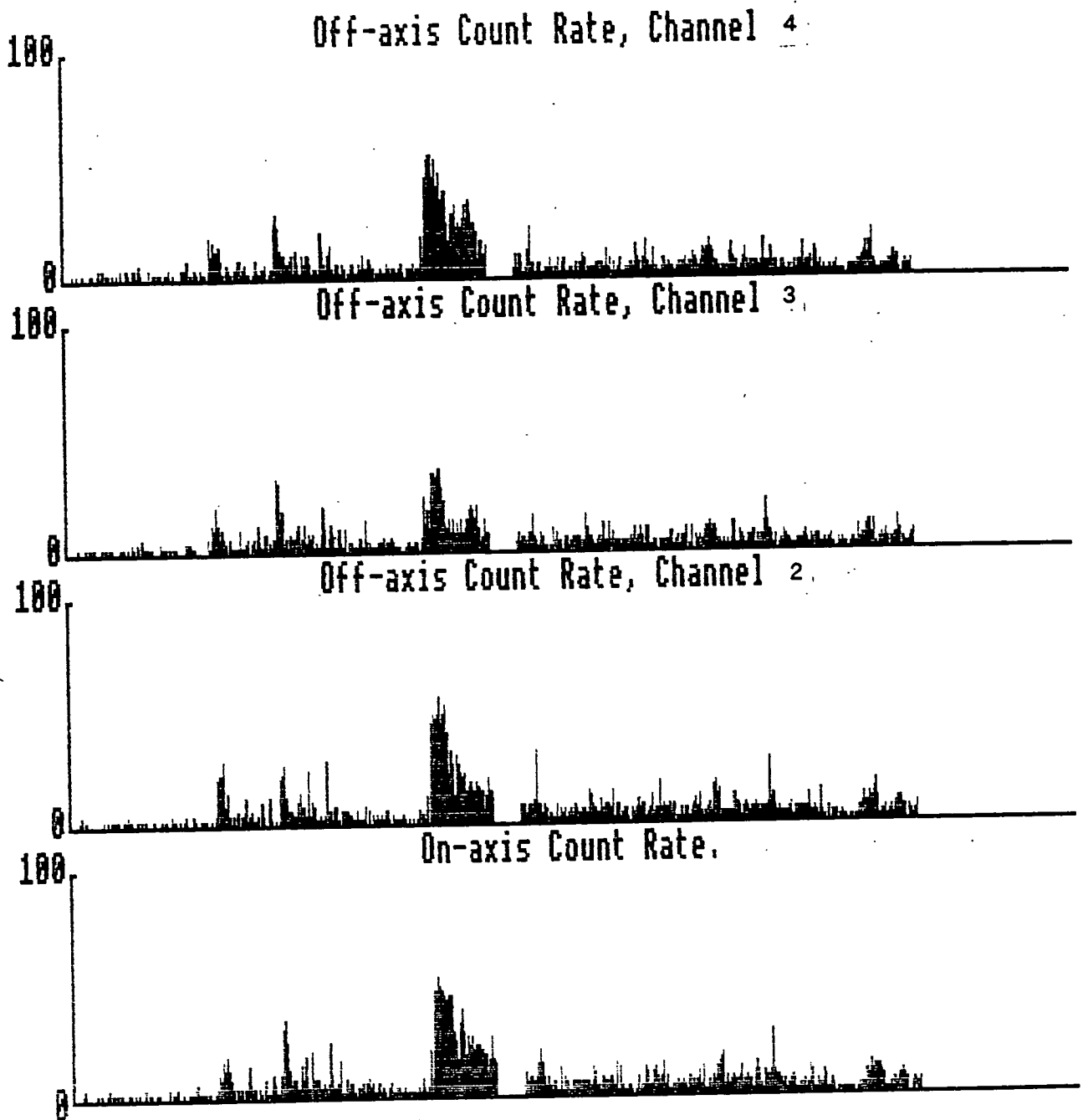
Figure 2.11 Online printout for the 28th June 1987

CHAPTER 3

STANDARD DATA ANALYSIS

3.1. Data Pre-processing

Thorough and efficient analysis requires not only the characteristics of each event, but also details of the telescope performance plus any general information that might be useful. The actual event analysis requires the accurate time of each event and the "fire pattern". Software cutting (see chapter 7) requires the QT's from each tube for every event. For purposes of quality control, it is necessary to know the position of the telscope at each event, so that the accuracy of the steering can be checked. It is also necessary to have a record of anode currents and singlefold rates, thus allowing tube performance to be checked. Weather details are printed out after each night and inserted in the observers' log (see chapter 2). For general information, it is also vital to know the date of the observation and useful to know the identities of the observers.

For every source observation, there are 3 relevant files that are recorded at the time of the observation. The first is the Run Start file. This is recorded at the start of the night and contains a description of the weather, the names of the observers, the Civil and Julian dates of the observation and a telescope status record. The second is the Source Start file. This is recorded before each individual source observation and

contains the source name and position, the starting time of the observation, the observatory position, the telescope steering offsets and the observers' comments, which will usually include a description of the weather. The third is the Data file. For each event, this file contains the event time; the QT's from all 21 tubes; the anode currents from 3 on-source and 3 off-source tubes (channels 1 and 3); the target direction for the telescope; the direction in which the telescope was actually pointing; and the drive voltage being applied to the motors. Only 6 anode currents are recorded due to lack of space in the 64-byte event "word" originally written by the 68000 computer. These files are transferred from 67 Mb 3M DC600 Data tape to the Vax 11/750 of the Durham Starlink Vax cluster. For a typical observing window of 2 to 3 weeks around the new Moon, two DC600 tapes are required, with the second being somewhat less than half full. Since the analysis programs use the event arrival times, the times, "fire patterns" and QT's are stripped out from the raw files and formatted into S-files, each of which contains information on one observation of one object.

Event times must then be transformed to the equivalent arrival time of the photon at the solar system barycentre to remove the effects of the observers' terrestrial motion. This transformation has 3 components: a correction for the orbital position of the Earth; a correction for the point of observation not being at the centre of the Earth; and a correction for the relativistic effects on the observers' timescale arising from the difference in gravitational potential between the point of observation and

the solar system barycentre and from the Earth's motion. This transformation is done by a program called BARY, which uses the JPL DE200 Earth Ephemeris available on-line on the Durham Starlink Vax cluster. The program stores the transformed times in unformatted files to conserve storage space. These files are known as C-files. Raw files, S-files and C-files are all backed up separately onto 9-track tape.

The C-files are transferred from the Vax to one of the V.H.E. Astronomy group's hard disc storage units. At this stage, the files are ready for analysis. Analysis is done on Acorn Cambridge 4 MByte workstations using programs written in Fortran-77. The files are checked against the observers' log as a quality control measure. Poor weather does not necessarily invalidate a search for periodicity in the data. Intermittent bands of cloud can introduce periods of the order of a few minutes into the data. A file showing this characteristic blemish would have to be rejected if the target object had a period of the order of seconds, but a search for millisecond periods would be unaffected. In data suffering from this problem, the sidebands due to atmospheric effects can be easily recognised when examining the results of a period search . Nights during which the weather is very poor are not analysed.

For analysis purposes, it is customary to reject all events that fire off source channels as well as the on source channel since the centre of the light pool producing such events will almost always be outside the on source channel's field of view. Thus, the rejected events do not emanate from the region of sky

containing the source and are, in general, caused by proton-initiated showers within the field of view of the Mark III and the Mark IV. The more PMTs that surround the on source channel, the better the efficiency of this protection. This is an important consideration when performing analysis of data taken in the chopping mode of operation (see chapter 5).

3.2. Testing for Pulsed Emission

When the telescope is operated in the tracking mode, detection of a count rate excess is not reliable since any test must rely on a comparison either between the count rate of the centre channel and those of the outer channels or between the count rate of the centre channel at various times during an observation. The first approach suffers from the uncertain differences between the sensitivities of the various channels. The second is prone to unquantified effects introduced by varying sky conditions. Hence, conclusive evidence of excess counts on source will not be easy to find. However, many potential V.H.E. γ-ray sources are pulsars and their emission is expected to be pulsed at the pulsar frequency. Searching for this pulsed emission is an important method of analysis. For full details of all methods used for testing for pulsed emission, see Chadwick (1987), Batschelet (1981) or Mardia (1972).

3.2.1. The Histogram Test - Epoch Folding

To apply this test for periodicity at a given period, it is necessary to convert the arrival times of the events to phases by folding the data modulo the period. This process is known as epoch folding. If the duration of the file is not very much longer than the period, then the file should be truncated to the largest possible integral number of test periods. This is known as Poincare's correction. For a typical file of duration 2 hours or more this is necessary only if the period being tested is unusually long such as that of Vela X-1, with its period of 283s. This correction is applied to all data files where necessary. The phases can be binned into phase bins of arbitrary width to produce a histogram. Pearson's χ^2-test can then be applied to test the null hypothesis that the phases should be distributed uniformly if there is no signal, in accordance with Poincare's theorem. The χ^2 test takes no account of the order of the bins in a histogram. Shuffling bins around will not affect the value of χ^2. A way to use this neglected order information is to apply the run test. For a given histogram, the number of separate sequences of bins either above or below the mean is evaluated. The distribution of this statistic is well known and the probability that it is derived from a random population can be found from a table (Walpole, 1982). There are a number of drawbacks to this technique. The definition of the phase origin is entirely arbitrary. The pulse may thus be spread between two or more bins even if it is narrow enough to fit into one. This will decrease the significance of the test result. This problem can be overcome

by sliding the origin and rebinning the phases, but this introduces a number of new degrees of freedom, which will also reduce the significance of the result. It is not clear what the exact quantitative effect of these extra degrees of freedom will be. To find this, each specific situation would need to be modelled separately. Another possible problem is that the test is most sensitive to γ-ray light curves that contain a sharp peak equal to one bin width and is relatively insensitive to broad-peaked light curves. Another difficulty may arise if the period of the source is not very accurately known. There is no way to combine separate light curves if there is an unknown phase shift between them. Hence light curves produced for a single object from separate nights must 'hold phase' if they are to be added together to obtain a composite light curve. If the uncertainty in frequency at the start of a series of observations is δv and the uncertainty in the first time derivative is $\delta v'$, then the uncertainty in the phase, $\delta \varphi$, is given by:

$$\delta \varphi = T * \delta v + \frac{T^2 * \delta v'}{2} \qquad (3.1)$$

where T is the time interval from the start of the first observation to the end of the last. If a 20 bin light curve is to be produced, $\delta \varphi$ must be less than 0.05.

The χ^2-test is thus best used for objects with very accurately known periods and narrow-peaked light curves. This makes it ideal for the Crab, which satisfies both these criteria very well. It should be used only with care for objects with accurate ephemerides, but unknown or broad light curves or for objects

31

with narrow light curves, but uncertain *periods.*

3.2.2. The Rayleigh Test

An alternative which overcomes many of the problems of the Histogram test is the Rayleigh test. This is described in detail in Mardia (1972). To perform this test, convert the arrival times of the events in a file to phases (see section 3.2.1), θ_i. Then evaluate

$$R^2 = \frac{1}{n^2}\left[\sum_{i=1}^{n} \sin\theta_i\right]^2 + \frac{1}{n^2}\left[\sum_{i=1}^{n} \cos\theta_i\right]^2 \qquad (3.2)$$

where n is the total number of events. If n is very large, $2nR^2$ is distributed as χ^2 with 2 degrees of freedom,

i.e. $\text{Probability}(nR^2 > K) = e^{-K}$

This is asymptotically exact. The approximate expression for smaller n is

$$\text{Probability}(nR^2 > K) = e^{-K} * \left[1 + \frac{2K - K^2}{4n}\right] \qquad (3.3)$$

Since R is the magnitude of the vector sum of the arrival times represented as unit vectors on a phasor *diagram,* the Rayleigh test is sensitive to single-peaked light curves only. A double-peaked light curve will have a relatively small value of R, since the two peaks will add up out of phase. Many pulsars,

32

such as the Crab' or PSR 1937+21 are known to produce an interpulse in their emission at other energies, so this problem must be borne in mind. One way round it if the two peaks of the light curve are half a period apart, is to fold the data at half the main pulse period. This will mean that the two peaks will now add up in phase. A refinement to the test to overcome the problem posed by multi-peaked light curves or those with significant power in high harmonics was suggested by Buccheri et al. (1983). This involves calculating the statistic $(R_m)^2$ given by

$$(R_m)^2 = \frac{2}{n} \sum_{k=1}^{m} \left[\left[\sum_{i=1}^{n} \cos k\theta_i \right]^2 + \left[\sum_{i=1}^{n} \sin k\theta_i \right]^2 \right] \quad (3.4)$$

where m is the number of harmonics to be included. $(R_m)^2$ is distributed as χ^2 with 2m degrees of freedom. This is, of course, identical to the standard test if m is chosen to be 1.

The Rayleigh test tests for power in the fundamental of any periodic variation in the data. Hence it is most sensitive to broad light curves, the ideal being a pure sinusoidal variation. It is relatively insensitive to narrow-peaked light curves, for which the histogram test may be appropriate (see above). If, however, the shape of the light curve is unknown, then the Rayleigh test is the best test to apply, although it will not produce the lowest chance probability in all cases. However, in these circumstances, it is better to apply an over-conservative test than to risk a false detection. The Rayleigh test is suitably conservative and is a reasonable one to apply, since any

33

light curve will have some power in the fundamental and thus be detected by the test at some level.

Unless the ephemeris for the object in question is extremely accurate, it will be necessary to search the data over a range of periods. Each independent period in the range must be tested. The separation of independent periods is known as the Fourier Interval. For an observation of length T, the phase of the last event, φ, is given by $\varphi = T / P_1$ cycles, where P_1 is the period being tested. As the test period is increased, the last event phase slips. At a test period of P_2, φ has slipped by a whole period and there is no phase coherence with the phases produced with P_1. P_2 is thus the next independent period. The Fourier Interval is given by F.I. = $P_2 - P_1$.

But
$$\frac{T}{P_1} - 1 = \frac{T}{P_2}$$

$\Rightarrow \quad TP_2 - P_1 P_2 = TP_1$

$\Rightarrow \quad T * F.I. = P_1 P_2$

$\Rightarrow \quad F.I. = \dfrac{P_1 P_2}{T} \qquad\qquad\qquad (3.5)$

For $P \ll T$ (which is usually the case), $P_1 P_2 \approx (P_1)^2$

$\Rightarrow \quad F.I. \approx (P_1)^2 / T \qquad\qquad\qquad (3.6)$

In order to maximise the chance of testing very close to the right period, it is our practice to test three periods per Fourier Interval. It is important to bear in mind the number of degrees of freedom used in searching over a range of periods, since this will lessen the significance of any result, e.g. a search over 10^3 periods that produces a chance probability for

34

one period of 10^{-6} is significant only at the 10^{-3} level.

3.2.3. Calculation of Fluxes and Flux Limits

    To translate a detected signal strength into a measurement of flux, it is necessary to know the effective field of view; the telescope threshold energy; and the integral cosmic ray flux at the threshold energy. The threshold energy is defined as that energy at which the counting rate calculated from the integral cosmic ray flux for a collecting area and aperture equivalent to those of our telescope is equal to that observed with the instrument. It is thus not an absolute limit to the telescope's sensitivity (See Kirkman (1985) for further details). For the Mark III, the field of view is 0.9° ± 0.2° and the threshold energy has been calculated to be about 250 GeV (Chadwick, 1987; Brazier et al., 1989a). At threshold, the integral cosmic ray flux is about 2.02 x 10^{-5} cm^{-2} s^{-1} str^{-1}, assuming the integral cosmic ray spectral index is -1.6 (Craig, 1984). The field of view of the Mark III channel 1 only is 3.27 x 10^{-4} str, so 1% of the cosmic ray flux at this energy is 6.6 x 10^{-11} cm^{-2} s^{-1}. Hence, for a detected signal strength of P%, detected flux is given by

$$\varphi = 6.6 * 10^{-11} * P \quad cm^{-2} \ s^{-1} \quad\quad\quad (3.7)$$

For the Mark IV, the threshold energy is 400 GeV due to the smaller collecting area, whilst the field of view is the same as that of the Mark III. This leads to a similar expression for Mark IV flux measurements:

$$\varphi_{IV} = 3.1 * 10^{-11} * P \ cm^{-2} \ s^{-1} \qquad (3.8)$$

For objects that show no significant signal, it is useful to convert this to an upper limit to the flux from the object. This is done by determining the flux that would have given a 3σ detection for the total duration of the observations and using this as the limit.

If a histogram test has been applied, then the procedure is as follows. For a 20 bin light curve, assume the pulsar has a 5% duty cycle. An excess of δ is required in one bin to produce a 3σ effect from the χ^2 test. If N is the total number of events in the light curve, this leads to the relation

$$\frac{\delta}{(N/20)^{1/2}} = 3.8 \qquad (3.9)$$

The percentage of pulsed γ-rays, P, is then given by:

$$P = 100\delta \ / \ N$$

This value of P can then be inserted into the expression (1) or (2) to give the required 5% duty cycle flux limit.

If a Rayleigh test has been performed, then the signal strength for a 3σ effect is given by

$$Probability(3\sigma) = exp(-N*P/100)$$

The Rayleigh probability corresponding to a 3σ one-tailed effect is $1.384 * 10^{-3}$, so the above expression yields

$$P^2 = - \frac{10^4}{N * \ln(1.384*10^{-3})} \qquad (3.10)$$

It is, of course, possible to apply the Rayleigh test to the 20 bins of a histogram, assigning to each event the phase of the middle of its phase bin. The above relation will then yield what

is known as the 'time-averaged' flux, which is a more sensitive measure of any broad pulsed emission than flux derived from the χ^2 test.

Evaluating fluxes and flux limits accurately requires assumptions concerning sensitive area of the telescope, telescope aperture and the size of a Cerenkov light pool. Different assumptions, especially about the last of these quantities, will produce different results. Thus, comparing flux measurements made by different groups using different instruments should be done with caution.

2.3. Testing for Unpulsed Emission

This section contains a relatively brief discussion of the standard procedure for analysis of chopped data which contains either no periodicity or has no known period to test. For details of other methods and a comparison between them, see chapter 5. When operating in chopping mode, the telescope moves in azimuth such that channel 1 points at the target object for two minutes with channel 3 pointing ~2° off source, then channel 3 points at the target for two minutes while channel 1 points off source. the pattern then repeats. The movement is timed such that channel 1 is on source for the first two minutes of every hour. One bit of the "fire pattern" byte associated with each event in a file indicates which channel was on source when the event was detected. This byte is read by the analysis programs and used to sort events according to which channel fired and whether it was

on source at the time. The basis of the technique is to count the numbers of events recorded on and off source and use a maximum likelihood method to test for the significance of any on source excess. For details of the test, see Gibson et al. (1982).

The maximum likelihood ratio, λ, is defined as

$$\lambda = \frac{\max\ L(N|S=0)}{\max\ L(N|S=s)} \qquad (3.12)$$

where $L(N|S=\alpha)$ is the likelihood of observing N counts given that the source strength is α. It is distributed as χ^2 with one degree of freedom. For a chopped file, suitably truncated so that equal times are spent on and off source, in which N counts are seen on source and B counts are seen off source, it can be shown (Orford, private communication; Dowthwaite, 1987; Gibson et al., 1982) that:

$$\lambda = \left[\frac{N+B}{2N} \right]^N \left[\frac{N+B}{2B} \right]^B \qquad (3.12)$$

S, the number of events due to the source, is given by

$$S = N - B$$

The error in this quantity is given by relaxing the value of λ to S_+ and S_- which are 1σ from S. For a discussion of the refinements required to minimise the effects of varying zenith angle and unequal detector sensitivity, see chapter 5.

/

CHAPTER 4

ISOLATED PULSARS

4.1. Introduction

There is a fundamental difference between isolated and binary pulsars in regard to their emission of V.H.E. γ-rays. The energy source for V.H.E. emission from binaries is the gravitational potential energy of accreting matter, whereas the source for an isolated pulsar is the rotational energy of the body itself. For a review of V.H.E. γ-rays observed from binary systems, see Mannings (PhD. Thesis, in preparation). The model of Cheng, Ho and Ruderman (1986a,b) provides a mechanism by which V.H.E. γ-rays are produced in isolated pulsars. Briefly, a region of charge depletion in the outer magnetosphere of a spinning magnetised neutron star allows the existence of a strong electric field with a potential difference between the opposite sides of the gap of the order of 10^{15}V. A region of charge depletion is required since, in regions containing significant quantities of freely moving charges, any electric field will cause current flows in the plasma that prevent the developement of large potential differences. The field in the depletion region accelerates particle pairs produced from γ-rays in the gap up to TeV energies. γ-rays are then produced by the inverse Compton effect. Since the energy source is ultimately rotational, candidate sources should ideally have small periods, high spin-

down rates and high mass. To satisfy the requirements of the models, a high degree of magnetisation is also required.

4.2. The Vela Pulsar (PSR 0833-45)

4.2.1. Background

The Vela pulsar is a relatively young pulsar associated with a supernova remnant. Pulsations at 89 ms have been detected at radio (Large et al., 1968), optical (Wallace et al., 1977) and γ-ray energies (Bennett et al., 1977; Kanbach et al., 1980; Tumer et al., 1984). In fact, it is the brightest source in the sky in the energy range 50MeV to 3 GeV (Bennett et al., 1977). So far, no evidence for pulsation in the X-ray emission from this object has been reported (Ogelman and Zimmermann, 1988). V.H.E. γ-ray observations of this object have been made by Grindlay et al. (1975b) and by the Tata Institute group at Ootacamund in India (Bhat et al., 1980; Gupta et al., 1982; Bhat et al., 1986a, 1987). Grindlay et al. published an upper limit to the flux at energies similar to the threshold of the Mark III of $(1.0 \pm 0.33) * 10^{-11}$ cm^{-2} s^{-1} and a limit to emission above ~5 TeV of $(7 \pm 3) * 10^{-13}$ cm^{-2} s^{-1}. The Indian group reported some positive observations at energies ~10 TeV.

4.2.2. Data and Results

The object was observed for 40 hours in 1987. The results of these observations are given in detail by Chadwick (1987).

They are not compatible with the Indian results, but there are problems about the statistical significance of these (Chadwick, 1987) and they show considerable time variability. The Ootacamund observations were taken shortly after a 'glitch' was observed (Manchester et al., 1976) in the pulsar's period. It is possible that this is linked to V.H.E. γ-ray emission in the following months. A similar large spin-up was detected by Flanagan (1988) on Christmas Eve of 1988. To test this, observations were made for 22 hours in March 1989, 30849 events being observed. Further observations were planned, but were prevented by poor weather.

The events were folded using a contemporary ephemeris supplied by C. Flanagan of the Hartebeesthoek Radio Astronomy Observatory, Johannesburg (Flanagan, private communication, 1989). The histogram produced is shown in fig. 4.1. Whilst there is a peak significant at the 2σ level in the light curve, there is an equally significant trough. Hence there is no evidence for pulsed emission in this light curve, leading to a 3σ flux limit to 5% duty cycle emission of $3.2*10^{-11}$ cm^{-2} s^{-1} and a 3σ 'time-averaged' flux limit of $9.7*10^{-11}$ cm^{-2} s^{-1}. The observations were taken over an 8 day period, so it is possible that the pulsar was in a low emission state for this relatively short time. The observations therefore conflict with the hypothesis that period glitches are followed by periods of high emission of V.H.E. γ-rays on a timescale of a few months.
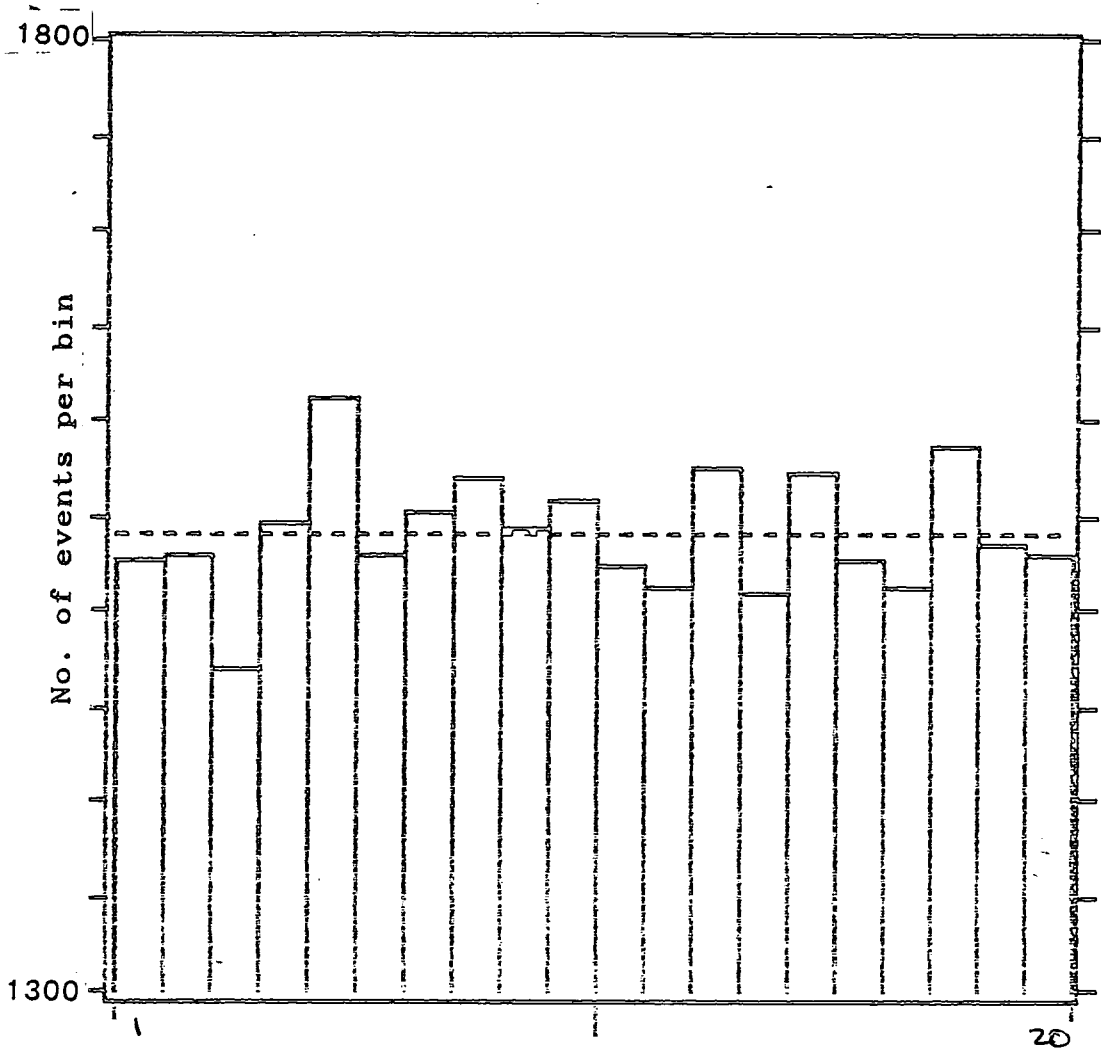
Figure 4.1 V.H.E. γ-ray light curve for 1989 observations of the Vela pulsar

4.3. The Crab Pulsar (PSR 0531+21)

4.3.1. Background

The Crab pulsar is the remnant of the supernova of 1054 AD recorded by Chinese astronomers. It was one of the first pulsars to be discovered (Staelin and Reifenstein, 1968) only a few months after the very first detection of a pulsar by Hewish et al. (1968). The Crab has been studied extensively at every wavelength since. It was first observed in V.H.E. γ-rays at the Smithsonian Astrophysical Observatory by Grindlay et al. (1976). Other observations followed, giving conflicting results (Porter et al.; 1976; Erickson et al., 1976; Gupta et al., 1978). This object was first observed by the Durham group with the mark I telescope in 1981. Two 15 minute bursts were found to be periodic at the radio period with chance probabilities of 10^{-4} and 10^{-6} (Gibson et al., 1982). Observations in 1982 and 1983 showed evidence for persistent weak emission at a period of 33 ms with a chance probability of 10^{-5} (Dowthwaite et al., 1984). As well as this low level of constant emission, there have been a number of reports of bursts lasting a few minutes (Gibson et al., 1982; Resvanis et al., 1987; Vishwanath, 1987).

4.3.2. Data and Results

Observations were made on four nights in October 1988 with the Mark IV telescope at La Palma. A total of 33413 on-axis events were collected in 7·5 hours. The new data were folded with the period taken from the contemporary ephemeris supplied by Lyne and

Pritchard (private communication). This is from a highly accurate and regularly repeated measurement which makes the Crab unique as the only object for which the the radio phase of each event arrival time is known accurately. Thus any excess due to the source should appear at phase 0. The resulting light curve is shown in fig. 4.2. There is no significant excess in any bin, which is not surprising, given the relatively short exposure. There is a non-significant peak at phase 0.75. The analysis has been studied in detail to see if a spurious phase shift has been introduced that would mean that this might be due to the Crab. To this end, the standard barycentring program was tested by using it to transform idividual arrival times that were then transformed using a calculator and tables from the Astronomical Almanac. The results from the two methods were compared and found to be the same to an accuracy much better than that required to produce a phase shift of 0.25 in the Crab light curve. The Rubidium oscillator used has been measured over a long time base against an off-air signal and found to be operating well within specification. No source of any phase offset has been found. Hence the data yield a 3σ flux limit of $1.4 * 10^{-11}$ cm^{-2} s^{-1}, which is compatible with our earlier flux measurements (Dowthwaite et al., 1984).

To test for the presence of any transient activity in our data on similar timescales to that previously reported, the files were divided into 15 minute segments, overlapping by 7.5 minutes. A Rayleigh test was performed on each segment. No significant peaks were seen.

43
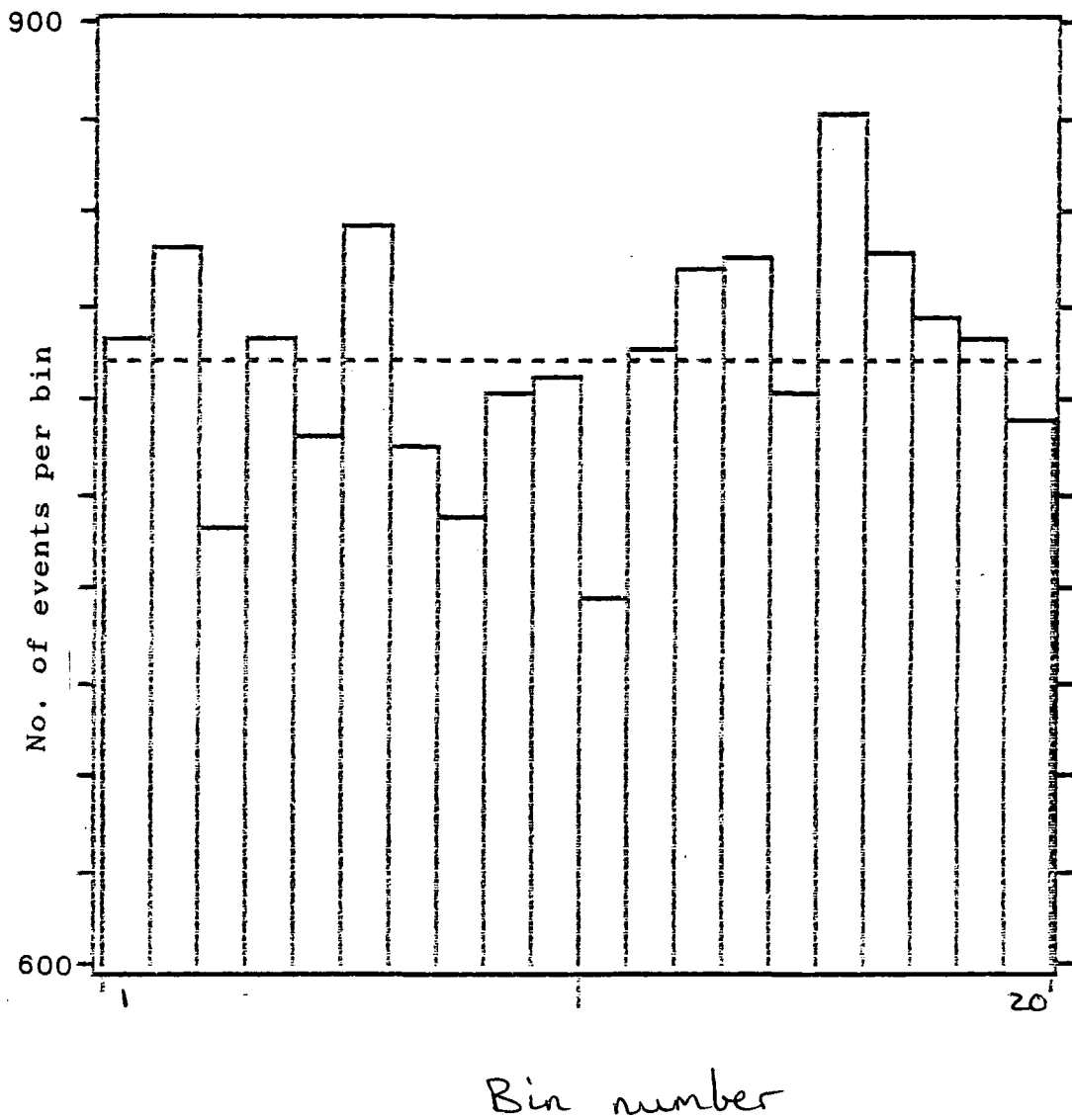
Figure 4.2 V.H.E. γ-ray light curve for 1988 observations of the Crab pulsar

4.4. PSR 1055-52

4.4.1. Background

The radio pulsar PSR 1055-52 was first discovered by Vaughan and Large (1972). The period of 0.197 s was among the shortest 5% known at the time, although this was before the discovery of millisecond pulsars. The period derivative of $5.8*10^{-15}$ ss^{-1}, which is among the highest 10% known implies a rotational energy loss rate of about $3*10^{34}$ $ergs^{-1}$. The distance to the object, as determined from the dispersion measure and a model of the intervening free electron density, is 920 pc (Manchester and Taylor, 1981). The object was detected as a source of soft X-rays by Cheng and Helfand (1983), using the Einstein Observatory and later by Brinkmann and Ogelman (1987), using EXOSAT. The X-ray emission is not significantly pulsed. The calculated luminosity in this region of the spectrum is of the order of 10^{32} $ergs^{-1}$. This accounts for only 1% of the rotational energy loss rate. The relative proximity and high energy loss rate suggest that this object might well emit V.H.E. γ-rays and is thus a good candidate for observation.

4.4.2. Data and Results

PSR 1055-52 was observed on 12 nights between February and June 1987. A total of 33 hours data was collected, comprising 53370 events on-axis. The most accurate ephemeris available is that given by Brinkmann and Ogelman (1987), which is based on radio observations by Manchester made in 1984. The ephemeris is

44

accurate enough for us to hold relative phase over the 4 month duration of observation, but not accurate enough to allow determination of the absolute phase of each event.

The arrival times of all the on-axis events were folded modulo the period to produce a light curve (see fig. 4.3). Taking the null hypothesis that there is no periodic signal and that therefore the event times should be uniformly distributed in accordance with Poincare's theorem, we find a value for χ^2 of 25.6. Since absolute phase is unknown, emission is not expected preferentially in any one bin or group of bins, so there are up to 19 degrees of freedom associated with this test, depending on the width of the light curve. The value of 19 corresponds to the case where the pulse has a 5% duty cycle. For a 50% duty cycle, the number of degrees of freedom would be 2. It is our practice to assume a value of 19 for the number of degrees of freedom to make the test the most conservative possible. The value of χ^2 falls within the 90% confidence interval for acceptance of the null hypothesis. There is thus no evidence for pulsed emission of V.H.E. γ-rays from this object. This leads to a 3σ flux limit to 5% duty cycle emission (see section 3.2.3) of $2.4*10^{-11}$ cm^{-2} s^{-1} and a 3σ 'time-averaged' flux limit of $7.3*10^{-11}$ cm^{-2} s^{-1}.

4.5. PSR 1509-58

4.5.1. Background

PSR 1509-58 was first detected in the X-ray region by Seward and Harnden (1982), using the Einstein Observatory. The
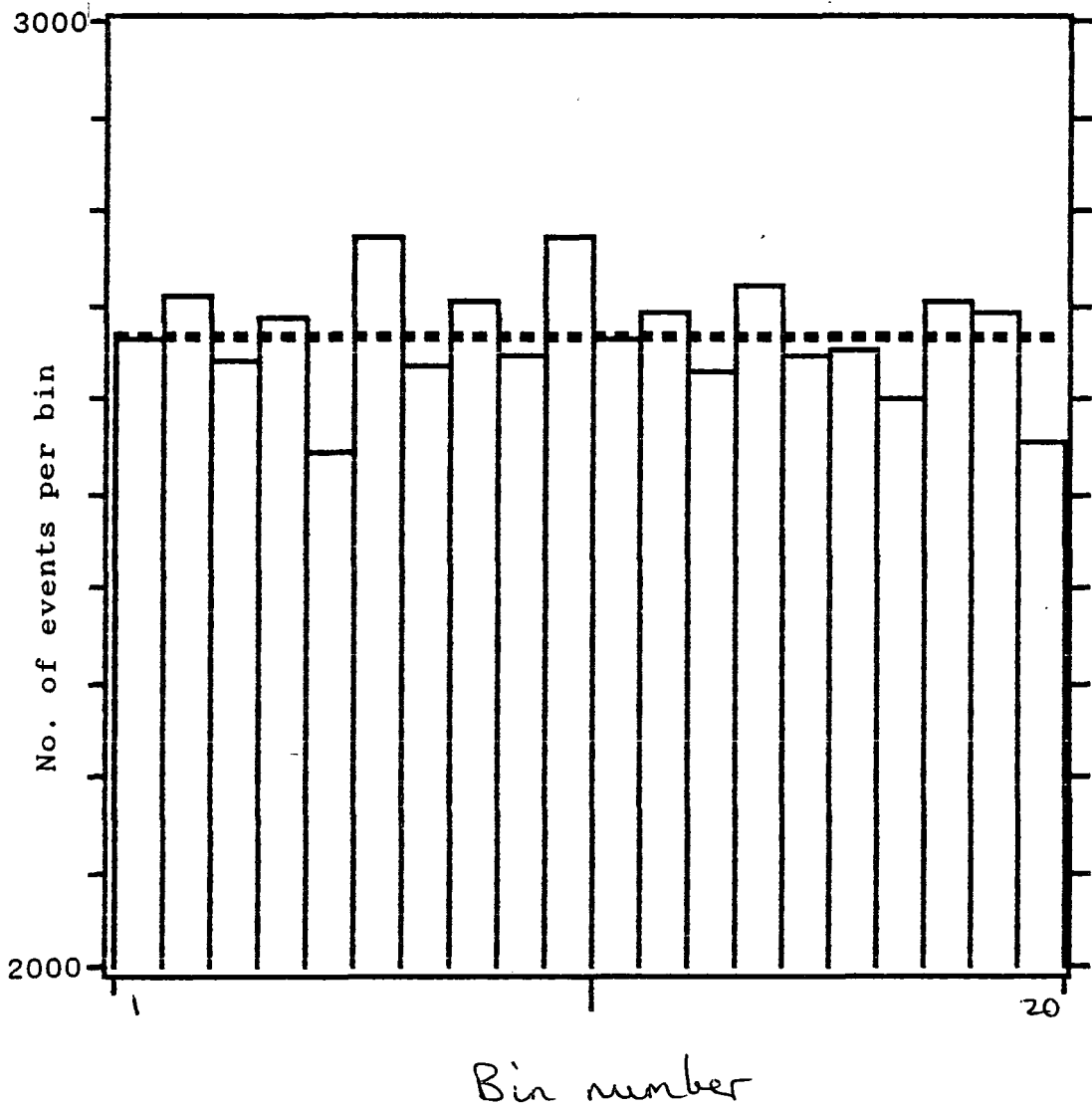
Figure 4.3 V.H.E. γ-ray light curve for PSR 1055-52'

The y-axis is labeled "No. of events per bin" with markings at 2000 and 3000. The x-axis is labeled "Bin number" with markings at 1 and 20.

measured period was 0.15 s, making this object one of the fastest known at the time. When the observations were made in 1979 and 1980, a large period derivative was noted, but the exposure was too short to rule out the possibility that the effect was due to orbital motion of a pulsar in a binary system. Radio pulsations were detected in observations made during 1981 and 1982 by Manchester et al. (1982), using the Parkes radio telescope. If the X-ray period measurements and the radio measurements are plotted as a function of time, the data points are well fitted by a straight line, implying that the large period derivative initially measured in X-rays is not due to orbital effects. Further radio observations (Manchester et al., 1985) have allowed very accurate measurement of the variation of the period with time. The distance, as determined by Caswell et al. (1975) is 4.2 kpc. This is close enough that the signal is not likely to be severely attenuated.

The period derivative of $1.5*10^{-12}$ ss^{-1} is the largest known, being about 3 times larger than that of the Crab, the second largest. In fact, the object shows remarkable similarities to the Crab. They are both associated with supernova remnants; they have comparable ages; and they both have well-behaved periods, allowing the second period derivative to be measured accurately (Manchester et al., 1985). The Crab is one of the few well-established sources of TeV γ-rays, so PSR 1509-58 must be considered a good prospect for emission. Indeed De Jager et al. (1988) have reported detection of TeV γ-rays from PSR 1509-58 from observations made with the Potchefstroom telescope. Their

detection, significant at the 10^{-3} level, produces a triple-peaked light curve which has yet to be explained. Further measurements by the same group are claimed to confirm this detection (Nel et al., 1989). The high period derivative, proximity, and detection at TeV energies make this a prime object for study.

4.5.2   Data and Results

Two separate observing runs were made on this object. Data was taken on 6 nights in March and April 1987 with 10 days between first and last observations. A total of 37821 events in 25 hours were observed on source during this run. Data was also taken on 5 nights during March 1989 with 7 days between first and last observations. A total of 26641 events in 16 hours were observed on source during the second set of observations.

The ephemeris was taken from Manchester et al. (1985). It is possible to hold phase within each dataset, but not over the two years separating the two, so separate histograms were produced (see figs 4.4 and 4.5). The combined chance probability of these is 0.1. A period search, using the Rayleigh test, over a wide range of periods including the radio period and that suggested by De Jager et al.(1988) showed no significant peaks (see figs. 4.6 and 4.7).

There is thus no evidence for significant pulsed emission from this object. The 3σ flux limit to 5% duty cycle emission derived from the first set of observations is $2.9*10^{-11} cm^{-2}$ s^{-1}, whilst
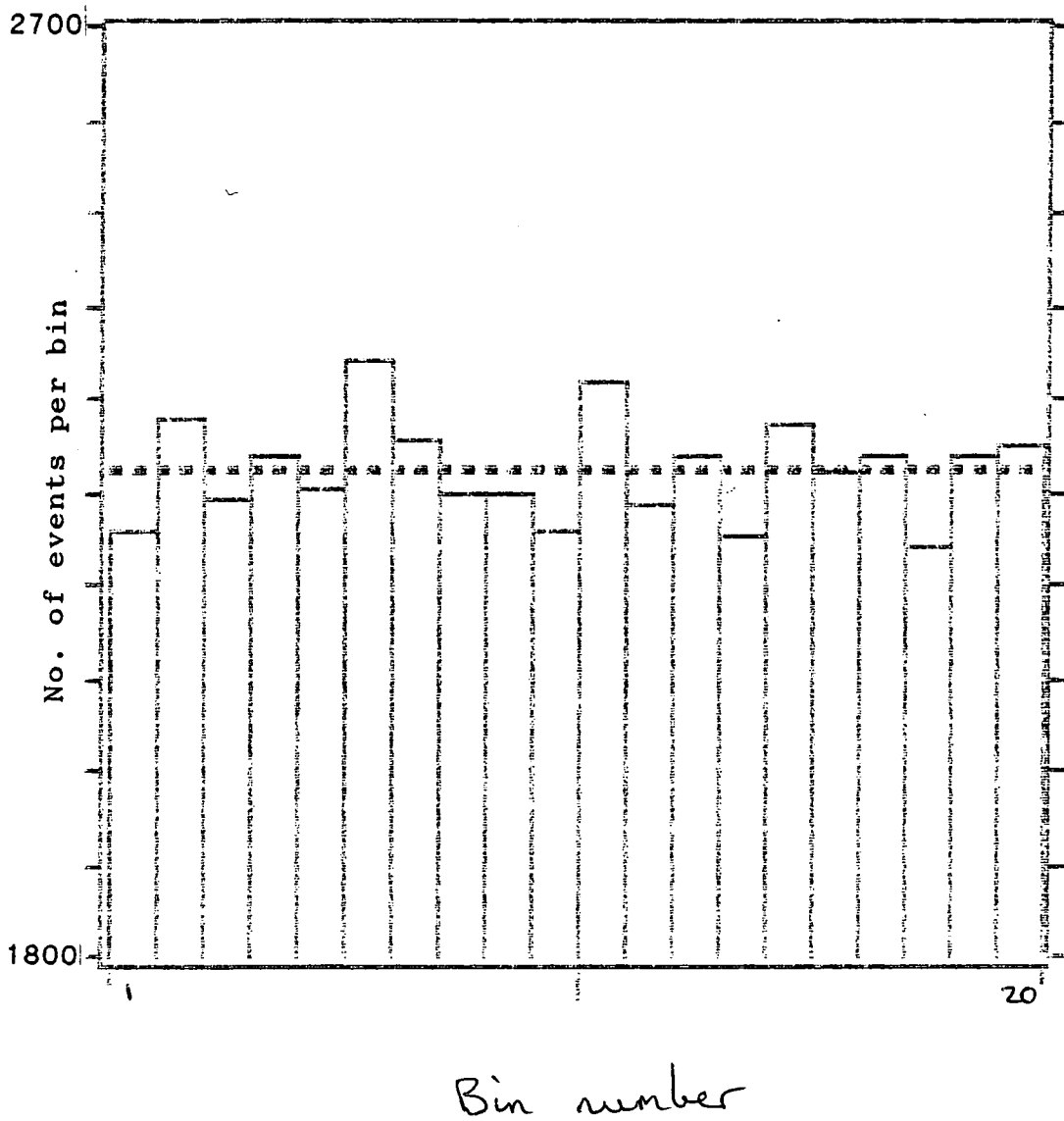
Figure 4.4 V.H.E. γ-ray light curve for 1987 observations of PSR
1509-58
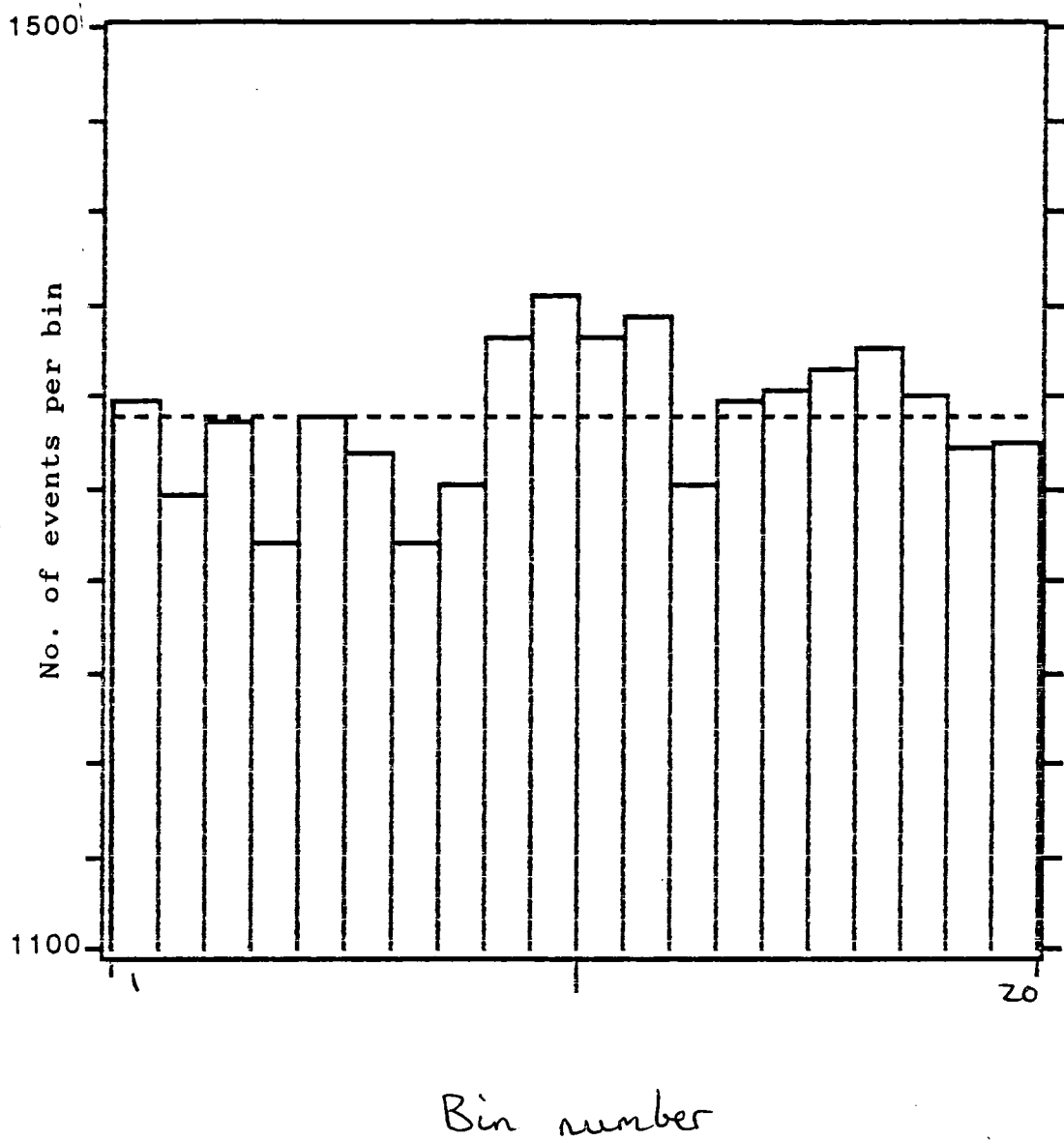
Figure 4.5 V.H.E. γ-ray light curve for 1989 observations of PSR
1509-58
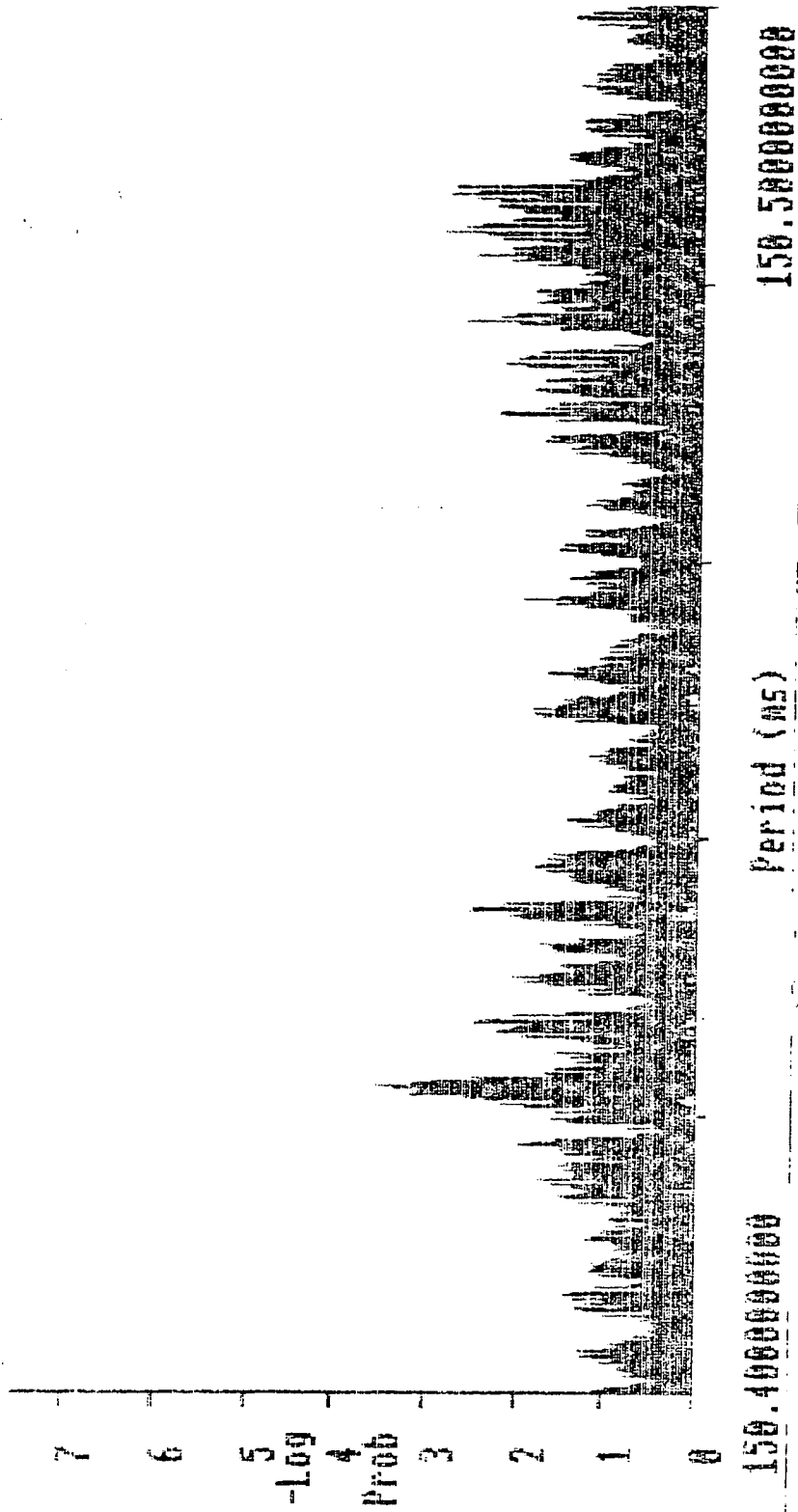
Figure 4.6 Plot of Rayleigh probability of chance occurrence against trial period for 1987 observations of PSR 1509-58
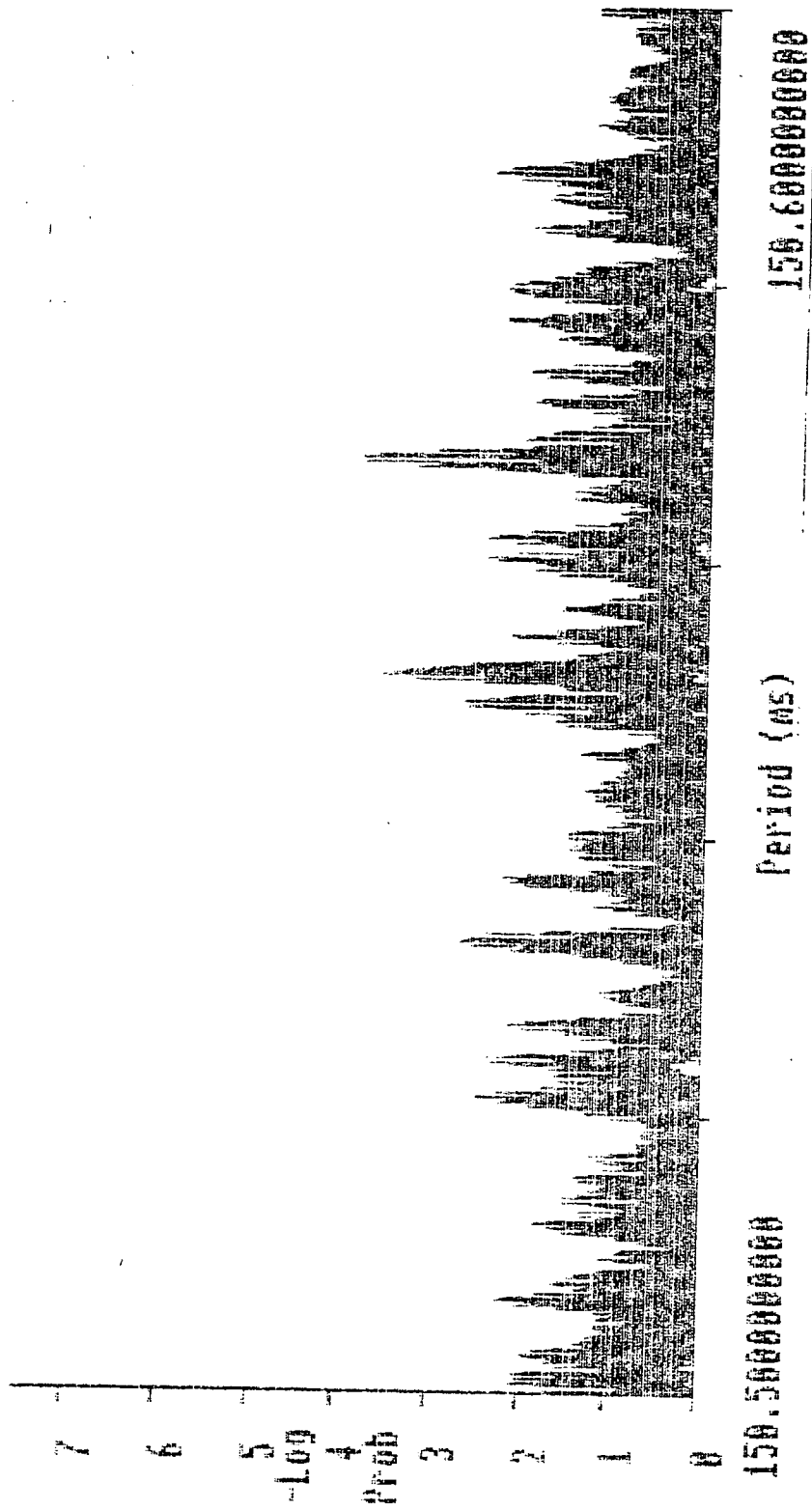
Figure 4.7 Plot of Rayleigh probability of chance occurrence against trial period for 1989 observations of PSR 1509-58

that derived from the second is $3.4*10^{-11}$ cm^{-2} s^{-1}. This yields a composite upper limit of $2.2*10^{-11}$ cm^{-2} s^{-1}. The corresponding 'time averaged' limit is $6.7*10^{-10}$ cm^{-2} s^{-1}.

The value of the flux given by De Jager et al. (1988) is $2.1*10^{-11}$ cm^{-2} s^{-1} for a threshold energy of 1000 GeV. However, there appears to be an over-estimation of the sensitive area of the telescope in the South Africans' flux calculations (De Jager, private communication) as the Cerenkov light pool size corresponding to showers occurring at the zenith has been used for all observations. A conservative estimate of the effect of this is that it will introduce a factor of about 0.5 into the flux calculations. Using this and extrapolating back to our threshold gives a flux of $3.9*10^{-10}$ cm^{-2} s^{-1}. This is not compatible with our result if PSR 1509-58 is a steady emitter of V.H.E. γ-rays. There is, however, some doubt as to the true significance of the detection. An estimator is used to determine the shape of the light curve before the existence of any emission is demonstrated. The result of this estimator is used to indicate how many harmonics to use in the Z^2 test which is then applied to the data. No allowance for this 'bootstrapping' procedure is made in the final significance of the detection, which is only $\approx 10^{-3}$. Also, in Nel et al. (1989), the Potchefstroom group publish evidence for the object being variable and claim confirmation of the original effect. There are a number of problems with the data used, however. The most significant effect comes from a series of drift scans of Circinus X-1. The paper quotes a field of view for the telescope of 2.2° (FWHM). During a drift scan, the centre of

48

Dates	Location	Signal ?
10/06/85 - 21/06/85	Potchefstroom	yes
10/07/85 - 20/07/85	Potchefstroom	yes
27/03/87 - 06/04/87	Narrabri	no
29/04/87 - 28/06/87	Potchefstroom	yes
05/03/89 - 14/03/89	Narrabri	no

Table 4.1 Comparison of Observations of PSR 1509-58

the field of view describes a line of constant declination on the sky. PSR 1509-58 is 1.97° away from Circinus X-1 in declination. Hence, at closest approach, PSR 1509-58 was 0.87° beyond the edge of the field of view. Little importance should be attached to this dataset, therefore. The significance of the other observation is $2*10^{-2}$ and thus not compelling.

If the object is indeed variable, our result can be reconciled with those from Potchefstroom, since there were no simultaneous observations made (see table 4.1). If the object emits for 3 out of every 4 10-day periods on average, as claimed, then the chances of quiet phases coinciding with both of our observing periods is 0.06. However, the results conflict with any claim for steady emission above the limit quoted.

4.6. Conclusions

Details of recent observations of 4 different pulsars have been presented in this chapter. The results are summarised in table 4.2. The result from the Crab is based on a relatively small dataset and is largely inconclusive as a consequence. The other three objects, however, show no sign of detectable emission. Whilst these pulsars do not represent an exhaustive survey of this class of object, they have been selected as the most promising candidates for V.H.E. emission. Thus, it is possible to infer from the lack of detectable emission from these few that isolated pulsars are not, in general, strong sources of observeable V.H.E. γ-rays. There are two possible explanations

Object	Energy Threshold (GeV)	3σ Flux limit / cm^{-2} s^{-1}	
		5% duty cycle	time averaged
PSR 0833-45 (Vela Pulsar)	250	$3.2 * 10^{-11}$	$9.7 * 10^{-11}$
PSR 0531+21 (Crab Pulsar)	400	$1.4 * 10^{-11}$	N/A*
PSR 1055-52	250	$2.4 * 10^{-11}$	$7.3 * 10^{-11}$
PSR 1509-58	250	$2.2 * 10^{-11}$	$6.7 * 10^{-11}$

*The light curve for the Crab is known to contain a sharp peak, so the 'time averaged' flux limit is not meaningful.

Table 4.2 Summary of results of observations of isolated pulsars

for this. One is that emission from these objects is intrinsically weak. This is attested to by the persistent and statistically significant 0.2% signal found in the Dugway experiment. The other is that the emission is in the form of well-collimated beams which are not always oriented in the right direction to reach the Earth and thus allow the emission to be detected.

Cheng, Ho and Ruderman (1986b) state that the potential drop that will develop in an outer magnetosphere gap and the created particle flow through it are both roughly proportional to $\Omega^2 B$. Assuming that the pulsar rotational energy loss rate is largely due to magnetic dipole radiation and that the sin of the angle between the rotation axis and the magnetic axis is roughly 1, then the relation between $\dot{\Omega}$ and B is given by

$$\dot{\Omega} = - \frac{2B^2 R^6 \Omega^3}{3c^3 I} \qquad (4.1)$$

(Katz, 1987) where R and I are the neutron star radius and moment of inertia respectively. These quantities may not vary much between neutron stars, leading to the relation

$$B^2 \ \alpha \ \frac{\dot{\Omega}}{\Omega^3} \qquad (4.2)$$

But

$$\dot{\Omega} \ \alpha \ \frac{\dot{P}}{P^2} \qquad (4.3)$$

Hence

$$\Omega^2 B \ \alpha \ \left[\frac{\dot{P}}{P^3} \right]^{1/2} \qquad (4.4)$$

OBJECT	Period (ms)	$\dot{P}$ (ss^{-1})	$(\dot{P}/P^3)^{1/2}$ (arbitrary)	Distance (kpc)	$(\dot{P}/P^3)^{1/2}/r^2$ (arbitrary)
CRAB	33	$4.2 * 10^{-13}$	0.11	2.0	2.8
VELA	89	$1.2 * 10^{-13}$	0.013	0.5	5.2
PSR 1509-58	150	$1.5 * 10^{-12}$	0.021	4.2	1.0
PSR 1055-52	197	$5.8 * 10^{-15}$	$8.7 * 10^{-4}$	0.92	0.1

Table 4.3 Comparison of pulsar parameters governing outer gap formation

The values of $\dot{P}/P^3$ for the pulsars studied in this chapter are given in table 4.3, along with the distances to the objects. From this it can be seen that the Crab Pulsar has the most favourable combination of parameters for the formation of a large potential drop in an outer gap, although the Vela Pulsar would be expected to produce a larger flux at the Earth if its V.H.E. luminosity were proportional to $(\dot{P}/P^3)^{1/2}$. It may be that there is a sharp cut-off in the energy emission spectrum at the energy corresponding to the total potential drop along the gap and that the pulsars other than the Crab have a cut-off below the V.H.E. γ-ray region.

The angular spread of the fan beam produced is dependent on the thickness of the gap. A thicker gap will produce a smaller angle. Since the larger gaps will produce larger fluxes of particles, those pulsars producing the largest quantities of V.H.E. radiation may well be those with the narrowest beams. Thus, objects chosen as most likely a priori sources of V.H.E. γ-rays would be the ones with the smallest probability of the beam geometry being favourable enough to allow observation from the position of the Earth.

Hence, the prerequisite for observing V.H.E. emission from an isolated pulsar may not simply be values of magnetic field (B) and angular velocity (Ω) that are as large as possible. The fact that the Crab produces a detectable flux of γ-rays is likely to be the result of an optimal combination of B and Ω which is not always produced by objects with higher values of either quantity. Substantial emission from the Crab must also be accompanied by a

certain amount of geometric good fortune to allow such emission to be observable.

The lack of detectable V.H.E. emission from the objects studied in this chapter does not therefore require the abandonment of the standard model. Indeed, the model that explains why some isolated pulsars emit detectable fluxes of V.H.E. γ-rays may well itself provide the best explanation of why others do not.

CHAPTER 5

NEW ANALYSIS TECHNIQUES FOR DC DATA

5.1. Problems to be Solved

The root of the problem posed in trying to measure a steady
excess signal from a V.H.E. source lies in the low flux of V.H.E.
photons relative to the flux of protons of similar energy and
hence the low signal to noise ratio. The ideal technique should
involve a measurement of counts from an area of sky containing
the source and a measurement of counts from another area of sky
under identical conditions; the only difference between the two
being the presence of the source in one and its lack in the
other.

Measurements must be made over a long period for the excess to
be significant due to the low signal to noise ratio. The count
rate produced by a tube depends on its gain. A tube's gain and
the dependence of the gain on external factors such as anode
current, temperature, humidity etc. is unique to each tube.
Hence, simultaneous observations of the source and a nearby area
of sky will not produce on and off source datasets that are
comparable. Also, the maximum enhancement of signal to noise
produced by rejecting events that trigger more than one tube is
only possible for channel 1 with its complete guard ring. The
chopping mode of operation (see section 3.3) for the telescope
attempts to overcome this problem. Channels 1 and 3, which are in

the same horizontal plane, each view the source and a nearby area of sky alternately. Thus each tube produces an on and off source dataset generated with identical tube characteristics. PMT gain will vary with anode current and thus sky brightness. Hence it is vital to have some form of gain control to compensate for the fact that the two areas of sky sampled are unlikely to have equal brightnesses. This is the justification for the AGC (see section 2.4.2) system that keeps the anode currents in each tube constant despite varying sky brightness. The count rate dependency on factors such as ambient temperature and humidity is small compared with the zenith angle effect, so the tube response characteristics can thus be taken to be constant throughout an observation. Hence, simulated data need only contain a zenith angle-determined variation in the count rate.

The one major factor affecting the count rate during an observation is the change in the zenith angle of the source. Cerenkov light is attenuated in the atmosphere. Extensive air showers initiated by V.H.E. γ-ray photons generally start at about 10 km above sea level. This means that an observer recording Cerenkov pulses from an object that is low in the sky will record fewer counts than an observer studying a higher object (see fig. 5.1). This dependency of count rate with zenith angle has previously been determined (Macrae, 1985) to be of the form

$$\text{count rate} \, \alpha \, \cos^n \theta \qquad (5.1)$$

where $n = 2.3 \pm 0.5$ (Brazier et al., 1989a). One result of the change in count rate with zenith angle is that each two minute
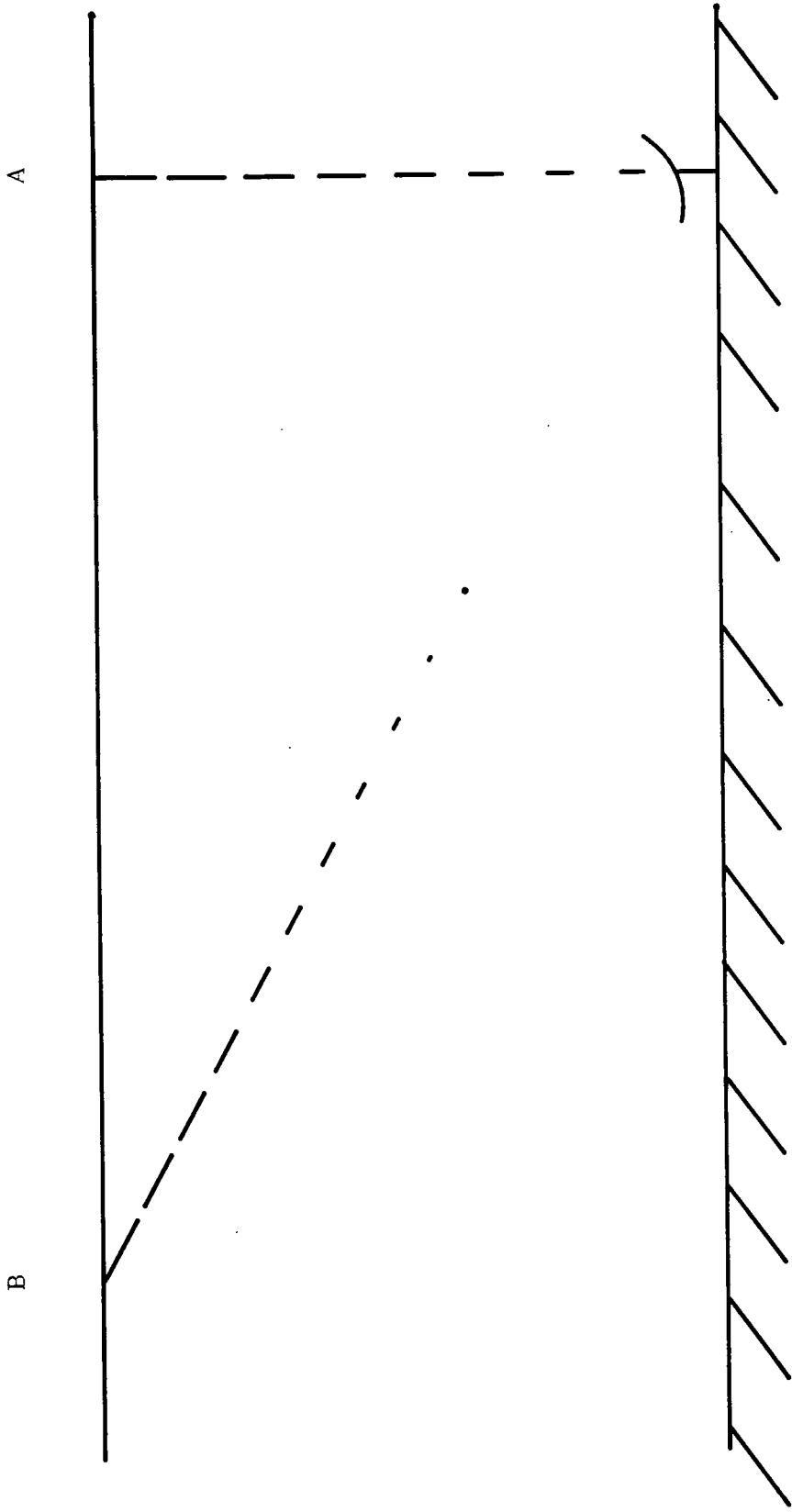
Figure 5.1 Attenuation in the atmosphere causes the variation of count rate with zenith angle. The Cerenkov flash from shower B is attenuated more than that from shower A.

segment of the 'chopped' observation is made at a different underlying count rate to the last. This can introduce a bias into the on and off source datasets (see fig. 5.2). Any analysis technique used on this sort of data should address itself to reducing this bias to a minimum.

5.2. The Counting Heads Method

5.2.1. Outline of Method

This method is the simplest of those to be presented in this chapter. It consists of just counting the number of events from on and off source for a particular tube and comparing them using the maximum likelihood method described in section 3.2.3. Observations do not in general start at the beginning of a two minute chop period, so chopped data files need to be cut so that equal amounts of time are spent on and off source. If a file is cut to start with channel 1 starting an on or off source segment and to finish with the same channel finishing a spell in its alternative position, then a consistently rising or falling count rate will introduce a bias (see fig. 5.2). If, however, the file is cut to start half way through a chop segment and finish halfway through a segment in the same position, then any linear variation in count rate is eliminated. To clarify this, consider a dataset during which the count rate increases linearly with time according to the relation
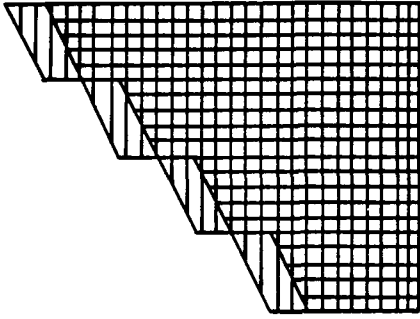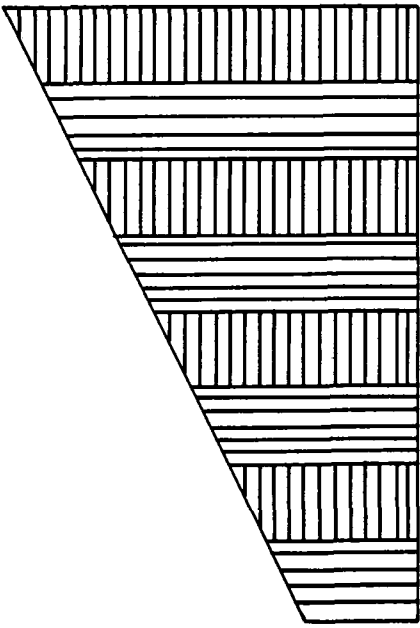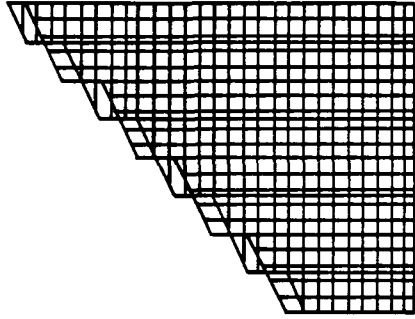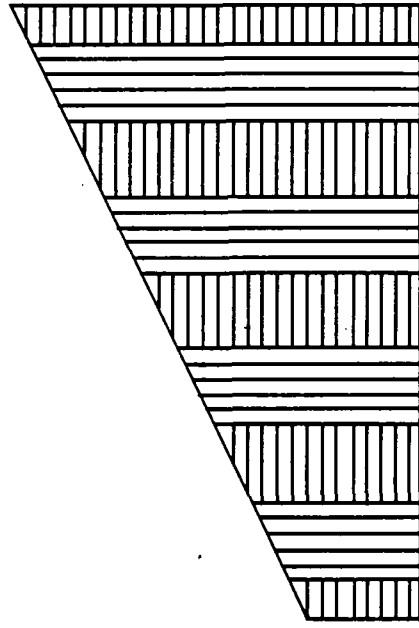
$$\text{rate} = R_0 + k(t - t_0) \qquad\qquad (5.2)$$

Figure 5.2 Graphs of chopped data with a linearly rising count rate. In case (1), cutting the data such that it starts at the beginning of an on-source or off-source segment leads to a bias. In case (2), this bias is removed if the data starts in the middle of a segment.

If there are n on source segments and n off source segments, starting with a complete on source segment, then the total on source counts, disregarding any from the source itself is given by

$$nR_0\tau + \sum_{i=1}^{n} \frac{k(4i-3)\tau^2}{2} \qquad (5.3)$$

whereas the off source counts are given by

$$nR_0\tau + \sum_{i=1}^{n} \frac{k(4i-1)\tau^2}{2} \qquad (5.4)$$

where τ is the length of a chopping segment. Thus, there is an excess off source of $nk\tau^2$. If the data selection begins in the middle of an on source segment, such that there are n off source segments and n-1 whole and two half on source segments, then the off source counts are given by

$$nR_0\tau + \sum_{i=1}^{n} (2i-1)k\tau^2 \qquad (5.5)$$

and the on source counts are given by

$$nR_0\tau + \sum_{i=1}^{n-1} 2ik\tau^2 + \frac{1}{8}k\tau^2 + \left[n - \frac{1}{8}\right]k\tau^2 \qquad (5.6)$$

which can be rewritten as

$$nR_0\tau + \sum_{i=1}^{n-1} (2i-1)k\tau^2 + (n-1)k\tau^2 + nk\tau^2 \qquad (5.7)$$

which is the same as the expression for the off source counts. This method of cutting the data will compensate totally for any linear term in the zenith angle dependence of the count rate. However, this dependence is more complex than a simple linear relation. A reasonable order of magnitude estimate of the errors in the event totals for on and off source data introduced by the non-linearity in a typical observation would be less than 1%. Attempts to compensate more comprehensively for the zenith angle effect should thus be more sophisticated.

5.2.2. Advantages and Disadvantages

The main advantages of this method are its simplicity and the simplicity of its underlying assumption that the zenith angle variation can be approximated by a linear relation. If, as is often the case, the observation starts and finishes around the same zenith angle with culmination occurring in the middle, then it does not matter what the zenith angle - count rate relation is, since any bias introduced as the object rises is automatically cancelled as it sets. No assumption is made as to the exact nature of the relation or even the linear part thereof.

The method had a serious disadvantage when only channels 1 to 4 contributed to the "fire pattern". Channel 1 was surrounded by 3 contributing tubes, which allowed rejection of events from any direction. Channel 3 on the other hand was much less well protected. It had only one adjacent tube to provide rejection. Hence the dataset from channel 3 was considerably poorer than

that from Channel 1, with ~50% more events which were all noise. Thus, best results were obtained by ignoring channel 3 and using only channel 1 data. This meant that only half the time spent looking at the source was being used. Since January 1989, however, all 7 channels have contributed to the fire pattern. As a result, Channel 3 has 3 adjacent channels to provide rejection. It now produces only ~10% more noise or nucleon-initiated events than channel 1 and the two datasets can be added together to improve the counting statistics and thus make maximum use of all the data. There is still the disadvantage that the observations have to be cut and that therefore some observing time is lost. In the worst case, a total of nearly four minutes could be lost. Since typical observations last in excess of two and a half hours, this is not too serious a problem.

5.3. The Ratio Method

5.3.1. Outline of Method

For a given observation, assume the rate of background events measured by channel 1 is R and the rate of signal events is s, say. Then the number of events recorded by channel 1 in all the time it spends looking at the source is given by

$$n1on = \int_{on-source} (R + s)dt = B + S \qquad (5.8)$$

Similarly, the number of events recorded by channel 1 in all the time it spends off source is given by

$$n1off = B \qquad (5.9)$$

Assume channel 3 counts at α times the rate of channel 1. The corresponding expressions for these channels are

$$n3on = \alpha\,(B + S) \tag{5.10}$$

$$n3off = \alpha B \tag{5.11}$$

Hence,

$$\frac{n1on}{n3off} = \frac{B + S}{\alpha B} = f1 \quad , \quad \frac{n1off}{n3on} = \frac{B}{\alpha\,(B + S)} = f2 \tag{5.12}$$

$$\Rightarrow \quad \frac{f1}{f2} = \frac{(B + S)^2}{B^2} = (1 + S/B)^2$$

$$\Rightarrow \quad S/B = (f1/f2)^{1/2} - 1 = X, \text{ say} \tag{5.13}$$

Hence X provides an measurement of signal strength. The variance of X is given by

$$\sigma^2(X) = \sigma^2_{f1} \left[\frac{\partial X}{\partial f1} \right]^2 + \sigma^2_{f2} \left[\frac{\partial X}{\partial f2} \right]^2$$

$$= \sigma^2_{f1}\,(1/4f1f2) + \sigma^2_{f2}\,(f1/4f2^3) \tag{5.14}$$

Assuming n1on, n1off, n3on, n3off follow Poisson statistics, then

$$\sigma^2_{f1} = \left[\frac{n1on}{n3off^2} + \frac{n1on^2}{n3off^3} \right] \quad \text{since } \sigma^2(n1on) = n1on \text{ etc.} \tag{5.15}$$

Similarly,

$$\sigma^2_{f2} = \left[\frac{n1off}{n3on^2} + \frac{n1off^2}{n3on^3} \right] \tag{5.16}$$

Hence the error in X, the estimate of the signal strength, is calculated from the event totals using the above relations.

5.3.2. Advantages and Disadvantages

The major advantage of this method is that it makes no assumptions about the dependency of count rate on zenith angle or even variations in sky clarity. All it assumes is that the ratio of channel sensitivities remains constant despite varying observing conditions. The technique allows full use of all channel 1 and channel 3 events. However, to make the events counted by channel 1 and channel 3 comparable, no rejection of events triggering more than one channel is possible. Also, it depends on the assumption of a constant sensitivity ratio.

5.4. Fitting Methods

5.4.1. Outline of Methods

This method involves fitting functions to plots of on and off source count rates against zenith angle. The two channels that point at the source are analysed individually to make sure the sensitivity is the same on and off source. The total number of events recorded in a two minute segment from a channel is considered as a data point on a count rate versus zenith angle graph. The same function is fitted separately to the on source and then the off source data points from the channel being considered. If there is a steady excess on source, this should be reflected in the coefficients of the two fits. The value of the two fits for a given zenith angle are then calculated. The signal strength can be determined from the difference between them.

Two different types of function have been used for fitting

purposes. Macrae (1985) gives the functional relationship between the count rate of a Cerenkov detector and zenith angle as

$$\text{count rate } \alpha \cos^{2.35}(\text{zenith angle})$$

$$\Rightarrow \quad \log(\text{count rate}) \alpha \log(\cos(\text{zenith angle})) \qquad (5.17)$$

Hence, a linear fit of log(count rate) against log(cos(zenith angle)) should be a good choice of functions. The other type of function used for this method is a third order polynomial. Third order polynomials were chosen as they were found empirically to give the smoothest fit. An orthogonal polynomial set was chosen since the covariances of the coefficients are zero. Thus, calculating the overall error is relatively straightforward, since the errors on the coefficients are independent. Chebyshev polynomials were chosen since they produce the fit with the least maximum error in the interval between the end data points.

5.4.2. Advantages and Disadvantages

This method uses channel 1 data only in order to maintain constant detector sensitivity. This has the advantage of allowing full off source event rejection. If the dependence of the count rate on zenith angle follows a power law of cos(zenith angle) or can be approximated to a third order polynomial in zenith angle, then this method should be able to eliminate the effect.

Using only channel 1 data has the disadvantage that half the data has been 'wasted'. Another possible problem is that the count rate – zenith angle relation may not be well fitted by either of the functions used; either because of the esentially

random nature of the background and the finite number of events collected or because the true relation is not well approximated by the functions.

5.5. Data Simulation

To test the effectiveness of analysis programs that use the techniques outlined in the last few sections, it is necessary to generate simulated data files.

To specify the output file characteristics, the user must input to the simulation program the count rate at zero zenith angle; the signal strength; the period of the signal; the time from the start of the run to transit of the hypothetical source; the duration of the run; the declination of the hypothetical source; and the output filename. The program produces a background event and a signal event. It then compares the times of the two and writes the earlier one to the output data file. A replacement is generated for the event written to the file and the comparison is repeated. Events are generated only in channels 1 and 3. Hence, no enhancement of the dataset by event rejection is possible (see section 5.6.2).

Data simulation relies on the generation of pseudo-random numbers by the computer used. Thus, the quality of the simulations is dependent on the quality of the random number generator. This was tested in two ways. The first approach was to generate sets of 10^3 numbers and bin them into 10 equally spaced bins according to size. This was done 10^3 times and the variances

of the totals in each bin noted. The expected mean population variance is 100. When the above process was repeated 100 times, involving the generation of a total of 10^8 numbers, the observed mean variance was 100·2114. The mean value of the generated numbers, converted to integers in the range from 1 to 10 was 5·499697. The second approach was to plot 50,000 pairs of random numbers and check visually whether a pattern was present. To check whether the generator produced a small 'cycle' of numbers, this was repeated with the first and second numbers modulo n, where n was an integer varied from 3 to 13. No pattern was observed on any of these plots (see fig 5.3). It was concluded that the random number generator had no obvious defects and was good enough for the task it was intended to perform.

A poissonian background is simulated by calculating the interval to the next background event using

$$\text{interval} = -(1/\text{rate})\log(\text{rnd1}) \qquad (5.18)$$

where rnd1 is a random number which can take values from 0 to 1 and rate is the count rate that was current for the last event time. The current rate is calculated from

$$\text{rate} = r_0 \cos^{2.35}(\text{zenith angle}) \qquad (5.19)$$

where r_0 is the rate at zero zenith angle, a figure which is supplied by the user when running the program. All signals generated are periodic to allow the output data files to be checked using reliable periodic analysis programs during the development of the simulation program. The interval between the last signal event and the next is calculated using a similar
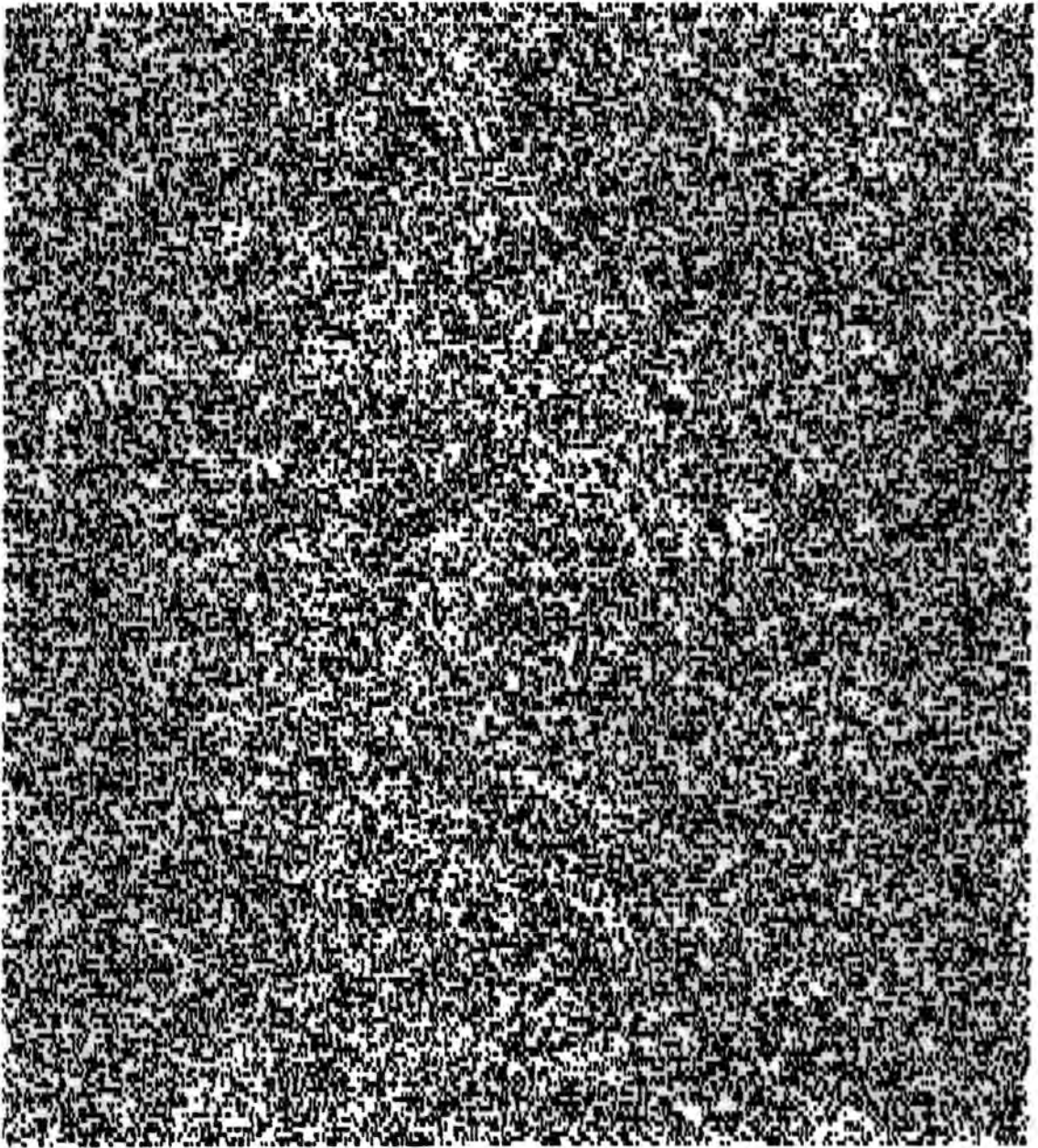
Figure 5.3 Pairs of random numbers plotted as x, y coordinates

relation to that used for background events, with the 'signal rate' replacing the background rate. The resulting event time is then rounded to the nearest whole period. This should not affect the distribution of signal events provided the period used is very much less than the average interval between events.

A χ^2 test was performed on a file produced with the zenith angle variation disabled to test the null hypothesis that the counts were distributed in accordance with poisson statistics. This produced a value of 20.86 for 20 degrees of freedom, indicating that the null hypothesis was quite acceptable.

5.6. Results from Simulated Data

Files were generated with signal strengths of 5%, 3%, 2%, and 1%. For each signal strength, 20 3-hour files were generated, which is typical of a long exposure on a source. The files ended at culmination at zero zenith angle. Thus, they cover a wide range of zenith angles and the zenith angle changes rapidly, providing as severe a test as possible for the analysis methods. The results from the various analysis techniques are summarised in tables 5.1 to 5.4.

RESULTS FROM VARIOUS DC ANALYSIS PROGRAMS ON SIMULATED DATA CONTAINING 5 % SIGNAL

File Number	'Counting heads' %	Ratios Method %	Log Fit %	Polynomial Fit %
1	4.9 ± 1.6	4.7 ± 1.6	6.9 ± 3.3	7.1 ± 10.4
2	5.1 ± 1.6	4.7 ± 1.6	11.8 ± 3.3	3.2 ± 10.7
3	7.7 ± 1.6	7.0 ± 1.7	8.9 ± 3.4	6.0 ± 10.6
4	3.8 ± 1.6	3.2 ± 1.6	0.0 ± 3.4	6.8 ± 10.7
5	6.8 ± 1.6	6.3 ± 1.7	5.7 ± 3.3	2.7 ± 10.8
6	7.4 ± 1.6	7.3 ± 1.7	9.2 ± 4.0	3.7 ± 10.6
7	10.3 ± 1.6	10.1 ± 1.7	14.1 ± 3.4	13.6 ± 11.1
8	6.1 ± 1.6	5.6 ± 1.6	4.2 ± 3.7	1.7 ± 10.5
9	6.7 ± 1.6	6.4 ± 1.7	5.9 ± 3.0	5.6 ± 10.5
10	6.3 ± 1.6	6.3 ± 1.7	10.6 ± 3.3	12.8 ± 10.8
11	3.5 ± 1.6	3.5 ± 1.6	0.9 ± 3.6	5.0 ± 11.0
12	2.0 ± 1.6	2.2 ± 1.6	3.0 ± 3.0	3.0 ± 10.6
13	4.3 ± 1.6	3.4 ± 1.6	3.0 ± 4.0	1.7 ± 10.8
14	1.3 ± 1.6	1.1 ± 1.6	1.8 ± 4.2	-6.7 ± 9.8
15	6.2 ± 1.6	5.6 ± 1.6	1.4 ± 3.7	1.9 ± 10.6
16	3.8 ± 1.6	3.5 ± 1.6	3.9 ± 3.4	4.4 ± 10.6
17	2.7 ± 1.6	2.2 ± 1.6	-0.9 ± 3.1	0.9 ± 10.6
18	3.3 ± 1.6	3.5 ± 1.6	8.2 ± 3.5	9.1 ± 10.9
19	7.8 ± 1.6	7.4 ± 1.7	14.7 ± 3.2	12.5 ± 11.5
20	7.3 ± 1.6	7.0 ± 1.7	5.4 ± 3.9	6.6 ± 10.8
Average	5.37 ± 0.36	5.05 ± 0.37	5.9 ± 0.8	5.08 ± 2.37

Table 5.1

RESULTS FROM VARIOUS DC ANALYSIS PROGRAMS ON SIMULATED DATA CONTAINING 3 % SIGNAL

File Number	'Counting heads' %	Ratios Method %	Log Fit %	Polynomial Fit %
1	4.1 ± 1.6	3.8 ± 1.6	3.1 ± 3.5	4.0 ± 10.2
2	3.8 ± 1.7	3.7 ± 1.6	11.5 ± 3.3	10.5 ± 11.5
3	1.1 ± 1.6	0.9 ± 1.6	-2.7 ± 2.9	-3.5 ± 10.2
4	5.6 ± 1.7	5.2 ± 1.6	7.4 ± 3.6	3.9 ± 11.0
5	4.5 ± 1.7	4.0 ± 1.6	-0.8 ± 3.6	-3.6 ± 10.7
6	3.4 ± 1.6	3.5 ± 1.6	2.1 ± 3.6	0.3 ± 10.8
7	1.0 ± 1.6	0.7 ± 1.6	3.7 ± 2.8	1.7 ± 10.9
8	4.3 ± 1.6	4.0 ± 1.6	6.4 ± 3.8	1.4 ± 10.6
9	6.0 ± 1.7	5.9 ± 1.7	9.5 ± 3.5	5.6 ± 11.0
10	3.4 ± 1.6	3.4 ± 1.6	3.5 ± 3.2	1.9 ± 10.5
11	2.1 ± 1.6	2.3 ± 1.6	3.0 ± 3.2	5.9 ± 10.9
12	0.0 ± 1.6	-0.2 ± 1.6	-0.4 ± 3.6	-3.7 ± 10.4
13	2.3 ± 1.6	2.1 ± 1.6	3.5 ± 3.7	-1.2 ± 10.5
14	1.3 ± 1.6	1.4 ± 1.6	2.7 ± 3.2	9.5 ± 11.1
15	4.5 ± 1.6	4.5 ± 1.6	6.4 ± 3.1	10.6 ± 11.2
16	4.7 ± 1.6	4.0 ± 1.6	9.6 ± 3.1	11.8 ± 11.2
17	-0.1 ± 1.6	0.4 ± 1.6	0.4 ± 3.4	1.1 ± 10.9
18	5.2 ± 1.7	5.0 ± 1.7	0.4 ± 3.8	0.6 ± 10.8
19	4.3 ± 1.6	4.4 ± 1.6	3.0 ± 3.0	3.2 ± 10.8
20	5.7 ± 1.7	5.0 ± 1.6	2.3 ± 3.5	0.8 ± 10.8
Average	3.36 ± 0.36	3.20 ± 0.36	3.73 ± 0.76	3.04 ± 2.42

Table 5.2

RESULTS FROM VARIOUS DC ANALYSIS PROGRAMS ON SIMULATED DATA CONTAINING 2 % SIGNAL

File Number	'Counting heads' %	Ratios Method %	Log Fit %	Polynomial Fit %
1	1.9 ± 1.6	2.4 ± 1.6	-0.3 ± 3.9	-4.6 ± 10.3
2	2.7 ± 1.6	2.7 ± 1.6	-1.0 ± 3.6	-0.2 ± 10.6
3	2.7 ± 1.6	2.5 ± 1.6	1.2 ± 3.2	9.8 ± 10.8
4	0.0 ± 1.6	-0.1 ± 1.5	-4.9 ± 3.5	-5.1 ± 10.2
5	5.6 ± 1.6	5.5 ± 1.7	8.2 ± 2.9	6.7 ± 10.8
6	5.1 ± 1.7	5.1 ± 1.6	1.5 ± 2.8	0.4 ± 10.7
7	-0.6 ± 1.7	-0.3 ± 1.6	-1.9 ± 3.9	-5.1 ± 10.8
8	3.9 ± 1.6	4.1 ± 1.6	3.0 ± 3.4	4.5 ± 10.8
9	1.7 ± 1.6	1.6 ± 1.6	6.2 ± 3.2	3.0 ± 10.9
10	4.1 ± 1.7	4.4 ± 1.6	7.1 ± 3.8	3.2 ± 10.8
11	1.8 ± 1.6	1.3 ± 1.6	-2.5 ± 3.2	2.1 ± 10.6
12	-0.5 ± 1.6	-0.3 ± 1.5	-3.1 ± 3.6	3.7 ± 10.7
13	2.2 ± 1.6	1.9 ± 1.6	-1.0 ± 3.5	-4.3 ± 10.3
14	4.3 ± 1.7	4.4 ± 1.6	4.2 ± 3.6	4.9 ± 11.5
15	-0.1 ± 1.6	-0.4 ± 1.6	-2.0 ± 3.8	-4.0 ± 10.2
16	3.3 ± 1.7	4.0 ± 1.6	5.1 ± 3.5	4.4 ± 11.1
17	1.7 ± 1.7	1.4 ± 1.6	0.8 ± 3.6	1.0 ± 10.8
18	6.2 ± 1.7	6.2 ± 1.7	2.2 ± 3.3	5.7 ± 11.1
19	1.8 ± 1.6	1.6 ± 1.6	1.9 ± 3.4	-1.8 ± 10.7
20	-0.1 ± 1.6	-0.2 ± 1.6	0.7 ± 3.5	6.9 ± 10.9
Average	2.39 ± 0.36	2.39 ± 0.36	1.27 ± 0.78	1.56 ± 2.40

Table 5.3

RESULTS FROM VARIOUS DC ANALYSIS PROGRAMS ON SIMULATED DATA CONTAINING 1 % SIGNAL

File Number	'Counting heads' %	Ratios Method %	Log Fit %	Polynomial Fit %
1	1.2 ± 1.6	1.0 ± 1.6	-1.7 ± 3.4	-1.3 ± 10.6
2	1.5 ± 1.6	1.6 ± 1.6	3.2 ± 3.9	8.1 ± 11.0
3	-2.9 ± 1.6	-3.0 ± 1.5	-2.3 ± 2.8	-5.5 ± 10.4
4	-0.3 ± 1.6	-0.2 ± 1.6	2.4 ± 3.6	-2.6 ± 10.1
5	-1.2 ± 1.6	-0.8 ± 1.6	-5.8 ± 3.8	-2.9 ± 10.8
6	1.0 ± 1.6	1.1 ± 1.6	-4.8 ± 3.3	2.6 ± 10.5
7	0.3 ± 1.6	0.5 ± 1.5	10.5 ± 4.0	3.0 ± 10.7
8	2.3 ± 1.7	2.6 ± 1.6	7.6 ± 3.7	7.1 ± 11.0
9	1.6 ± 1.6	1.0 ± 1.6	-2.1 ± 3.5	-4.8 ± 10.4
10	1.4 ± 1.7	0.7 ± 1.6	-2.4 ± 3.6	-0.7 ± 11.3
11	0.3 ± 1.6	0.6 ± 1.6	5.0 ± 3.5	-1.7 ± 11.0
12	1.5 ± 1.6	1.0 ± 1.6	4.7 ± 3.9	3.4 ± 10.9
13	0.2 ± 1.6	0.3 ± 1.5	0.8 ± 3.6	2.2 ± 10.7
14	2.9 ± 1.7	2.4 ± 1.6	5.0 ± 3.5	0.0 ± 10.4
15	5.1 ± 1.7	4.8 ± 1.6	7.0 ± 3.6	11.9 ± 11.4
16	3.4 ± 1.7	2.8 ± 1.7	4.0 ± 4.0	9.7 ± 11.2
17	1.2 ± 1.6	1.4 ± 1.6	1.6 ± 3.8	7.1 ± 10.9
18	1.6 ± 1.6	1.4 ± 1.6	0.8 ± 3.3	-0.5 ± 10.5
19	2.3 ± 1.6	2.7 ± 1.6	-1.8 ± 3.5	-6.4 ± 9.9
20	3.2 ± 1.6	3.4 ± 1.6	3.6 ± 3.7	-1.6 ± 10.9
Average	1.33 ± 0.36	1.27 ± 0.36	2.06 ± 0.81	1.36 ± 2.40

5.7. Comparison of the Various Methods

The Counting Heads method and the Ratios method give comparable results which suggest that they are effective approaches for detecting sources of these strengths from a dataset of this size. Even for a signal strength of 1%, they both give a positive detection significant at the 4σ level.

Both fitting methods are clearly inferior to the simpler techniques, even though one is using the same functional form of zenith angle count rate relation as that used to generate the data. For the 1% signal files, the polynomial fit yields a detection significance of 0.5σ, whilst the log(cos(zenith angle)) fit is not much better at 2.5σ. These two approaches do not seem effective in their aim of compensating for zenith angle effects.

The two simpler techniques give almost identical results throughout. However, they are being performed on a dataset containing exclusively events that fire one channel. Real data will contain events that fire more than one channel. These would normally be rejected for the purposes of analysis of tracked data (see section 3.1), since this rejection improves the signal to noise ratio and has been observed to improve the statistical significance of any detection (Brazier et al., 1989a). This is still possible for the counting heads method, but not for the ratios method (see section 5.3.1). Hence, for any given real observation, the ratios method is effectively being applied to a file with a much weaker signal and so will give a less significant result. Hence the most effective method to emerge

from this investigation appears to be the 'Counting Heads'
approach.

CHAPTER 6

NON-PULSATING OBJECTS

6.1. Introduction

There are a number of potential V.H.E. γ-ray sources with no
known pulse period. In some cases, such as Scorpius X-1, the
emitting body may well be a pulsar, but a semi-opaque envelope
surrounding the object prevents the observation of   pulsed
emission. In others, such as Centaurus-A, the emission is not
pulsed on a short enough timescale to be detectable, because the
source is an extended one. Detecting V.H.E. emission at a high
level of significance is more difficult, since, apart from the
anisotropy, the signal does not differ from the background in any
of its other properties. It is therefore necessary to detect an
excess of counts from the region of sky containing the source
candidate compared with the general background. Signal strengths
are of the order of 1% of the background counting rate. This is
much smaller than the statistical fluctuations of the background
in a typical single file.   In this chapter, results of
observations of the 3 most promising V.H.E. source candidates
with no, or no known, pulse period are presented.

6.2. Centaurus A

6.2.1. Background

Centaurus A is the nearest active galaxy. At 5 Mpc, it is about 500 times more distant than a typical galactic source candidate. By inverse square law, the radiation from this object will be attenuated by a factor of about 10^5 more than that from a galactic one. This drawback may, however, be compensated for by a high luminosity in V.H.E. γ-rays due to the very energetic processes occurring in the galactic nucleus.

The radio map of this galaxy shows inner and outer lobes of emission (Moffet, 1966), suggesting that at least two violent explosions have happened in the past. Measurements at 10.7 GHz show that the flux density from Centaurus A increased by a factor of roughly 3/2 between September 1973 and March 1974. Emission then appeared to pass through a minimum in July 1975, which was followed by a second increase later in the year and a subsequent decrease in mid 1976 (Price and Stull, 1973; Beall et al., 1978).

Centaurus A is also a strong source of X-rays. It was observed by many early rocket and balloon experiments (Bowyer et al., 1970; Kellogg et al., 1971; Lampton et al., 1972). Fiegelson et al. (1981) observed an X-ray jet emanating from the centre of the galaxy. The longest set of observations of this source were made by the Vela 5B satellite, which operated for 10 years from 1969 to 1979 (Terrell, 1986). The results of these observations (see fig.6.1) showed that Centaurus A entered an active phase in 1973, which continued for approximately 3 years. During this period, the X-ray flux was about 3 times greater than its former value.
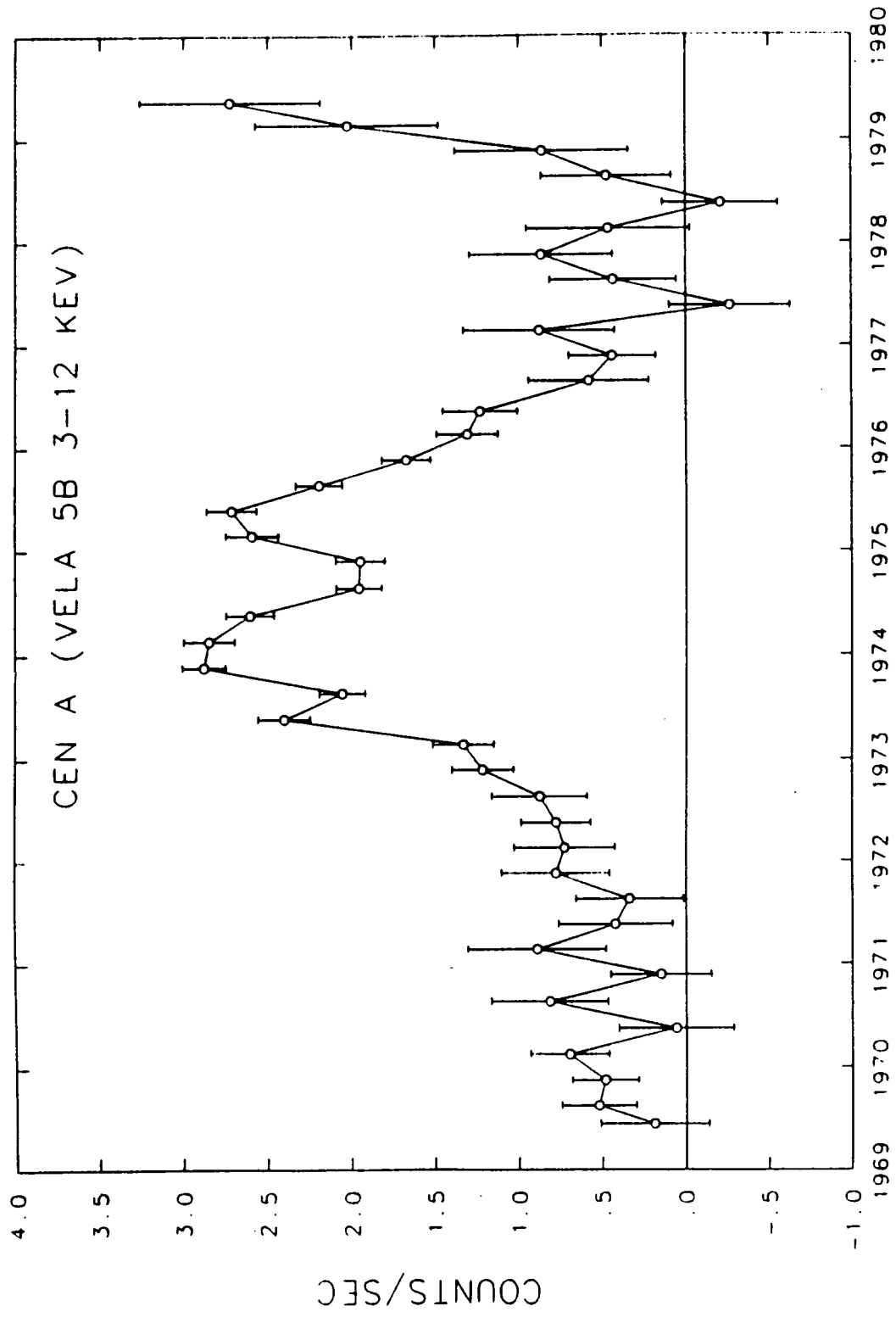
Figure 6.1 Vela 5B measurements of 3-12 keV flux from Cen A
(after Terrell, 1986)

The object then entered a quiet phase until the X-ray flux once more increased at the end of the life of the satellite. This history is confirmed by observations made with other satellites and balloons up to 1977 (Beall et al., 1978). The Vela 5B data also show variability on timescales of days.

Clay et al. (1986) have reported a 2.7σ excess in U.H.E. cosmic ray showers from the direction of Centaurus A. However, the most interesting observations in the context of the current work are those made by Grindlay et al. (1975a). The data were recorded during 1972, 1973 and 1974, using a stellar interferometer as a V.H.E. γ-ray telescope employing the Atmospheric Cerenkov Technique. Over the period of these observations an overall excess, at a similar energy threshold to that of the Mark III, significant at the 4.6σ level was detected, corresponding to a counting rate of 0.66 ± 0.16 photons min^{-1} or a flux of $(4.4 \pm 1)*10^{-11}$ cm^{-2} s^{-1}. The former result is very useful, as it provides an hypothesis to test that is not dependent on the sensitive area or aperture of the telescope or the size of the Cerenkov light pool.

Whilst extragalactic objects are not normally good candidates for detectable sources of V.H.E. emission, Centaurus A is exceptional in many ways. It is a relatively close neighbour of our galaxy; it is the site of extremely energetic processes; and it has been detected in the energy range to which our telescope is sensitive, providing a particularly simple consistency test. This combination of factors makes it a very interesting object to observe.

6.2.2. Data and Results

Observations were made on 25 nights between March 29th 1987 and April 20th 1988. A total of 90 hours of data were collected. Table 6.1 gives the observing log. Selecting only those observations made under clear, stable skies, produces a subset of 44 hours. All these observations were made in 1988.

Using the measurement of Grindlay et al. (1975a), we should expect a total of 1736 ± 421 γ-ray events from our 2631 minutes of data. The results from our observations are shown in table 6.2. Combining the totals for channels 1 and 3 yields an excess on source of 25 ± 504 events, where the error is calculated using the method given in section 2.3. This is equivalent to an average rate of 0.01 ± 0.19 events min^{-1}. Thus, there is no significant excess for the duration of the observations, corresponding to a 3σ limit of 0.58 ± 0.19 photons min^{-1} or 1512 events in total. The 3σ flux limit is 7.8*10^{-11} cm^{-2} s^{-1} for energies above 300 GeV.

During 1988, when the observations were made, only channels 1 to 4 contributed to the fire pattern, seriously limiting the sensitivity of channel 3 (see section 5.3.2). Considering channel 1 only, therefore, there are 52443 events on source and 52469 events off source. This corresponds to a 3σ flux limit for this channel alone of 1.5*10^{-10} cm^{-2} s^{-1}.

6.2.3. Conclusions

The flux limit given in the preceding section appears

DATE	OBSERVATION LENGTH (MIN)
1987 Mar 29	213
1987 Apr 2	225
1987 Apr 3	232
1987 Apr 5	306
1988 Feb 14	181
1988 Feb 16	225
1988 Feb 20	234
1988 Feb 21	250
1988 Feb 22	199
1988 Feb 23	221
1988 Feb 27	170
1988 Mar 15	160
1988 Mar 16	230
1988 Mar 17	293
1988 Mar 18	400
1988 Mar 20	87
1988 Mar 21	59
1988 Mar 22	184
1988 Mar 24	287
1988 Mar 25	234
1988 Mar 26	211
1988 Apr 12	60
1988 Apr 14	143
1988 Apr 20	224

Table 6.1. The Centaurus A observing log.

Date	Events ON	Events OFF	ON-OFF	ON-OFF (min^{-1})
1988 Feb 14	8380	8449	−69	−0.38
1988 Feb 16	12219	12082	137	0.61
1988 Feb 20	12080	11949	131	0.56
1988 Feb 21	12367	12425	−58	−0.23
1988 Mar 15	6915	6957	−42	−0.26
1988 Mar 17	13108	13352	−244	−0.83
1988 Mar 18	16625	16504	121	0.30
1988 Mar 24	10477	10458	−11	−0.04
1988 Mar 25	7951	8010	−59	−0.25
1988 Apr 14	16553	16356	188	1.31
1988 Apr 20	10361	10430	−69	−0.31
TOTAL	127006	126981	25	9.5×10^{-3}

Table 6.2. The number of events in the on-source and off-source categories during each of the observations made under clear and stable conditions.

compatible with the flux measurement of Grindlay et al. (1975a), but, for reasons given earlier (section 3.2.3), comparing fluxes from different telescopes is unreliable. However, the photon counting rate measurement given by Grindlay et al. does not suffer from this disadvantage. The well-known z-test (Freedman et al., 1978) was applied to test the null hypothesis that our value of 0.01 ± 0.19 was compatible with Grindlay et al.'s value of 0.66 ± 0.16. The result of this is that there is only a 0.9% chance that the two are indeed compatible, representing a rejection at the 2.6σ level. This may not appear to be a very significant result, but since the original effect was only significant at the 4.6σ level and has a large standard error, the significance with which the hypothesis of compatibility can be rejected can never be greater than 4.1σ, even if an infinite dataset containing no signal were used.

Centaurus A is known to show long-term variability in both radio and X-rays. Looking again at the results from Vela 5B (see fig. 6.1), it can be seen that previous V.H.E. observations were made during or shortly after a prolonged X-ray outburst, when the flux was at about 3 times its former value. In his model, Grindlay (1975) suggests that synchrotron emission is responsible for the detected X-ray flux and that higher energy emission is produced by inverse Compton scattering of these photons with the same high energy particles producing the synchrotron emission. If this is the case, then X-ray and V.H.E. emission must emanate from the same source volume. No X-ray data are available for the period of our observations, but preliminary results of an

observation of this source made by Ginga show that Centaurus A was in a low X-ray state in March 1989 (Inoue, private communication, 1989). This suggests that X-ray emission was low during our observation. Hence our result tends to support the idea that the X-ray and V.H.E. γ-ray emission may be related.

6.3. Supernova 1987a In The Large Magellanic Cloud

6.3.1. Background

On the 23rd of February, 1987, the blue B-type supergiant Senduleak -69 202 in the Large Magellenic Cloud went supernova (Shelton, 1987). It has since been studied extensively at many wavelengths.

A prompt neutrino burst was reported by three experiments, although only two of these were simultaneous. The Mont Blanc Neutrino Observatory observed a burst of neutrinos (Castagnoli, 1987a,b) 5 hours before simultaneous detections by the Kamiokande II collaboration (Koshiba, 1987; Hirata et al., 1987) and the IMB collaboration (Svoboda, 1987; Bionta et al., 1987).

About eighteen hours after the simultaneous neutrino bursts, the supernova was detected optically (Shelton, 1987). It reached 5th magnitude within a day and peaked at visual magnitude 2.8 around the 20th of May (Hamuy and Phillips, 1987). Since then, optical luminosity has decayed nearly exponentially, with a mean life of somewhere between 100 and 111 days (Catchpole et al., 1987). This provides support for the theory that the main energy source is radioactive decay of ^{56}Co, which has a mean life of

111.26 days. Early ultra violet observations made with the IUE show that the initial photosphere temperature was high, in excess of 14,000 K, whilst the initial radius of the star was small, ~10 solar radii (Panagia et al., 1987).

A radio outburst was detected from the supernova 2 days after the optical flare-up (Turtle et al., 1987). Hard X-rays were finally detected about 6 months after the initial explosion by the Mir-Kvant Observatory (Sunyaev et al., 1987) and by Ginga (Dotani et al., 1987). At about the same time, the γ-ray spectrometer on NASA's Solar Maximum Mission satellite detected γ-ray lines at 843 keV and 1238 keV, characteristic of ^{56}Co decay (Matz et al., 1988).

Many supernova models (Brezinsky and Prilutsky, 1978; Shapiro and Silverberg, 1979) predict the acceleration of particles to very high energies. Gaisser et al. (1987) suggest a model of SN1987a which involves production of a detectable flux of V.H.E. γ-rays. In the early stages following the core collapse, the envelope of supernova ejecta is opaque to V.H.E. γ-rays (Protheroe, 1987), so any emission in the course of the explosion itself is unlikely to be detectable. The most likely source of detectable V.H.E. γ-rays would be a new, rapidly-spinning pulsar in the supernova remnant. The recent report by Kristian et al. (1989) of a 0.5 ms optical pulsar in SN1987a is very exciting. Clearly, continual monitoring of this object is required, since a pulsar of this sort is a very strong candidate for V.H.E. emission. The time profile of any V.H.E. flux detected will provide important constraints on pulsar and pulsar formation

models.

6.3.2. Data and Results

In the February of 1987, the Mark III telescope in Narrabri was observing PSR0540-69 as part of the planned observing programme. During these observations, Senduleak -69 202 was within the field of view of the central channel (see fig. 6.2). The telescope was operating in tracking mode since the target object was a pulsar. This makes detection of a DC signal quite difficult. It is possible , however, that a strong signal will produce a significant excess of counts in the central channel. At this stage, channels 5, 6 and 7 did not contribute to the fire pattern. Two observations were made on February 18.5 and 20.5, shortly before core collapse. A total of 6108 events was recorded in channel 1, whilst a total of 19951 events was recorded in the other three. After core collapse, observations were made on February 23.4 and 24.4.The corresponding totals were 3810 events in channel 1 and 12834 events in the other three. The ratio of on source to off source events from the observations immediately preceding the explosion is 0.306 ± 0.004. The corresponding ratio for the later observations is 0.297 ± 0.005. There is clearly no significant excess and the 3σ limit to the number of γ-ray photons detected during the second observation is 357 (Orford and Turver, 1988).

Observations of the supernova itself were started in March 1987 and it has been observed at every opportunity since. The
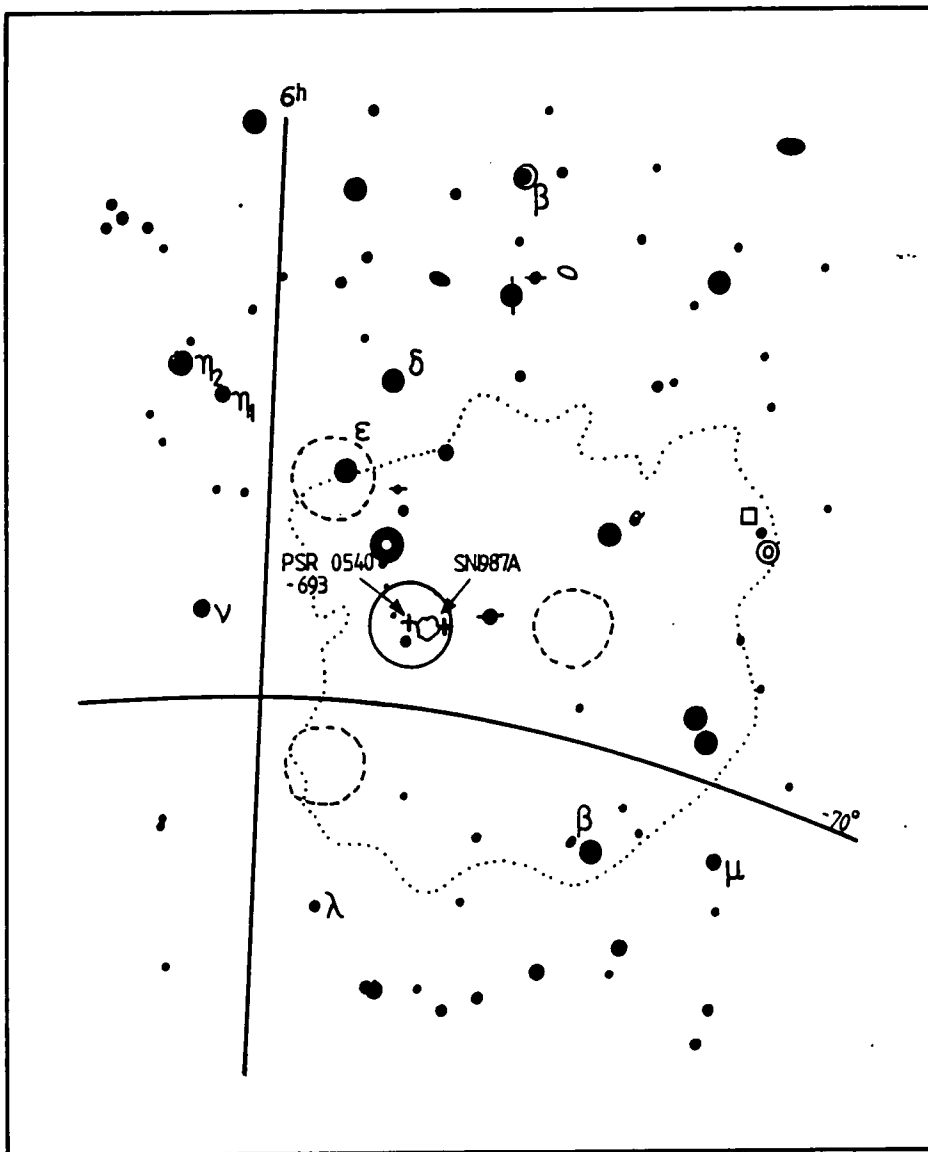
KEY TO STAR MAP.

LARGE MAGELLANIC CLOUD.

FIELD OF VIEW OF THE MARK
II TELESCOPE'S 'ON SOURCE'
CHANNEL.

FIELD OF VIEW OF ONE OF
THE MARK II TELESCOPE'S
'OFF SOURCE' CHANNELS.

Figure 6.2 Sky chart showing PSR 0540, Senduleak 69-202 and the
telescope f.o.v. when observing the former

Date	Duration / mins
22 Mar 1987	240
14 Jan 1988	150
15 Jan 1988	120
18 Jan 1988	210
21 Jan 1988	150
24 Jan 1988	150
11 Feb 1988	160
15 Feb 1988	196
17 Feb 1988	185
19 Feb 1988	187
20 Feb 1988	211
21 Feb 1988	166
22 Feb 1988	137
23 Feb 1988	99
10 Mar 1988	150
19 Mar 1988	150
12 Apr 1988	88
14 Apr 1988	90
15 Apr 1988	25
16 Apr 1988	89
17 Apr 1988	94
07 Sep 1988	120
09 Sep 1988	138
13 Sep 1988	109
14 Sep 1988	112
06 Oct 1988	124
07 Oct 1988	185
09 Oct 1988	193
07 Jan 1989	330
08 Jan 1989	140
31 Jan 1989	159
01 Feb 1989	73
02 Feb 1989	128
08 Feb 1989	176
05 Mar 1989	222
06 Mar 1989	144
07 Mar 1989	150
09 Mar 1989	156
10 Mar 1989	156
12 Mar 1989	150
04 Apr 1989	164
06 Apr 1989	173
08 Apr 1989	152
29 Apr 1989	90
30 Apr 1989	83
01 May 1989	94
02 May 1989	88
04 May 1989	92

Table 6.3 SN1987a Observing Log

Date	Channel 1 On Source	Channel 1 Off Source	Channel 3 On Source	Channel 3 Off Source	Ch. 1 + Ch. 3 On Source	Ch. 1 + Ch. 3 Off Source
14-01-88	2359	2313	3265	3262	5624	5575
18-01-88	3559	3556	4659	4574	8218	8130
24-01-88	2503	2503	2908	2881	5411	5384
11-02-88	2478	2487	3133	3214	5611	5701
15-02-88	3105	3065	3780	3924	6885	6989
17-02-88	2919	2831	3582	3589	6501	6420
19-02-88	2696	2749	3275	3366	5971	6115
20-02-88	2991	3000	3721	3683	6712	6683
21-02-88	2223	2161	2715	2756	4938	4917
22-02-88	1612	1576	1953	1997	3565	3573
23-02-88	1116	977	1327	1384	2443	2361
10-03-88	1669	1704	2121	2173	3790	3877
12-04-88	881	912	1176	1152	2057	2064
14-04-88	1021	1092	1345	1267	2366	2359
16-04-88	672	639	902	865	1574	1504
07-09-88	1771	1765	2043	2167	3814	3932
09-09-88	2133	2194	2561	2551	4694	4745
13-09-88	2251	2292	2766	2742	5017	5034
14-09-88	2111	2092	2548	2555	4659	4647
06-10-88	925	911	1055	1097	1980	2008
07-10-88	969	1054	1400	1491	2369	2545
09-10-88	4184	4076	4972	4894	9156	8970
07-01-89	5874	5822	6509	6519	12383	12341
08-01-89	2500	2412	2851	2821	5351	5233
31-01-89	2341	2304	2341	2338	4682	4642
01-02-89	1075	1035	1136	1137	2211	2172
02-02-89	1886	1880	1998	2021	3884	3901
08-02-89	1532	1477	1594	1550	3126	3027
07-03-89	1615	1556	1704	1693	3319	3249
09-03-89	1592	1648	1673	1672	3265	3320
10-03-89	1722	1649	1621	1680	3343	3329
12-03-89	807	823	794	801	1601	1624
29-04-89	981	990	997	1010	1978	2000
02-05-89	949	943	911	931	1860	1874
04-05-89	1048	1027	1034	994	2082	2021
Totals	70070	69515	82370	82196	152440	151711

Table 6.4 Results of SN1987a Observations

observing season lasts from August to the following April. A summary of the observations made is given in table 6.3. The results of these observations, selecting only those made under clear skies, are given in table 6.4.

The overall excess from channel 1 is 555 ± 373 events, which is significant at the 1.5σ level, whilst the excess from the sum of the channels 1 and 3 is 174 ± 552 events. The channel 1 figure leads to a time-averaged 3σ flux limit from the supernova of $5.5*10^{-11}$ cm^{-2} s^{-1}.

The supernova is not expected to produce a constant flux of γ-rays. Rather, the flux is expected to increase with time as the shell of debris around the putative central pulsar thins and becomes more transparent. It is also likely to fluctuate as whisps of gas move across the line of sight. The variation of any detected V.H.E. flux with time will therefore provide information, not only about energetic processes within the shell, but the nature and development of the shell itself. To examine any time variation the chopped data have ben divided into roughly three-month segments each segment being either the first or second half of the observing 'season' which runs from September to April. The signal strengths from these segments have been plotted in fig. 6.3. Clearly, there is no significant increase in signal over the course of the observations.

There is a discrepancy between the values of the count rate excess from the two channels. This is, of course, caused by the fact that for the majority of observations, only 4 tubes contributed to the "fire pattern" (see section 5.2.2). The change
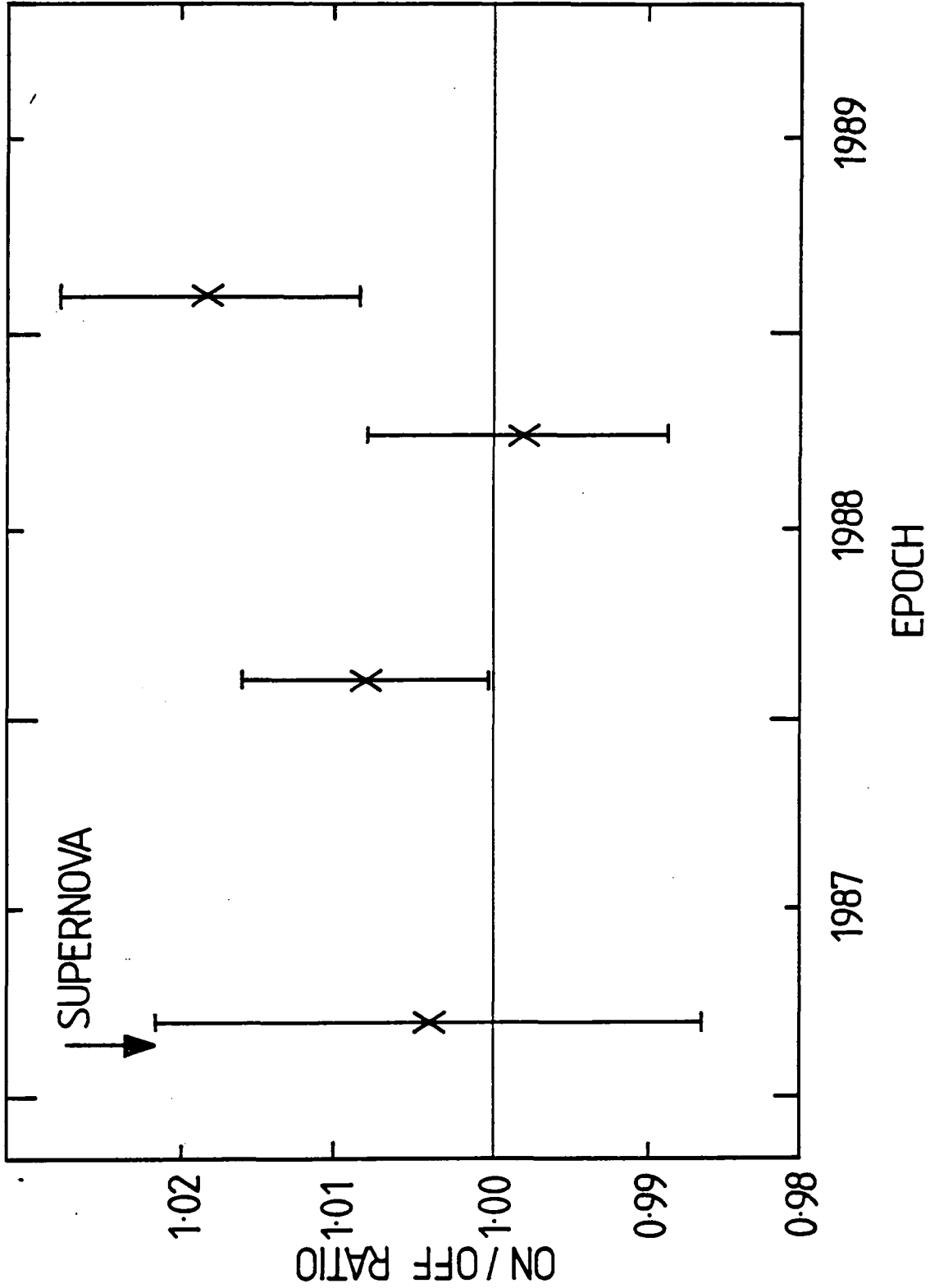
Figure 6.3 Ratios of on-source counts to off-source counts for SN1987a subdivided into 3-month segments.

to a 7-fold fire pattern was made in the latter part of January 1989. The effect of this can be seen in the event totals for channels 1 and 3. Before the change, channel 3 counted at about 1.4 times the rate of channel 1 after rejecting events that fired more than one channel. Afterwards, it counted at only about 1.1 times. Fortunately, this increase in sensitivity occurred shortly before the detection by Kristian et al. (1989) of a submillisecond optical pulsar in the supernova remnant. The data from this period onwards has therefore been examined separately. The excess on source from channel 1 is 356 $\pm$ 217 events, significant at the 1.6σ level. This yields a 3σ flux limit for the interval from the end of January to the beginning of May of $9.8*10^{-11}$ cm^{-2} s^{-1}.

6.3.3. Conclusions

There are two possible explanations for the lack of V.H.E. γ-rays from SN1987a. The first is that there is no central pulsar or that the pulsar is slow, and so incapable of producing such energetic radiation. This would agree with models that suggest that millisecond pulsars are old pulsars spun up by accretion from a now-evaporated companion and that new pulsars are relatively slow (Alpar et al., 1982; Backus et al., 1982). This conflicts with the observation of Kristian et al. (1989). Though the detection of the pulsar was confined to only 1 night in a series of observations and has yet to be confirmed, the significance of the detection puts it beyond question that some

periodic phenomenon was exposed.

The other possible explanation for the lack of γ-rays is that the shell of debris surrounding SN1987a is still opaque to this radiation. If this is the case, then continued observations are essential and will eventually bear fruit. The detection of the optical pulsar and the small excesses from every month of 1989 are very promising signs and suggest that the 1989-1990 observing season should yield a positive detection of this object.

6.4. Scorpius X-1

6.4.1. Background

Scorpius X-1 was the first extrasolar X-ray source to be discovered (Giaconni et al., 1962). It was also the first for which an optical counterpart (v818 Scorpii) was identified (Sandage et al., 1966). It is the brightest continuous X-ray source in the sky. The distance of the object is hard to determine, despite much study over the past 20 years. It is generally assumed to be about 1.5 kpc away. It is a Low Mass X-Ray Binary comprising a neutron star primary and late type secondary in a close orbit. The secondary fills its Roche lobe and is accreting mass onto the primary.

The 0.787 day orbital period of the system was first determined by Gottlieb et al. (1975) from photometric studies. The details of the determination of the orbital elements are complicated and are reviewed by LaSala and Thorstensen (1985). Evidence for modulation of the X-ray emission at the orbital

period is limited, but the X-ray minimum probably lags behind superior conjunction of the optical emission-line source by 0.09 ± 0.06 periods (Priedhorsky and Holt, 1987).

Scorpius X-1 is considered a strong candidate for a millisecond pulsar, though is no clear evidence of a stable period at any wavelength yet. Middleditch and Priedhorsky (1986) suggest 4.53 ms as a possible period, but since there was no evidence of a Doppler shift due to the binary orbit in their data, they reject any association of this periodicity with the rotation of a pulsar. Leahy (1987) reported detection of pulsations at 2.93 ms, but this has not been confirmed and the figure given is not accurate enough to allow us to test it properly.

X-ray binaries are the most common class of V.H.E. γ-ray emitters. Scorpius X-1 is one of the closest and the brightest of the X-ray binaries. Hence, it is a strong candidate for V.H.E. emission and has been the target of an extensive programme of observations.

6.4.2. Data and Results

Scorpius X-1 was observed in 1988 and again in 1989. Between the two sets of observations, the sensitivity of the telescope had been considerably improved by the addition of an extra stage of amplification in the PMT's and the introduction of 7-fold fire patterns (Brazier et al., 1989a). Thus, the two datasets will be treated separately, since they are qualitatively

different and there is no straightforward way of combining them.

In 1988, Scorpius X-1 was observed for a total of 45 hours on 12 nights between 10th May and 19th June. The results of these observations are summarised in table 6.5. The excess on source for channels 1 and 3 summed is 1306 ± 535, which is 0.95 ± 0.38 % of the background. This is significant at the 2.5σ level. Summing events for channel 1 only gives an excess of 1019 ± 332 or 1.85 ± 0.60 %. This is significant at the 3.1σ level. The channel 3 excess is, as expected, smaller at 287 ± 406 events. The totals for channel 1 translate to a γ-ray flux of (1.2 ± 0.4) * 10^{-11} cm^{-2} s^{-1} (see section 3.2.3). There is thus considerable evidence that this object is a source of V.H.E. γ-rays.

To investigate the possibility that the emission is modulated at the orbital period, the data files were binned into 10 phase bins. The results of this are given in table 6.6. Two alternative hypotheses were compared. The first was that the excess was independent of phase. The second was that the excess was 100% sine wave modulated at the orbital period. The likelihood ratio of these two was evaluated. The average ratio of counts on source to counts off source is given by

$$R_0 = \frac{\Sigma N_i}{\Sigma B_i} \qquad (6.1)$$

For a given observation with N counts recorded on source and B off, the likelihood that B and N are sampled from this average ratio is given by the binomial expansion of

Date	Ch 1 On	Ch 1 Off	Ch 3 On	Ch 3 Off	Total On	Total Off
10th May 1988	4462	4382	6000	5857	10462	10239
11th May 1988	4977	4859	4953	4955	9930	9814
12th May 1988	6881	6626	11485	11449	18366	18075
13th May 1988	8226	8128	13498	13201	21724	21329
14th May 1988	3269	3266	5508	5524	8777	8790
6th Jun 1988	2405	2329	2955	2935	5360	5264
7th Jun 1988	1601	1548	2103	2128	3704	3676
12th Jun 1988	6092	6059	8955	9104	15047	15163
15th Jun 1988	2156	2124	3226	3217	5382	5341
16th Jun 1988	5701	5622	8504	8446	14205	14068
18th Jun 1988	4492	4425	6922	6871	11414	11296
19th Jun 1988	5847	5722	8723	8858	14570	14580
Totals	56109	55090	82832	82545	138941	137635

Table 6.5 Scorpius X-1 observations

Date (1988)	Orbital Phase	No of Counts Channel 1		No of Counts Channel 3		No of Counts All		% Strength
		ON	OFF	ON	OFF	ON	OFF	
Jun 6	0.09	2405	2329	2955	2935	5360	5264	+3.3
May 11	0.12	2093	2094	2025	2050	4118	4144	-0.1
May 11	0.22	2884	2765	2928	2905	5812	5670	+4.3
Jun 18	0.31	4492	4425	6922	6871	11414	11296	+1.5
May 12	0.36	2020	1926	3335	3195	5355	5121	+4.9
Jun 7	0.43	1601	1548	2103	2128	3704	3676	+3.4
May 12	0.46	2576	2420	4249	4278	6825	6698	+6.4
May 12	0.56	2285	2280	3901	3976	6186	6256	+0.2
Jun 19	0.60	2958	2878	4438	4531	7396	7409	+2.8
Jun 15	0.64	2156	2124	3226	3217	5382	5341	+1.5
May 13	0.65	1956	2016	3330	3171	5286	5187	-3.0
Jun 19	0.72	2889	2844	4285	4327	7174	7171	+1.6
Jun 12	0.73	3163	3063	4595	4612	7758	7675	+3.3
May 13	0.74	2403	2436	4115	4086	6518	6522	-1.4
Jun 16	0.82	3093	3032	4790	4652	7883	7684	+2.0
May 13	0.83	2282	2183	3736	3644	6016	5827	+4.5
May 10	0.84	1877	1868	2479	2378	4356	4246	+0.5
Jun 12	0.85	2929	2996	4360	4492	7289	7488	-2.2
May 14	0.90	1426	1407	2309	2259	3735	3666	+1.4
May 13	0.92	1585	1493	2317	2300	3902	3793	+6.2
May 10	0.93	2585	2514	3521	3479	6106	5993	+2.8
Jun 16	0.95	2608	2590	3714	3794	6322	6384	+0.7
May 14	0.98	1843	1859	3199	3265	5042	5124	-0.9
Total		56109	55090	82832	82545	138941	137635	

Table 6.6 Scorpius X-1 observations subdivided by phase.

$$\left[\frac{R}{1 + R} + \frac{1}{1 + R} \right]^{N+B}$$

The likelihood under the first hypothesis is found by putting $R = R_0$. The maximum likelihood under the modulation hypothesis is obtained by evaluating the above expression using

$$R = 2R_0 \sin(\varphi + \alpha) \qquad (6.2)$$

where φ is the orbital phase and α is a phase offset chosen to maximise the likelihood. The likelihood ratio found using this method is 302, supporting the hypothesis that the emission is 100% modulated at the orbital period at the $3*10^{-3}$ probability level. This probability may be increased by up to a factor of 10 due to the degrees of freedom introduced by the ability to choose the peak of the γ-ray modulation to be in whichever of the 10 phase bins maximises the likelihood. In the worst case, however, the significance is still greater than 2σ. The peak of γ-ray emission occurs at $\varphi = 0.32 \pm 0.08$ relative to superior conjunction of the optical line emitting region as determined by Crampton et al. (1975). The phase distribution of the signal strengths along with the sine wave fitted to them are shown in fig. 6.4.

Observations were made on 3 nights in May 1989, for a total of 10.75 hours. The results are summarised in table 6.7. The sensitivity of channel 3 had been greatly improved compared with the 1988 data by the introduction of 7-fold fire patterns, as can be seen from the ratio of counts from the two channels, which is
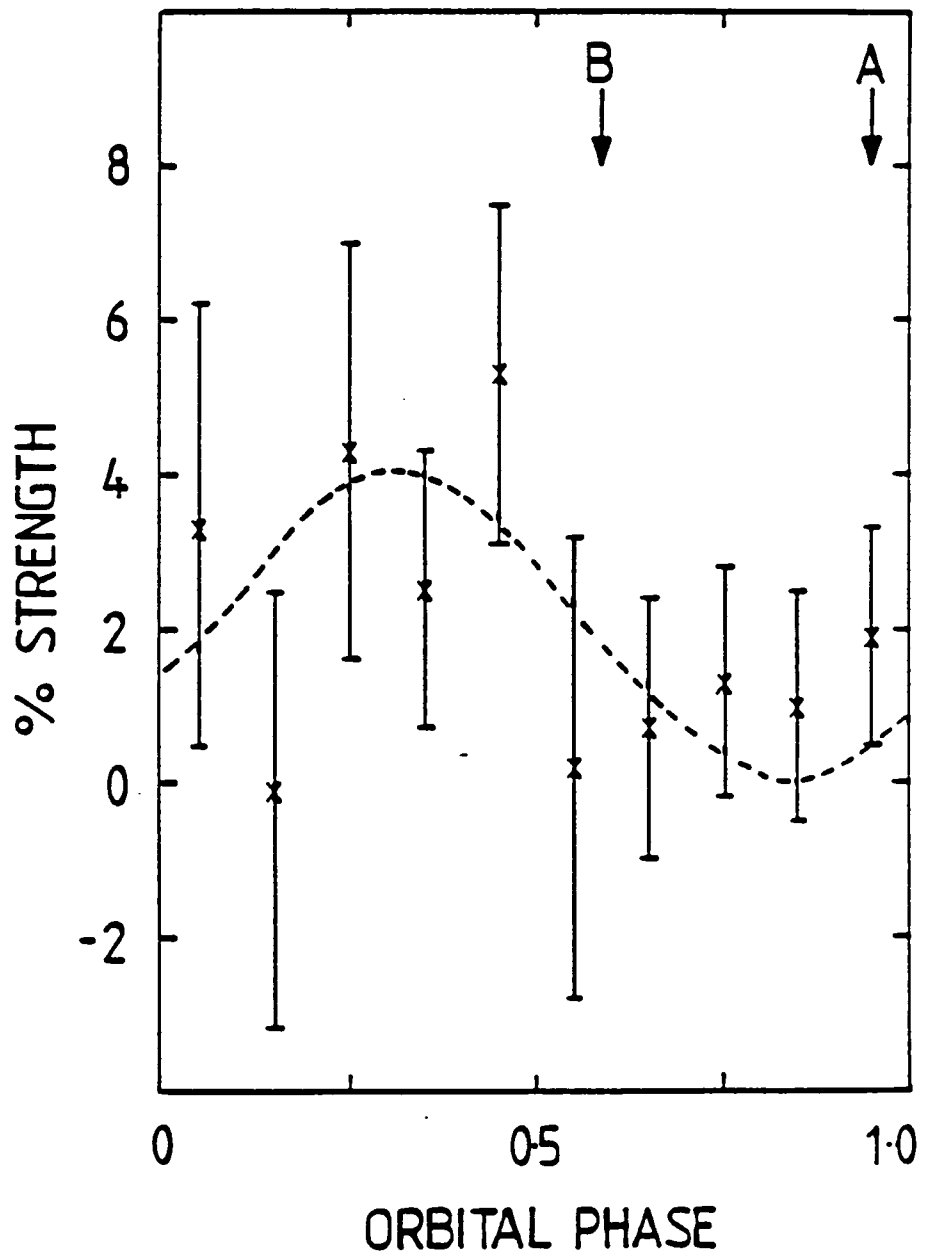
Figure 6.4 Scorpius X-1 signal strengths in 10 bins. A and B are
minima of optical line emission and X-ray emission respectively

Date (1989)	Orbital Phase	No of Counts Principal Channel		No of Counts Secondary Channel		No of Counts All		% Strength
		ON	OFF	ON	OFF	ON	OFF	
May 2	0.32	6854	6876	7073	6671	13927	13547	2.8
May 6	0.40	2250	2179	2209	2093	4459	4272	4.3
May 8	0.90	1797	1772	1872	1789	3669	3561	3.0
Total		10901	10827	11154	10553	22055	21380	
Excess		0.7%		5.7%		3.1%		
		0.5σ		4.1σ		3.3σ		

Table 6.7. Scorpius X-1 1989 data

not far from unity for the 1989 data. Hence, the data from channel 3 are almost as reliable as the data from channel 1 and most efficient use of the data is made by summing the events for both channels. For these nights alone, the excess is 675 ± 207 events, a signal strength of (3.2 ± 1.0) %. This represents confirmation of the 1988 result at the 3.3σ significance level. It is not possible to use the 1989 data to investigate further the possible orbital modulation, since the observations were deliberately chosen to have phases near the phase of maximum emission found from the 1988 data. Also, if the orbital dependence is real, the 1989 data would be modulated with a greater amplitude than the 1988 data, due to the increased sensitivity of the telscope in 1989.

Searches were made for periodicity in the data using a Rayleigh test over a range of periods around 2.93 ms as suggested by Leahy (1987) and around 4.53034 ms as suggested by Middleditch and Priedhorsky (1986). Since Scorpius X-1 is a binary system, any pulsed emission will be subject to Doppler shifting due to the orbital motion of the pulsar. The orbital parameters of the system need to be well known if this is to be compensated for in period searches. Whilst the orbital period of this object has been accurately measured, the size of the system is not so well known. Line emission measurements (LaSala and Thorstensen, 1985) suggest a value of $a\sin i^{\dagger}$ of the order of a few light seconds, which would make it impossible to find a single pulse period of a few milliseconds in a search throughout the orbit. Tests have therefore been run on each night individually. The results of

† i is orbital inclination and a is body separation

95

these tests on the night showing the strongest on source count excess whilst still short enough to prevent a periodic signal being too distorted by orbital motion are shown in figs. 6.5 and 6.6. There is no evidence for significant pulsed emission from any night, leading to a 3σ 'time-averaged' flux limit for pulsed emission of $\sim 2.6 * 10^{-10}$ cm^{-2} s^{-1}.

6.4.3. Conclusions

Previous V.H.E. γ-ray observations of Scorpius X-1 using the Nooitegedacht telescope suggested a flux of $1.7 \pm 0.2 * 10^{-10}$ cm^{-2} s^{-1} at energies greater than 1000 GeV (De Jager et al., 1986). However, the telescope was operating without background light stabilisation, as provided for the Mark III by the AGC system (see chapter 2). This means that a positive detection must be based on correcting the count rate for varying background light levels. Our measurements show a time-averaged signal strength of 1.85 ± 0.60 %, which translates to a γ-ray flux of $1.2 \pm 0.4 * 10^{-10}$ cm^{-2} s^{-1} at energies greater than 400 GeV. This translates to a flux of $2.8 \pm 0.9 * 10^{-11}$ cm^{-2} s^{-1} in the energy range of the South African instrument. The discrepency in these measurements is not as important as it appears, bearing in mind the uncertainties in the South African measurements and the difficulty of comparing fluxes from different experiments (see section 3.2.3).

Assuming the distance to Scorpius X-1 is 1.5 kpc, the V.H.E. luminosity of this object is $2.3 \pm 0.7 * 10^{34}$ erg s^{-1}. We have

Figure 6.5 Plot of Rayleigh probability of chance occurrence against trial periods in the region of 4.5ms for Sco X-1

The overall probability allowing for all degrees of freedom is 0.3
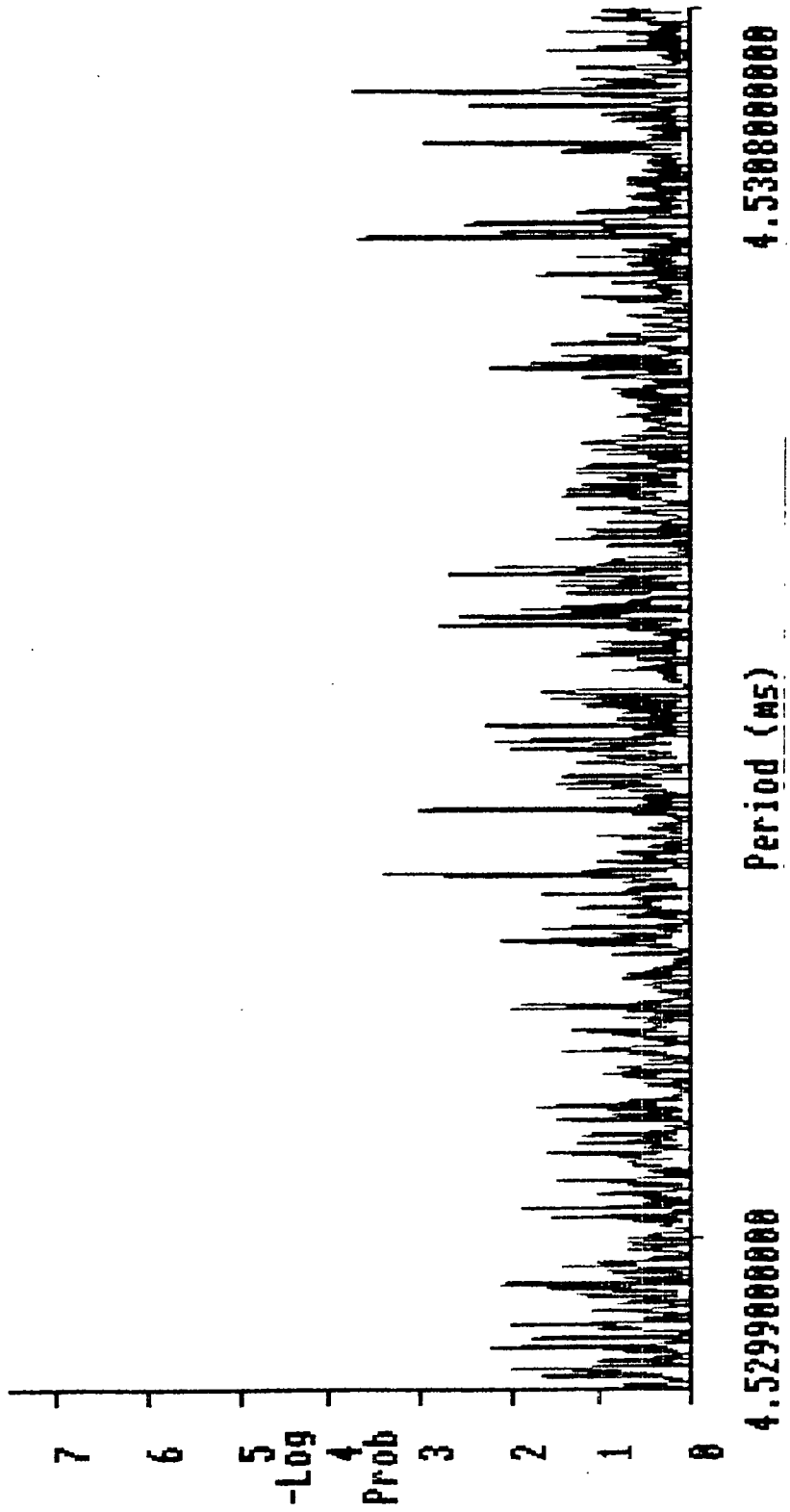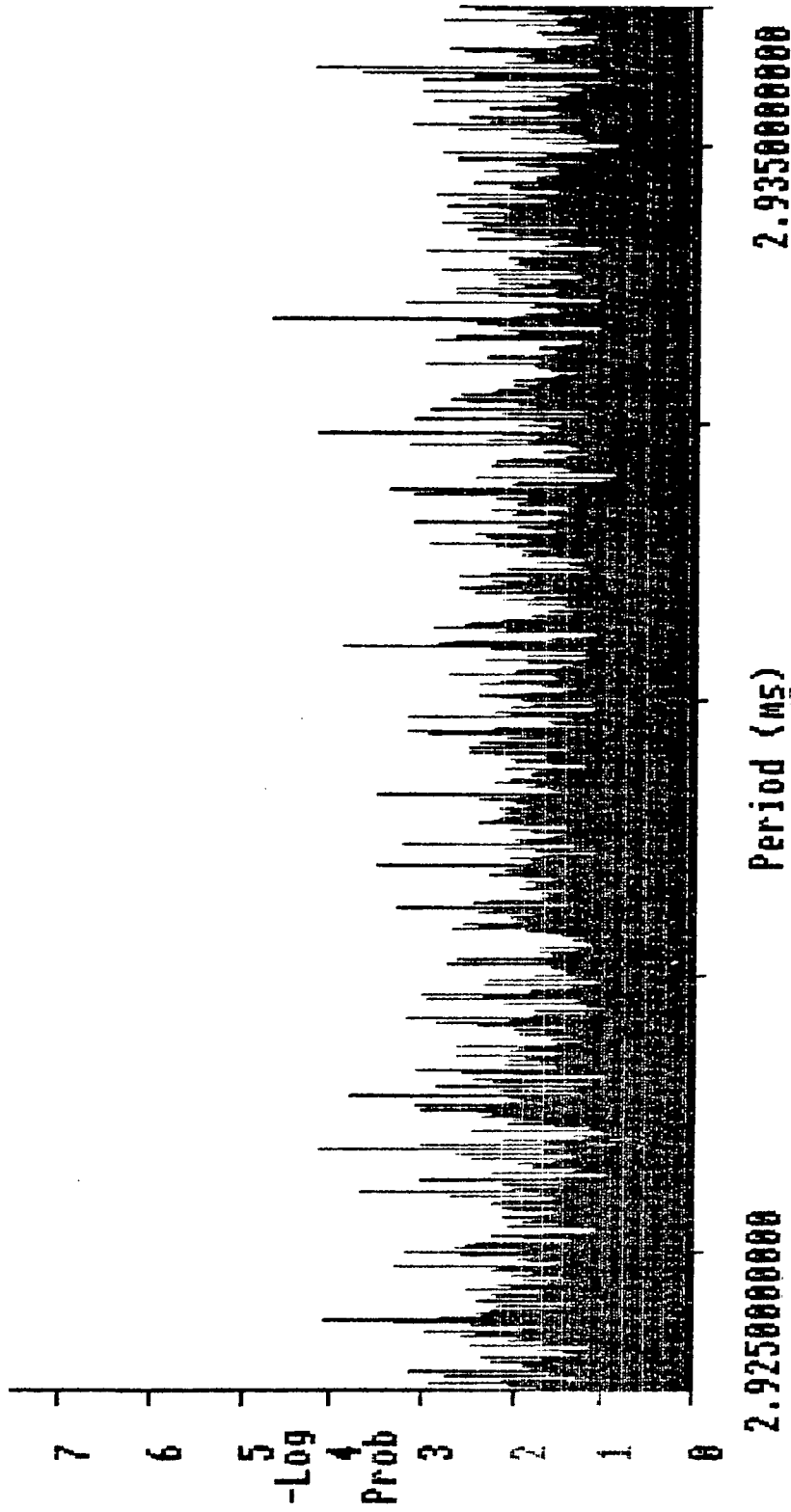
Figure 6.6 Plot of Rayleigh probability of chance occurrence against trial period in the region of 2.93ms for Sco X-1

The overall probability allowing for all degrees of freedom is 0.7

found evidence at better than the 2σ level that this is 100% modulated with the 0.878 day orbital period. The phase of γ-ray emission is not obviously related to the phase of maximum emission at other wavelengths. If the V.H.E. γ-rays we have detected are generated by a beam of relativistic particles in the region of a pulsar, the emission is likely to be periodic at the period of the pulsar. No convincing or accurate period has been found for this object. If and when this is achieved, there is a good chance of an extremely significant detection in the V.H.E. region.

CHAPTER 7

SUMMARY AND CONCLUSIONS

7.1. Isolated Pulsars

Few isolated pulsars have been positively detected as sources of V.H.E. γ-rays. However, the Crab, Vela and a few others have all been reported as sources at different times by different groups, at varying levels of significance.

Of the above, only the Crab is widely accepted as a source of V.H.E. γ-radiation. No evidence for emission was found in the 1988 observations made with the Mark IV telescope, but the observations were too short to contradict previous positive results from various groups, including this one (Dowthwaite et al., 1984; Gibson et al., 1982; Tumer et al., 1985; C.L. Bhat et al., 1986). More observations of these objects are required before a definite statement can be made about their emission. At time of writing, the Mark IV telescope has just started a second observing season at La Palma, running from June to October 1989. This may well furnish the necessary data.

The Vela pulsar has now been extensively observed with the Mark III telescope. No significant emission has been found from any of our observations. This is in conflict with the reports of P.N. Bhat et al. (1980,1986,1987) and Gupta et al. (1982). However, there are problems with these claims. For a full

discussion of them, see Chadwick (1987). The large radio period glitch observed at the end of 1988 has not been followed by a period of detectable V.H.E. γ-ray emission. To change our flux limit significantly would require at least as much data as we have already taken. Hence, there are no plans to re-observe this object.

There are no reports of V.H.E. γ-ray emission from PSR 1055-52. Our negative result stands alone, therefore. There is thus no reason to re-observe this object yet.

PSR 1509-58 has been observed for a total of about 38 hours. No evidence for emission from this object has been found. This is in conflict with the claims of De Jager et al. (1988) and Nel et al. (1989). However, there are serious doubts about these results (see section 4.5.2). Given the amount of data that would be required to make any significant difference to the flux limit we have measured so far, there is little benefit to be gained in re-observing this object in the near future.

7.2. Non-Pulsating Objects

7.2.1. New Analysis Techniques

It is clear from the results of the simulations shown in chapter 5 that the 'counting heads' method is superior to the fitting methods tested. Indeed, considering that one of the fits used a completely correct model of count rate dependence on zenith angle, it seems likely that the 'counting heads' approach would be superior to any fitting method.

Between the 'counting heads' and the 'ratios' methods, the choice is not so clear cut. The results of chapter 5 suggest that for a 4-fold fire pattern, the two tests have similar accuracies. The introduction of 7-fold fire patterns leaves the 'ratios' method unchanged, but greatly enhances the 'counting heads' method, effectively doubling the data it can operate on. Thus, 'counting heads' followed by a maximum likelihood ratio test has become the standard technique for analysis of chopped data.

7.2.2. Results of Analysis

The three DC objects discussed in chapter 6 are representatives of three entirely different classes of object, an active galaxy, a very young supernova remnant and an X-ray binary.

Centaurus A is an active galaxy. It has shown great variability in both its X-ray and its radio emission. The results of our observations suggest that in 1987 and 1988, this object was not emitting V.H.E. γ-rays at the rate measured by Grindlay et al. (1975a). This is not necessarily a problem, given the variability of the object. X-ray data contemporary with our observations are not available, but observations by Tenma (Wang et al., 1986) in 1984 and by Ginga (Inoue, Private Communication) in March 1989 both show that Centaurus A was in a low X-ray state. These two measurements strongly suggest that there was little X-ray activity during the period of our observations. Thus, Grindlay's contention (1975) that the V.H.E. emission and

the X-ray emission are intimately linked is supported by the combination of these X-ray results and our V.H.E. γ-ray measurement. Clearly, any subsequent X-ray outburst would make further observations of this object very interesting. Until such time as this occurs, however, there is little point in continuing to observe this object, since a large amount of data would be required to significantly alter our flux limit or the strength of our rejection of Grindlay et al.'s (1975a) measurement.

SN1987a has shown no significant emission so far. However, it is very young and still evolving rapidly. If there is a central pulsar, which seems possible after the report of Kristian et al. (1989), it is likely to be a source of V.H.E. γ-rays (Gaisser et al., 1987). The object is widely expected to begin to emit detectable γ-rays in the near future. Whilst not formally significant, the fact that the result from every month of 1989 is positive is very encouraging. If the supernova does begin to emit V.H.E. γ-rays, an intensive observing program over the next observing season should show how such emission varies with time. This will provide an insight, not only into high energy processes occurring near the supernova remnant, but also into the nature and development of the surrounding shell of debris. Further observations of this object should be given high priority, therefore.

Scorpius X-1 is an X-ray binary, the class of object responsible for more V.H.E. γ-rays detections than any other. Significant evidence for emission from this object was found in data from 1988 and this detection was confirmed in the data from

1989. Like Centaurus X-3 (Carramiñana et al., 1989) and Cygnus X-3 (Brazier et al., 1989b), V.H.E. emission from this object is modulated with the period of the binary orbit. To increase appreciably the significance of our detection would require about another 20 hours of data. There are no plans to re-observe this object in the near future therefore.

7.3. Techniques

A standard part of data processing involves the rejection of events that fire any off source channels, on the grounds that these are mainly produced by proton-initiated showers emanating from outside the field of view of the on source channel. This technique is known as hardware cutting since the rejection is based on whether the off axis channels exceeded the 50 mV threshold required to trigger a reliable event. Thus, the criterion is decided by the telescope's hardware and sub-trigger information is lost. The QT for each PMT is stored for each event (see section 2.4.2). This allows an extension to the above technique. High QT's from off source PMTs show that a considerable number of photons were arriving from an off axis direction, even though the event in question may have passed the hardware criterion. It is possible to reject such events, thus providing an extra enhancement of the signal to noise ratio, by rejecting events where the outer QT's rise above a given fraction of the central one. Since this rejection is done by software, the technique is referred to as software cutting.

Software cutting has been tried with a wide range of objects. Indications are that this has proved successful in a number of cases. The optimum enhancement for Centaurus X-3 is achieved by rejecting all events where any outer channel averaged QT is greater than 55% of the channel 1 value. This figure, however, may be a function of the zenith angle of the observations. Hardware cutting accepts a smaller fraction of the total events when the telescope is pointing at the zenith than when it is looking low in the sky, as does the fraction rejected by software cutting (see figs. 7.1, 7.2). This is explained qualitatively by the fact that when the telescope is looking low in the sky, when atmospheric attenuation is greatest, a smaller fraction of off-axis events have light pools wide enough to cause a response in the centre channel. However, it is not clear that the variation of the fraction of events accepted by the software cutting is the most efficient possible. It is not possible to vary the hardware criterion during the course of an observation, but this is possible with the software criterion. The best way to apply the software cut may be to use a rejection criterion that varies with zenith angle. Further investigation of all aspects of this promising technique is continuing (Brazier, PhD. Thesis, in preparation).

7.4. Equipment

There are two ways to increase the effectiveness of this branch of Astronomy: improve the signal to noise ratio to
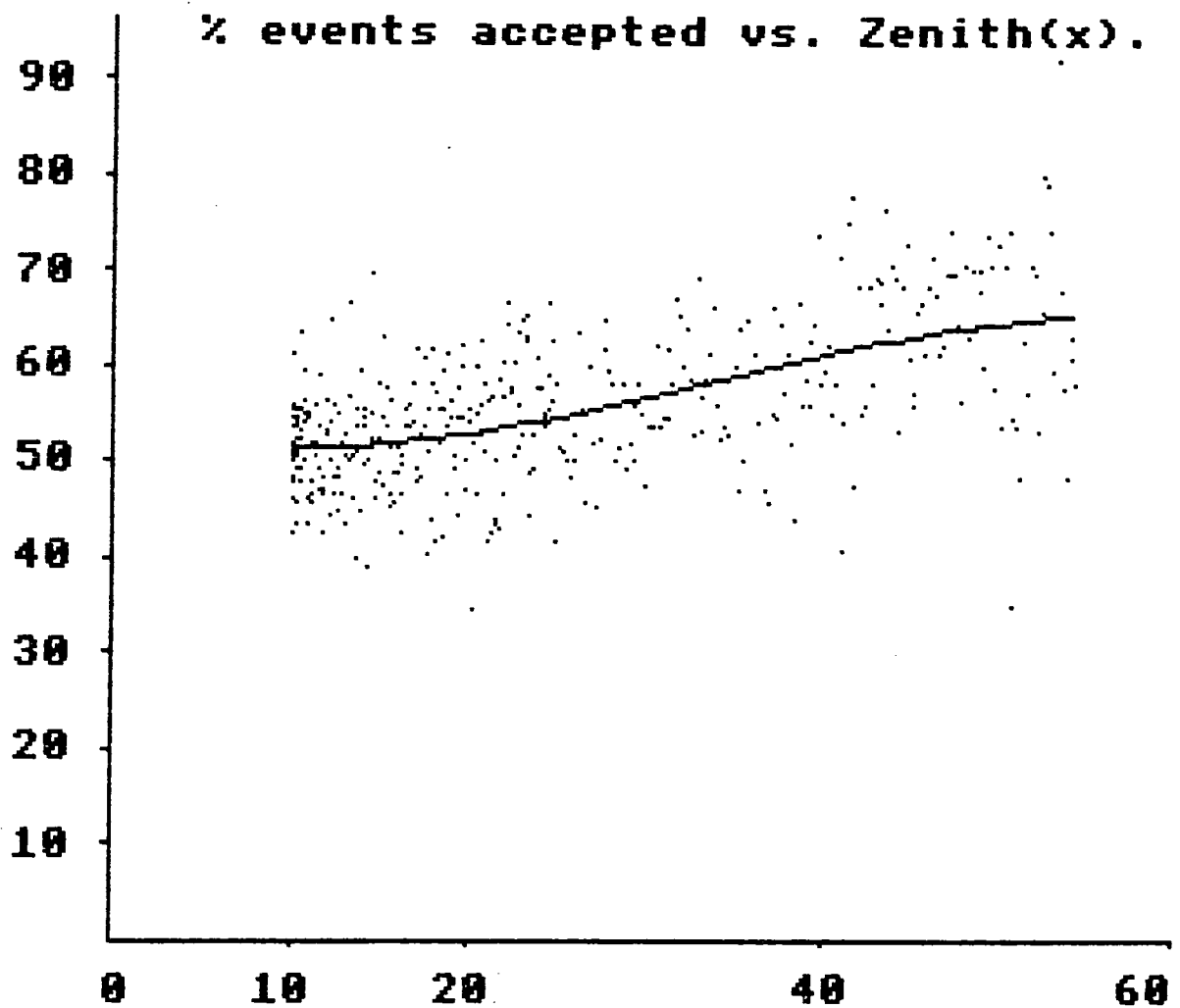
Figure 7.1 Plot of fraction of events accepted against zenith angle for hardware cut
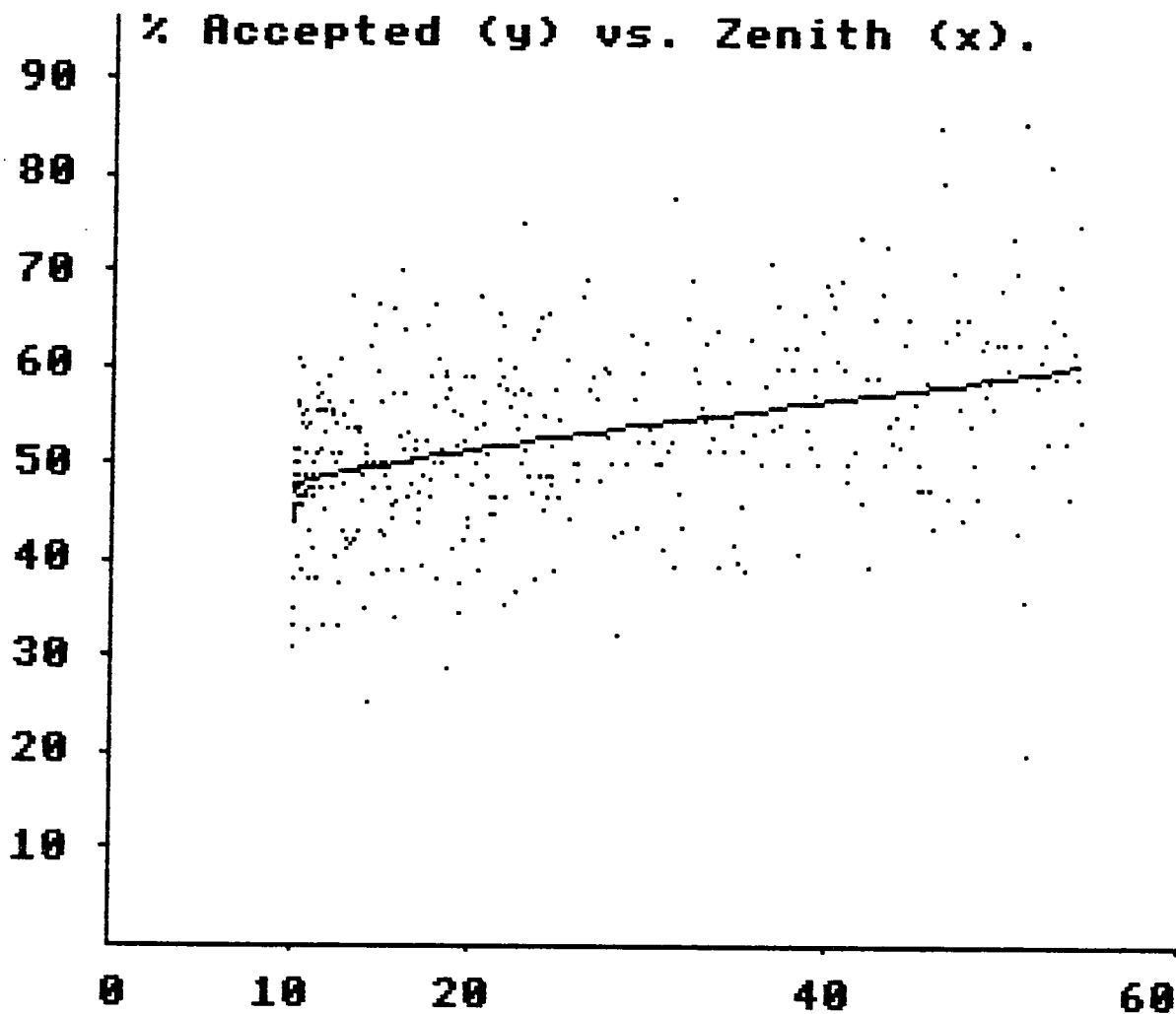
Figure 7.2 Plot of fraction of events accepted against zenith
angle for 55% software cut

increase the signal strength in a given dataset or increase the counting rate to improve the counting statistics of the background and thus the significance of detections. The former option is difficult to achieve due to the very low flux of V.H.E. γ-ray photons and the similarity between a proton-initiated and a photon-initiated shower. Nevertheless, the software cutting technique described above is likely to represent a considerable advance in this direction.

Increasing the count rate is relatively simple to achieve. Two telescopes placed far enough apart to avoid detecting the same showers will produce a dataset twice as large as a single telescope in the same time. Effectively, the count rate is twice that of a single telescope. An array of 10 telescopes of a similar design to the Mark IV could be operated by a single observing team and would have a count rate of about 1000 min^{-1} when pointing near the zenith. This means that the entire 1989 observation of Scorpius X-1 could be repeated in an hour and a half. This improvement would allow study of the form of the light curves of those objects from which pulsed emission has been detected with the present equipment. Furthermore, a DC signal as low as 2% could be detected at the 3σ level in a single 4 hour observation. A fast data acquisition rate will make the proposed array a very useful tool for studying emission from variable objects, such as SN1987a and possibly Centaurus A. Emission from these objects may well vary on a timescale of days. With the array, it would be possible to make an accurate measurement of the signal strength each night and thus follow closely any short-

term variability. This is an exciting development and should contribute greatly to the study of V.H.E. γ-Ray Astronomy in the 1990's.

REFERENCES

Alpar, M.A., Cheng, A.F., Ruderman, M.A. and Shaham, J. Nature, <u>300</u>, 728 (1982).

Backus, P.R., Taylor, J.H. and Damashek, M. Astrophys. J. Lett., <u>255</u>, L63 (1982).

Barthelmy, S., Gahrels, N., Teegarden, B.J., Tueller, J., Leventhal, M. and MacCallum, C.J. IAU Circ. no. 4703 (1989).

Batschelet, E. <u>Circular Statistics in Biology</u>, Academic Press, London (1981).

Beall, J.H., Rose, W.K., Graf, W., Price, K.M., Dent, W.A., Hobbs, R.W., Conklin, E.K., Ulich, B.L., Dennis, B.R., Crannell, C.J., Dolan, J.F., Frost, K.J. and Orwig, L.E. Astrophys. J., <u>219</u>, 836 (1978).

Bennett, K., Bignami, G.F., Boella, G., Buccheri, R., Hermsen, W., Kanbach, G., Lichti, G.G., Masnou, J.L., Mayer-Hasselwander, H.A., Paul, J.A., Scarsi, L., Swananburg, B.N., Taylor, B.G. and Wills, R.D. Astron. & Astrophys., <u>61</u>, 279 (1977).

Bergstrahl. T. and Schroeder, C. Phys. Rev., <u>81</u>, 461 (1952).

Bhat, P.N., Gupta, S.K., Ramanamurthy, P.V., Sreekantan, B.V., Tonwar,S.C. and Vishwanath, P.R. Astron. & Astrophys., <u>81</u>, L3 (1980).

Bhat, C.L., Sapru, M.L. and Razdan, H. Astrophys. J., <u>306</u>, 587 (1986a).

Bhat, P.N., Ramana Murthy, P.V., Sreekantan, B.V. and Vishwanath, P.R. Nature, <u>319</u>, 127 (1986b).

Bhat, P.N., Gupta, S.K., Ramanamurthy, P.V., Sreekantan, B.V., Tonwar,S.C. and Vishwanath, P.R. in <u>Proceedings of the NATO Advanced Research Workshop on Very High Energy γ-Ray Astronomy</u>, Turver, K.E. (ed.), Reidel, p. 143 (1987).

Bionta, R.M., Blewitt, G., Bratton, C.B., Casper, D., Ciocio, A., Claus, R., Cortez, B., Crouch, M., Dye, S.T., Errede, S., Foster, G.W., Gajewski, W., Ganezer, K.S., Goldhaber, M., Haines, T.J., Jones, T.W., Kielczewska, D., Kropp, W.R., Learned, J.G., LoSecco, J.M., Matthews, J., Miller, R., Mudan, M.S., Park, H.S., Price, L.R., Reines, F., Schultz, J., Seidel, S., Shumard, E., Sinclair, D., Sobel, H.W., Stone, J.L., Sulak, L.R., Svoboda, R., Thornton, G., van der Velde, J.C. and Wuest, C. Phys. Rev. Lett., 58, 1494 (1987).

Blackett, P.M.S., Emission Spectra of the Night Sky and Aurora, Rep. of the Gaissot Comm. of the Roy. Soc., p.34 (1948).

Bowyer, C.S., Lampton, M., Mack, J. and De Mondonca, F. Astrophys. J., 161, L1 (1970).

Brazier, K.T., Carramiñana, A., Chadwick, P.M., Currell, T.R., Dipper, N.A., Lincoln, E.W., Mannings, V.G., McComb, T.J.L., Orford, K.J., Rayner, S.M. and Turver, K.E., Experimental Astronomy, (In Press) (1989a).

Brazier, K.T., Carramiñana, A., Chadwick, P.M., Currell, T.R., Dipper, N.A., Lincoln, E.W., Mannings, V.G., McComb, T.J.L., Orford, K.J., Rayner, S.M. and Turver, K.E. submitted to Astrophys. J. (1989b).

Brezinsky, V.S. and Prilutsky, O.F. Astron. & Astrophys., 66, 325 (1978).

Brinkmann, W. and Ogelman, H. Astron. & Astrophys., 182, 271 (1987).

Buccheri, R., Bennett, K., Bignami, G.F., Bloemen, J.B.G.M., Boriakoff, V., Caraveo, P.A., Hermsen, W., Kanbach, G., Manchester, R.N., Masnou, J.L., Mayer-Hasselwander, H.A., Ozel, M.E., Paul, J.A., Sacco, B., Scarsi, L. and Strong, A.W. Astron. & Astrophys., 128, 245 (1983).

Carramiñana, A., Chadwick, P.M., Dipper, N.A., Lincoln, E.W., Mannings, V.G., McComb, T.J.L., Orford, K.J., Rayner, S.M., Turver, K.E. and Williams, D.G. in Timing Neutron Stars, Kluwer, Ogelman, H. and van den Heuvel, E.P.J. (eds.), p.369 (1989).

Castagnoli, C. IAU Circular 4323 (1987).

Castagnoli, C. IAU Circular 4332 (1987).

Caswell, J.L., Roger, R.S., Murray, J.D., Cole, D.J. and Cooke, D.J. Astron. & Astrophys., 45, 239 (1975).

Catchpole, R.M., Whitelock, P.A., Feast, M.W., Menzies, J.W., Glass, I.S., Marang, F., Laing, J.D., Spencer Jones, J.H., Roberts, G., Balona, L.A., Carter, B.S., Laney, C.D., Lloyd Evans, T., Sekiguchi, K., Hutchinson, M.G., Maddison, R., Albinson, J., Evans, A., Allen, D.A., Winkler, H., Fairall, A., Corbally, C., Davies, J.K. and Parker, Q.A. Mon. Not. R. Soc., 231, 75P (1987).

Cerenkov, P.A., Dokl. Akad. Nauk., 2, 451 (1934).

Cerenkov, P.A., Phys. Rev., 52, 378 (1937).

Chadwick, P.M., Very High Energy Cosmic Gamma-Rays From Radio and X-Ray Pulsars., PhD. Thesis, Durham (1987).

Cheng, A.F., and Helfand, D.J. Astrophys. J., 271, 271 (1983).

Cheng, K.S., Ho, C. and Ruderman, M., Astrophys. J., 300, 500 (1986a).

Cheng, K.S., Ho, C. and Ruderman, M., Astrophys. J., 300, 522 (1986b).

Chudakov, A.E., Zatsepin, V.I., Nesterova, N.M., and Dadykin, V.L., J. Phys. Soc. Japan, Sup. A-III, 106 (1962).

Clark, G.W., Garmire, G.P. and Kraushaar, W.L. Astrophys. J., 153, L203 (1968).

Clay, R.W., Gerhardy, P.R. and Liebing, D.F. Astrophys. J., 251, 31 (1986).

Craig, M.A.B., The Lateral Distribution of Cerenkov Light in Large Cosmic Ray Showers as a Measure of Longitudinal Development, PhD. Thesis, Durham (1984).

Crampton, D., Cowley, A.P., Hutchings, J.B. and Kaat, C. Astrophys. J., <u>207</u>, 907 (1975).

De Jager, H.I., De Jager, O.C., North, A.R., Raubenheimer, B.C., van der Walt, D.J. and van Urk, G. S. Afr. J. Phys., <u>9</u>, 107 (1986).

De Jager, O.C., Raubenheimer, B.C., North, A.R., Nel, H.I. and Van Urk, G. Astrophys. J., <u>329</u>, 831 (1988).

Derdeyn, S.M., Ehrmann, C.H., Fichtel, C.E., Kniffen, D.A. and Ross, R.W. Nucl. Instr. Methods, <u>98</u>, 557 (1972).

Dowthwaite, J.C., <u>Very Energetic Gamma Rays From Binary X-Ray Sources and Other Astronomical Objects.</u>, PhD Thesis, Durham (1987).

Dowthwaite, J.C., Harrison, A.B., Kirkman, I.W., Macrae, H.J., McComb, T.J.L., Orford, K.J., Turver K.E. and Walmsley, M. Astrophys. J., <u>286</u>, L35 (1984).

Dotani, T., Hayashida, K., Inoue, H., Itoh, M., Koyama, K., Makino, F., Mitsuda, K., Murakami, T., Yoshida, A., Makishima, K., Ohashi, T., Kawai, N., Matsuoka, M., Hoshi, R., Hayakawa, S., Kii, T., Kunieda, H., Nagase, F., Tawara, Y., Hatsukade, I., Kitamoto, S., Miyamoto, S., Tsunemi, H., Yamashita, K., Nakagawa, M., Yamauchi, M., Turner, M.J.L., Pounds, K.A., Thomas, H.D., Stewart, G.C., Cruise, A.M., Patchett, B.E. and Reading, D.H. Nature, <u>330</u>, 230 (1987).

Erickson, R.A., Fickle, R.K. and Lamb, R.C., Astrophys. J., <u>210</u>, 539 (1976).

Fichtel, C.E., Hartman, R.C., Kniffen, D.A., Thompson, D.J., Bignami, G.F., Ogelman, H., Ozel, M.E. and Tumer, T. Astrophys. J., <u>198</u>, 163 (1975).

Fiegelson, E.D., Schreier, E.J., Delvaille, J.P., Giaconni, R., Grindlay, J.E. and Lightman, A.P. Astrophys. J., <u>251</u>, 31 (1981).

Flanagan, C. IAU Circular 4695 (1988).

Frank, I.M. and Tamm, Ig., Dokl. Akad. Nauk., <u>14</u>, 109 (1937).

Freedman, D., Pisani, R. and Purves, R. Statistics., Norton (1978).

Gaisser, T.K., Harding, A. and Stanev, T. Nature, 329, 314 (1987).

Galbraith, W. and Jelley, J.V. Nature, 171, 349 (1953).

Giacconi, R., Gursky, H., Paolini, F. and Rossi, B. Phys. Rev. Lett., 9, 439 (1962).

Gibson, A.I., Harrison, A.B., Kirkman, I.W., Lotts, A.P., Macrae, J.H., Orford, K.J., Turver, K.E. and Walmsley, M. Nature, 296, 833 (1982).

Gottlieb, E.W., Wright, E.L. and Liller, W. Astrophys. J., 195, L33 (1975).

Grindlay, J.E. Astrophys. J., 199, 49 (1975).

Grindlay, J.E., Helmken, H.F., Hanbury Brown, R., Davis, J. and Allen, L.R. Astrophys. J., 197, L9 (1975a).

Grindlay, J.E., Helmken, H.F., Hanbury Brown, R., Davis, J. and Allen, L.R. Astrophys. J., 201, 82 (1975b).

Grindlay, J.E., Helmken, H.F. and Weekes, T.C., Astrophys. J., 209, 592 (1976).

Gupta, S.K., Ramana Murthy, P.V., Sreekantan, B.V. and Tonwar, S.C., Astrophys. J., 221, 268 (1978).

Gupta, S.K., Ramana Murthy, P.V., Sreekantan, B.V., Tonwar, S.C. and Vishwanath, P.R., in Proceedings of the International Workshop on Very High Energy γ-Ray Astronomy, Ramana Murthy, P.V. and Weekes, T.C. (Eds.), p.282 (1982).

Hamuy, M. and Phillips, M.M. IAU Circ. 4398 (1987).

Heaviside, O. Electrical Papers, 2, 494 (1892).

Hewish, A., Bell, S.J., Pilkington, J.D.H., Scott, P.F. and Collins, R.A. Nature, <u>217</u>, 709 (1968).

Hillas, A.M. and Patterson, J.R. in <u>Proceedings of the NATO Advanced Research Workshop on V.H.E. γ-ray Astronomy.</u>, Turver, K.E. (Ed.), Reidel (1987), p.243.

Hirata, K., Kajita, T., Koshiba, M., Nakahata, M., Oyama, Y., Sato, N., Suzuki, A., Takita, M., Totsuka, Y., Kifune, T., Suda, T., Takahashi, K., Tanimori, T., Miyano, K., Yamada, M., Beier, E.W., Kim, S.B., Mann, A.K., Newcomer, F.M., Van Berg, R. and Zhang, W. Phys. Rev. Lett., <u>58</u>, 1490 (1987).

Jelley, J.V. in <u>Proceedings of the NATO Advanced Research Workshop on V.H.E. γ-ray Astronomy.</u>, Turver, K.E. (Ed.), Reidel (1987), p.27.

Jelley, J.V. and Porter, N.A. Quarterly J. Roy. Ast. Soc., <u>4</u>, 275 (1963).

Johnson, Davies and Siry in <u>Rocket Exploration of the Upper Atmosphere.</u>, London, 1954, Seatom, M. and Boyd, R. (eds.), p.306.

Kanbach, G., Bennett, K., Bignami, G.F., Buccheri, R., Caraveo, P., D'Amico, N., Hermsen, W., Lichti, G.G., Masnou, J.L., Mayer-Hasselwander, H.A., Paul, J.A., Sacco, B., Swananburg, B.N. and Wills, R.d. Astron. & Astrophys., <u>90</u>, 163, (1980).

Katz, J.I. <u>High Energy Astrophysics</u>, Addison-Wesley (1987).

Kellogg, E., Gursky, H., Leong, C., Schreier, E., Tanenbaum, H. and Giaconni, R. Astrophys. J., <u>165</u>, L49 (1971).

Kirkman, I.W., <u>V.H.E. γ-Rays From Celestial Objects.</u>, PhD. Thesis, Durham (1985).

Koshiba, M. IAU Circular 4338 (1987).

Kraushaar, W.L., Clark, G.W., Garmire, G.P., Borken, R., Higbie, P., Leong, V. and Thursos, T. Astrophys. J., <u>177</u>, 341 (1972).

Kristian, J., Pennypacker, C.R., Middleditch, J., Hamuy, M.A., Imamura, J.N., Kunkel, W.E., Lucinio, R., Morris, D.E., Muller, R.A., Perlmutter, S., Rawlings, S.J., Sasseen, T.P., Shelton, I.K., Steiman-Cameron, T.Y. and Tuohy, I.R. Nature, 338, 234 (1989).

Lampton, M., Margon, B., Bowyer, S., Mahony, W. and Anderson, K. Astrophys. J., 171, L45 (1972).

Large, M.I., Vaughan, A.E. and Mills, B.Y. Nature, 220, 340 (1968).

LaSala, J. and Thorstensen, J.R. Astron. J., 90, 2077 (1985).

Leahy, D.A. IAU Circular 4485 (1987).

Macrae, J.H.K., The Detection of Very High Energy Cosmic γ-Rays using the Atmospheric Cerenkov Technique., PhD. Thesis, Durham 1985.

Manchester, R.N., Goss, W.M. and Hamilton, P.A. Nature, 259, 291 (1976).

Manchester, R.N. and Taylor, J.H. Astrophys. J., 86, 1953 (1981).

Manchester, R.N., Tuohy, I.R. and D'Amico, N. Astrophys. J., 262, L31 (1982)

Manchester, R.N., Durdin, J.M. and Newton, L.M., Nature, 313, 374 (1985).

Mardia, K.V., Statistics of Directional Data, Academic Press (1972).

Matz, S.M., Share, G.H., Leising, M.D., Chupp, E.L., Vestrand, W.T., Purcell, W.R., Strickman, M.S. and Reppin, C. Nature, 331, 416 (1988).

Middleditch, J. and Priedhorsky, W.C. Astrophys. J., 306, 230 (1986).

Moffett, A.T. Ann. Rev. Astron. Astrophys., 4, 145 (1966).

Morrison, P. Nuovo Cimento, 7, 858 (1958).

Nel, H.I., de Jager, O.C., Raubenheimer, B.C. and North, A.R., in Timing Neutron Stars, Kluwer, 1989, Ogelman, H. and van den Heuvel, E.P.J. (eds.), p.383.

Ogelman, H. and Zimmermann, H. preprint (1988).

Orford, K.J. and Turver, K.E. Nature, 331, 216 (1988).

Panagia, N., Gilmozzi, R., Clavel, J., Barylak, M., Gonzales Riesta, R., Lloyd, C., Sanz Fernandez de Cordoba, L. and Wamsteker, W. Astron. & Astrophys., 177, L25 (1987).

Pollock, A.M.T., Bennett, K., Bignami, G.F., Bloemen, J.B.G.M., Buccheri, R., Caraveo, P.A., Hermsen, W., Kanbach, G., Lebrun, F., Mayer-Hasselwander, H.A. and Strong, A.W. Astron. & Astrophys., 146, 352 (1985).

Porter, N.A., Delaney, T., Helmken, H.F. and Weekes, T.C., Nuovo Cimento, 32B, 515 (1976).

Price, K.M. and Stull, M.A. Nature, 245, 83 (1973).

Priedhorsky, W.C. and Holt, S.S. Astrophys. J., 312, 743 (1987).

Protheroe, R.J. Nature, 329, 135 (1987).

Raubenheimer, B.C., North, A.R., De Jager, O.C., Van Urk, G., and Van Tonder, A.J., Astrophys. J. (Lett), 307, L43 (1986).

Reiffel, L. and Burgwald, G.M. Phys. Rev., 95, 1294 (1954).

Resvanis, L., Learned, J., Stenger, V., Weeks, D., Gaidos, J., Loeffler, F., Olson, J., Palfrey, T., Sembroski, G., Camerini, U., Finley, J., Fry, W., Jaworski, M., Jennings, J., Kenter, A., Koepsel, R., Lomperski, M., Loveless, R., March, R., Matthews, J., Morse, R., Reeder, D., Sandler, P., Slane, P. and Szentgyorgyi, A. in Proceedings of the NATO Advanced Research Workshop on V.H.E. γ-ray Astronomy., Turver, K.E. (Ed.), Reidel (1987), p.155.

Richards, J.A. and Nordheim, L.W. Phys. Rev., 75, 444 (1949).

Sandage, A.R., Osmer, P., Giaconni, R., Gorenstein, P.,Gursky, H., Waters, J., Bradt, H., Garmire, G., Sreekantan, B.V., Oda, M., Osawa, K. and Jugaku, J. Astrophys. J. 146, 316 (1966).

Scarsi, L., Bennett, K., Bignami, G.F., Boella, G., Buccheri, R., Hermsen, W., Koch, L., Mayer-Hasselwander, H.A., Taylor, B.G. and Wills, R.D. Proceedings of the 12th ESLAB Symposium, ESA SP-124, p. 3, (1977).

Seward, F.D. and Harnden, J.R. Astrophys. J., 256, L45 (1982).

Shapiro, M.M. and Silverberg, R. in Relativity, Quanta and Cosmology., Johnson Reprint Corporation, 1979, De Finis, F. (ed.) vol. 2, p.745.

Shelton, I. IAU Circular 4316 (1987).

Staelin, D.H. and Reifenstein, E.C. IAU Circular 2110 (1968).

Sunyaev, R., Kaniovsky, A., Efremov, V., Gilfanov, M., Churazov, E., Grebenev, S., Kuznetsov, A., Melioranskiy, A., Yamburenko, N., Yunin, S., Stepanov, D., Chulkov, I., Pappe, N., Boyarskiy, M., Gavrilova, E., Loznikov, V., Prudkoglyad, A., Rodin, V., Reppin, C., Pietsch, W., Engelhauser, J., Trumper, J., Voges, W., Kendziorra, E., Bezler, M., Staubert, R., Brinkman, A.C., Heise, J., Mels, W.A., Jager, R., Skinner, G.K., Al-Emam, O., Patterson, T.G. and Willmore, A.P. Nature, 330, 227 (1987).

Svoboda, R. IAU Circ. 4340 (1987).

Terrell, J. Astrophys. J., 300, 669 (1986).

Tumer, O.T., Dayton, B., Long, J., O'Neill, T., Zych, A. and White, R.S. Nature, 310, 214 (1984).

Tumer, O.T., Wheaton, W.A., Godfrey, C.P. and Lamb, R.C. in Proceedings of the 19th International Conference on Cosmic Rays. (La Jolla), 1, 139 (1985).

Turtle, A.J., Campbell-Wilson, D., Bunton, J.D., Jauncey, D.L., Kesteven, M.J., Manchester, R.N., Norris, R.P., Storey, M.C. and Reynolds, J.E. Nature, 327, 38 (1987).

Vaughan, A.E. and Large, M.I. Mon. Not. Roy. Ast. Soc., 156, 26P (1972)

Vishwanath, P.R. J. Astrophys. Astr., 8, 69 (1987).

Wallace, P.T., Peterson. B.A., Murdin, P.G., Danziger, I.J., Manchester, R.N., Lyne, A.G., Goss, W.M., Smith, F.G., Disney, M.J., Hartley, D.F., Jones, D.H.P. and Wellgate, G.W. Nature, 266, 692 (1977).

Walpole, R.E., Introduction to Statistics, Macmillan (1982).

Wang, B., Inoue, H., Koyama, K. and Tanaka, Y. Publ. Astron. Soc. Japan, 38, 685 (1986).